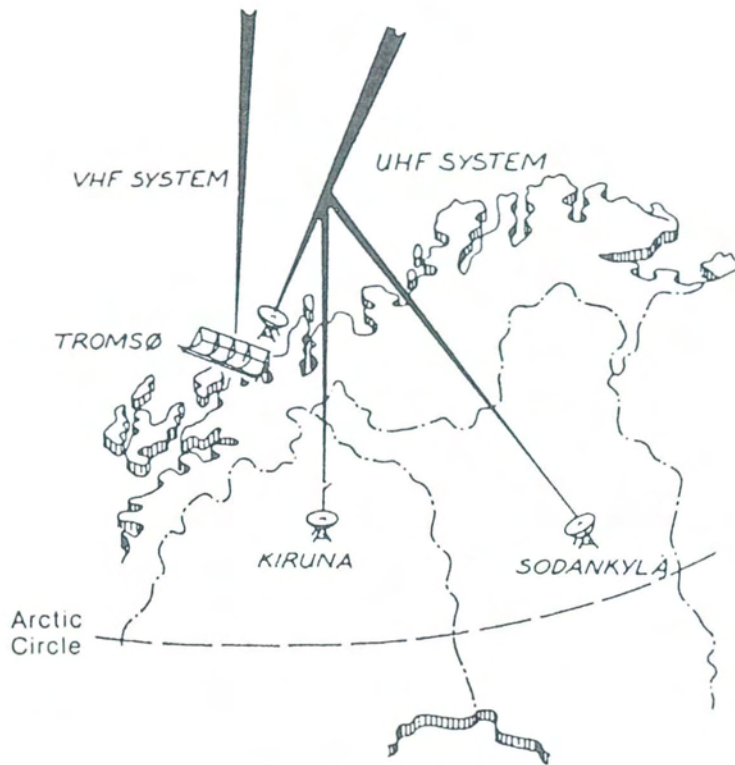


E I S C A T

EUROPEAN INCOHERENT SCATTER SCIENTIFIC
ASSOCIATION

ANNUAL REPORT 1988

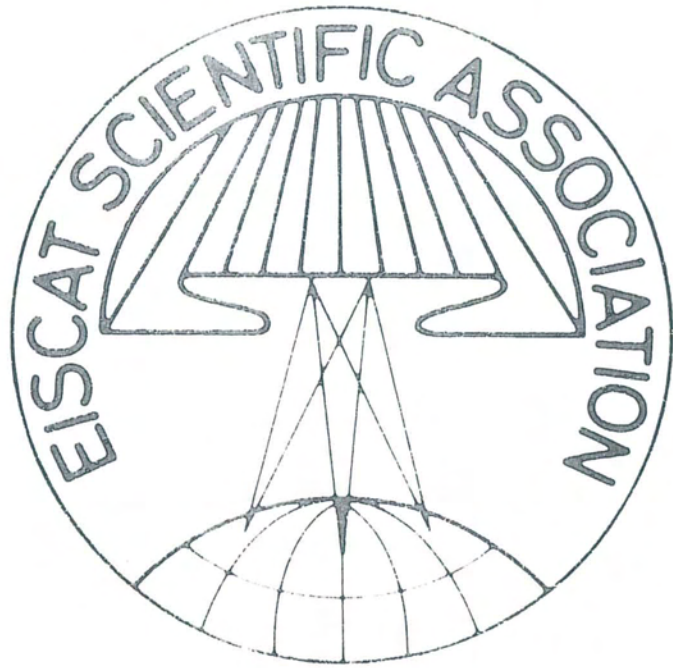
S-981 28 KIRUNA, SWEDEN, Phone (0980) 18740



The EISCAT Radar Systems

(see page 2 for a more detailed description)

The cover illustration shows a height-time-intensity plot of Polar Mesosphere Summer Echoes, called "PMSE". The altitude region is 80 km to 89 km and the time period is from 11:08 to 11:38 UT on 6 July 1988. These data were recorded with the VHF radar with vertical beam and about 1.2 MW peak power. This experiment was the first time a complementary code was applied with EISCAT yielding a height resolution of 150 meters. The colour code covers signal levels of about 0 dB (blue) to 25 dB (red) above the noise level. These Polar Mesosphere Summer Echoes are not caused by the conventional incoherent scatter process, but by some irregularity structure in the electron density profile, which may be related to steep electron density gradients, heavy positive ions, gravity waves and turbulence or other yet unknown mechanisms. These echoes frequently exhibit dramatic height and intensity variations as well as large variations in Doppler shift, i.e. vertical velocity (see pages 22-28 for more information on the PMSE).



ANNUAL REPORT 1988

EISCAT, the European Incoherent Scatter Scientific Association, is established to conduct research on the middle and upper atmosphere, ionosphere and aurora using the incoherent scatter radar technique. This technique is the most powerful groundbased tool for these research applications. EISCAT is also being used as a coherent scatter radar for studying instabilities in the ionosphere as well as for investigating the structure and dynamics of the middle atmosphere and as a diagnostic instrument in ionospheric modification experiments (Heating).

There exist seven incoherent scatter radars in the world, and EISCAT is one of the highest-standard facilities. The experimental sites of EISCAT are located in Scandinavia, north of the arctic circle. They consist of two independent radar systems (see scheme on the inside of the cover page).

The UHF radar of EISCAT operates in the 933 MHz band with a peak transmitter power of 1.5 MW and 32 m parabolic dish antennas, which can be steered omni-directionally. Transmitter and receiver are in Tromsø (Norway). Receiving sites are also in Kiruna (Sweden) and in Sodankylä (Finland), allowing tristatic measurements.

The VHF radar in Tromsø operates monostatically in the 224 MHz band with a peak transmitter power of 1.5 MW (to be raised to 5 MW) and a 120 m x 40 m parabolic cylinder antenna, which is subdivided into four sectors. It can be steered mechanically in the meridional plane from 30° south to 60° north of the zenith.

The basic data, which are measured with the incoherent scatter radar technique, are the profiles of electron density, electron and ion temperature and ion velocity. A selection of well-designed radar pulse schemes allows the adaption of the data taking routines to many particular phenomena, occurring at altitudes between about 60 km and more than 1000 km. Depending on geophysical conditions, a best time resolution of one second and an altitude resolution of a few hundred meters can be achieved, whereas typical resolutions are of the order of minutes and kilometers.

The operation of a total of 2000 hours per year is distributed equally between Common Programmes (CP) and Special Programmes (SP). At present five well-defined Common Programmes are run regularly about 30 times per year for 24 or more hours to provide a data base for long term synoptic studies. Three Unusual Programmes (UP) can be started ad hoc during particular geophysical conditions. A large number of Special Programmes, defined individually by associate scientists, are run to study a variety of particular geophysical events.

Details of the EISCAT system and operation can be found in EISCAT Technical Reports, which can be obtained from EISCAT Headquarters in Kiruna, Sweden.

The investments and operational costs of EISCAT are shared between:

Suomen Akatemia, Finland

Centre National de la Recherche Scientifique, France

Max-Planck-Gesellschaft, W.Germany

Norges Almenvitenskapelige Forskningsråd, Norway

Naturvetenskapliga Forskningsrådet, Sweden

Science and Engineering Research Council, United Kingdom

CONTENTS of the EISCAT ANNUAL REPORT 1988:	page
Council Chairman's Foreword	4
Director's Perspective on Some Highlights of the Past	5
Operations and Data Analysis	14
Experiment Operation	14
Incoherent Scatter Data Analysis at EISCAT	15
Common Programme Data Analysis	16
World Day Operations	16
New Techniques in Data Analysis	17
The EISCAT Common and Unusual Programmes	19
Scientific Research	21
Observations of the D-region and the Mesosphere	21
E-region Studies	29
E- and F-region Irregularities	35
Ionosphere - Thermosphere Coupling	42
The Excitation of Ionospheric Convection	43
Auroral Signatures of Magnetospheric Substorms	49
Artificial Modifications of the Ionosphere	55
Technical Evolution and Adaption of the System and Instrumentation	59
The NMT 900 Situation	60
The UHF Receivers	60
Problems Introduced by the NMT 900 System	62
Technical Parameters of the EISCAT Radar Facilities	64
 Appendix:	
Publications	65
Journals and Books 1988	65
Proceedings, Reports and Theses 1988	70
Supplements 1984-1987	71
EISCAT Reports and Meetings	72
Budget Balance Sheet 1988	73
EISCAT Council and Committee Members and Senior Staff	74
The EISCAT Associates	75
Addresses	76

Annual Report 1988 of the EISCAT Scientific Association

Edited and lay-out by
 J. Röttger, S. Buchert, T. van Eyken,
 Gurli Hultqvist and other EISCAT senior staff.

Finishing and printing by
 Birgitta Määttä and Stig Björklund,
 Institutet för Rymdfysik, Kiruna, Sweden.

ISSN 0349-2710

COUNCIL CHAIRMAN'S PAGE

The year 1988, my second year as chairman of the Council of EISCAT, was for me first of all the year when it became clear to everyone in the field that EISCAT and the EISCAT community have developed into dominating forces in important sectors of space physics research. This was demonstrated perhaps most clearly at the COSPAR Meeting in Helsinki. I shall not mention any individual contributions, but the amount and quality of the results that originated in EISCAT measurements impressed very much. After many years of development work we are now reaping rich fruits of the earlier efforts. The EISCAT community, the EISCAT staff and the EISCAT Council have good reasons to be happy and proud.

Yet we have hardly started to use the VHF radar. The year 1988 was also the year of interference problems and of problems with the permission to transmit. The permission to continue transmissions was granted at the end of the year but the interference problems are still with us and it is still unclear how we shall be able to solve them at a cost that we can afford. It is an economic problem rather than a technical one.

In 1988 we first dealt with a number of new plans for additional radio facilities in northernmost Europe: for the super-heater in Ramfjordmoen and for new incoherent scatter radars on Spitzbergen. Those plans are very exciting. It is unclear how they will affect EISCAT, however, if they come into existence. In the best case they will be coordinated with and complement EISCAT. In the worst case they may be uncoordinated with EISCAT and reduce the resources available for EISCAT. EISCAT will certainly have to prepare itself in the next few years for the new situations that may grow out of the present planning efforts.

During 1988 I had the pleasure of signing the contract with our Director, Dr. Jürgen Röttger, for an extension of his term by another four years. The Council also appointed the organization's first Deputy Director, Dr. Gudmund Wannberg in 1988 and it decided to hold only one Council meeting per year, as a rule, from 1989. This last-mentioned decision is to me an illustration that EISCAT has passed its main development phase and has come into a more stable situation in which it is run by a very experienced and competent Director and staff.

Bengt Hultqvist

DIRECTOR'S PERSPECTIVE ON SOME HIGHLIGHTS OF THE PAST

The past year has again been a very prosperous one for EISCAT operation, science and development. The UHF as well as the VHF system were used in more than 2000 hours of experiments, the quality of the data is further improving and has reached a respected recognition, the number of scientists and the number of scientific papers has increased and the financial, instrumental and personnel situation is under proper control.

Although slow progress has still to be reported on the improvement of the VHF system, several hundred hours of operation were performed on VHF and new experimental techniques have been introduced, which resulted in most valuable scientific results. The cover photo of this Annual Report shows for instance a representative example of a data record of VHF-radar echoes from the mesosphere, which was collected with the newly implemented complementary code. The altitude resolution of 150 m is the best resolution achieved so far in experimental data acquisition with the EISCAT radars.

Many more new and exciting developments took place and only a few can be mentioned here: Full application of alternating codes for improved spectrum and altitude resolution, the introduction of interferometer measurements with the VHF radar, the implementation of a new UHF receiver front-end in Tromsø to improve the system temperature by several ten Kelvin to presently 90 Kelvin, the full inclusion of two new Common Programmes to study the high latitudes as well as coupling processes in the lower thermosphere and the operation of Unusual Programmes to study, ad hoc, certain geophysical events.

Evolutionary developments were continued, such as the implementation and first tests of the digital chirp synthesizer, the design of the special digital preprocessor, the Multichannel FIR Filter and Integrator, and the FFT processor, the loading of codes into the correlator buffer memory and correlator, the CPU synchronization of all site computers and other hardware and software developments. As usual, these technical and instrumental developments are reported in the Proceedings of the EISCAT Annual Review Meeting (see list of

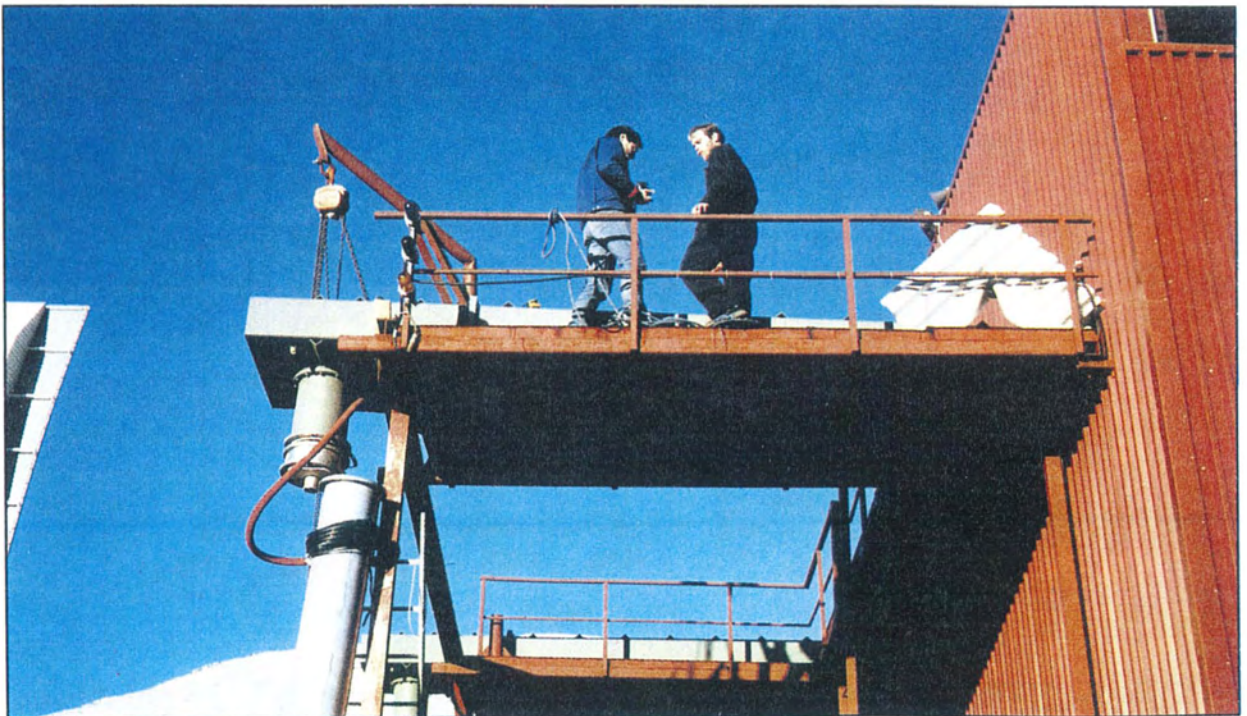


Fig. 1. Work on the transition from waveguide to coaxial cable of the VHF system

INTERFERENCE HAZARDS FACING EISCAT

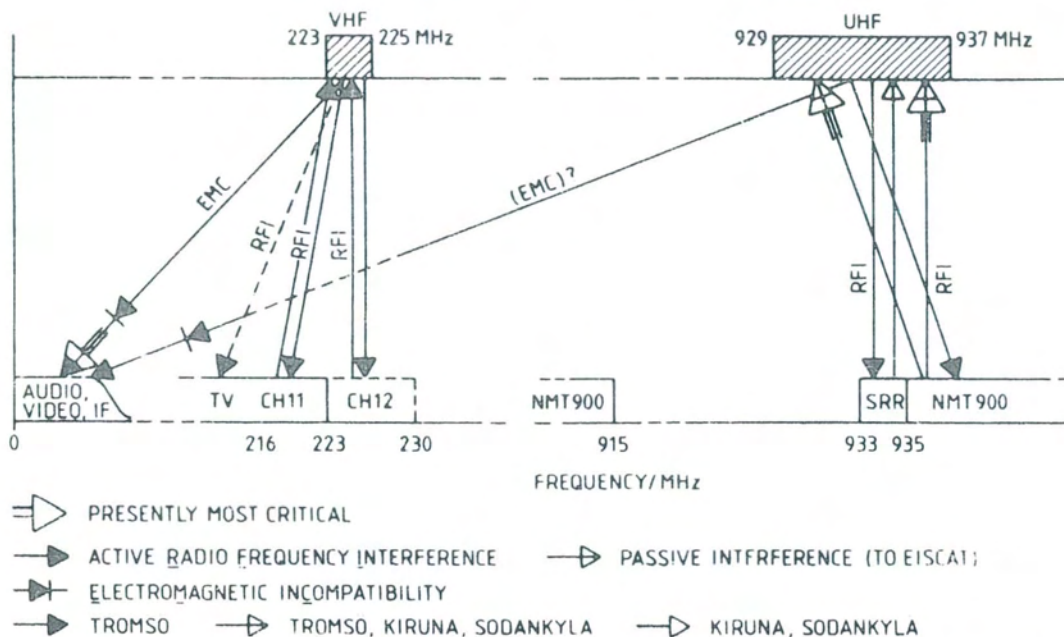


Fig. 2. Allocation of frequency bands to EISCAT (upper part) and to other services (lower part) in the same or adjacent frequency bands. The arrows show the direction of transmission and indicate the potential for Radio Frequency Interference (RFI), as well as for Electro Magnetic (in)Compatibility (EMC) of transmitter radiation to audio and video equipment. Indicated are the television channels TV CH11 and CH12 in the VHF band as well as the mobile telephone (NMT 900) and short-range-radio (SRR) channels in the UHF band.

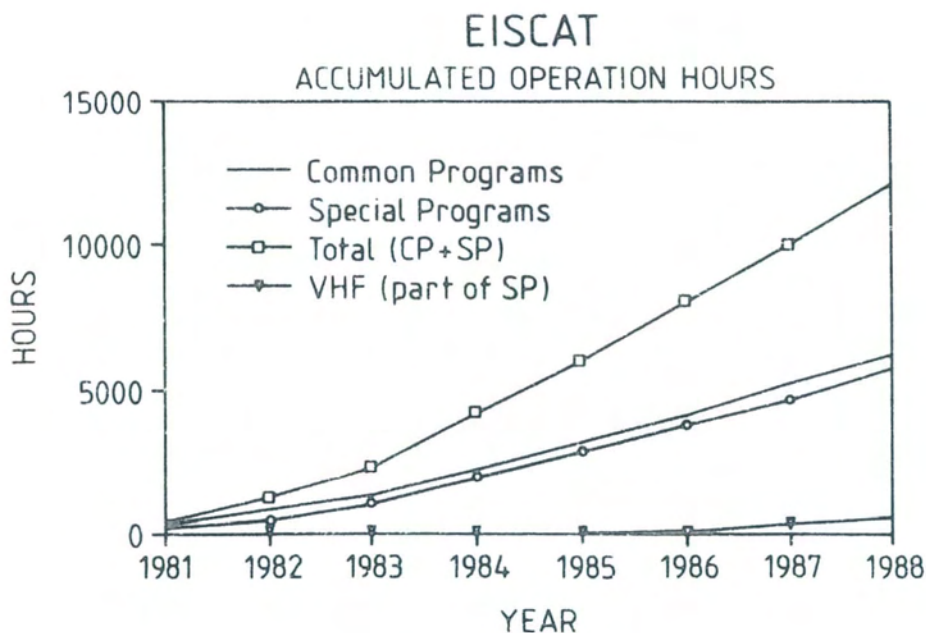


Fig. 3. Accumulated operating hours of Common Programmes (CP), Special Programmes (SP) and the Total of CP + SP. The Total and the SP operation time include the VHF operation, which is also displayed separately.

EISCAT publications on page 72), which in the year 1988 took place in Riksgränsen, Sweden.

A major part of the technical work was related to the ongoing development of the VHF radar system. In the beginning of the year the first rebuilt Valvo klystron was handed over to EISCAT after it had been aged, tuned and tested on-site in Tromsø. The operation was reliable throughout the year, though the transmitted power had to be limited to 1.5 MW and restrictions on antenna beam directions and operating time periods had to apply because of radio frequency interference. The second rebuilt VHF-klystron could not be implemented into the transmitter system as planned, because a failure of the waveguide-coax transition interrupted the tests at the end of October. The waveguide-coax repair, which is documented on the photo of Figure 1, allowed a later continuation of the tests in the next year.

Besides these casual problems which had to be solved, the main difficulty was the mitigation of different kinds of mutual radio-frequency interference (RFI). The multitude of the interference possibilities is displayed in Figure 2, and we note that it relates to the VHF as well as the UHF operation. The VHF problem results mainly from the electromagnetic non-compatibility of electronic installations (EMC), i.e. the EISCAT transmissions affect nearby audio and video equipment. The UHF problem arises due to near-band operation of communication transmitters of the NMT 900 (Nordic Mobile Telephone) system, which raise the noise level in EISCAT's receiving bands substantially. There are several technical possibilities to remedy these disturbances, and we are working hard on feasible solutions. These range from desensitizing electronic equipment to VHF-radar transmissions to contemplations for modifying the antenna radiation by electronic beam forming or shielding by mechanical structures. The UHF interference is being reduced by improving the receiver front-ends and implementing filters (see specific chapter on the Technical Evolution and Adaption of the System and Instrumentation on pages 59-63).

We are well aware of the fact that the operation of the EISCAT research radar systems are performed in frequency bands which are also allocated to other users. We therefore have to

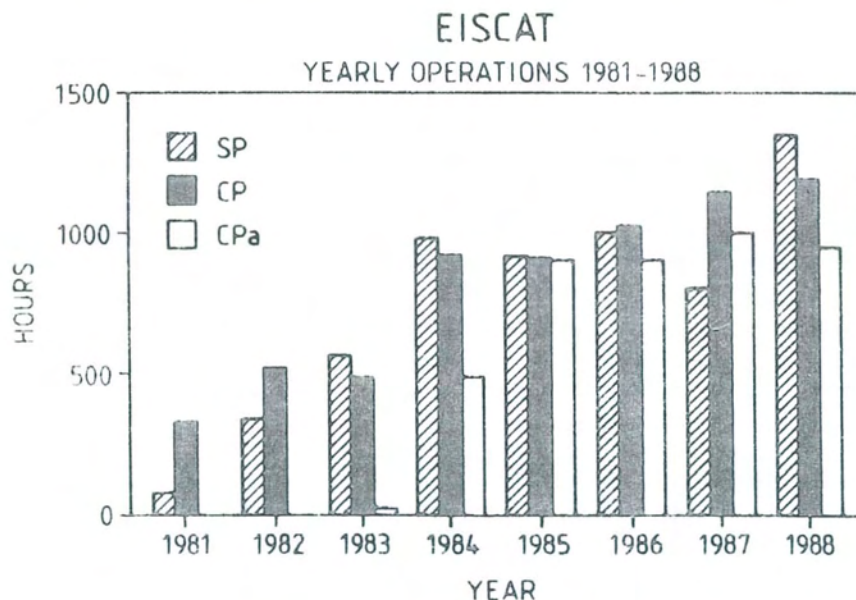


Fig. 4. The yearly operation hours of EISCAT for Special Programmes (SP), which includes the VHF operations, Common Programmes (CP) and the analyzed hours of Common Programme operation (CPa).

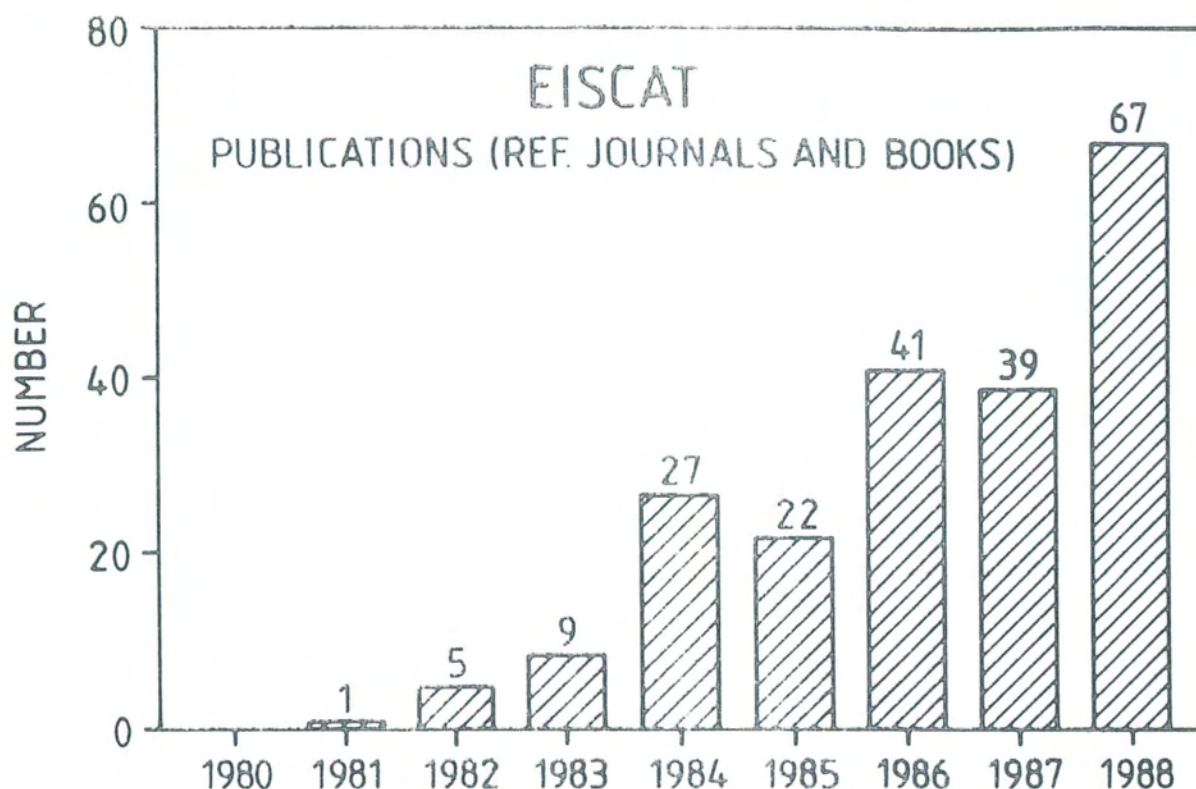


Fig. 5. Publications in refereed journals and books, which deal with EISCAT science and techniques (a complete list of publications in 1988 is found on pages 61 to 68 of this Annual Report).

undertake all possible means to diminish the mutual interference and to collaborate with the telecommunication administrations on this matter. It is a pleasure to acknowledge the cooperative attitude to optimise the frequency allocation planning in order to minimise the interference in the EISCAT bands, which has been developing by the administrations in the Scandinavian countries.

In the context of all the measures to mitigate the interference we have also carefully evaluated the possibilities of radiation hazard in the surrounding of the EISCAT antennas. Extensive investigations have shown that, provided the precautions advised to staff and visitors are obeyed, the electromagnetic power levels are well below official safety limits and radiation by the EISCAT radars presents no safety hazards to persons at the site or in its surroundings.

More than 2000 hours of experiment operation again took place in the year 1988 (the operation statistics are found in the special section on page 14 of this Annual report). At the beginning of the year EISCAT crossed the representative milestone of 10000 hours of total experiment operation since the first experiments took place in 1981 (see Fig. 3). As envisaged, about half of these are Special Programme (SP) and the other half are Common Programme (CP) operations. In Figure 4 the development of these operations since 1981 is depicted. We note that since about 1984 the total number of operating hours per year has roughly stabilized close to 1000 hours per CP as well as SP, adding up to the prospected total number of 2000 hours per year. Since 1985 the Common Programme data are almost completely analysed, which also proves the high quality of the data. The present status of the analysis procedure is described in the special section on page 18. The accumulated Special Programme time is 28% for United Kingdom, 22% for France, 22% for Germany,

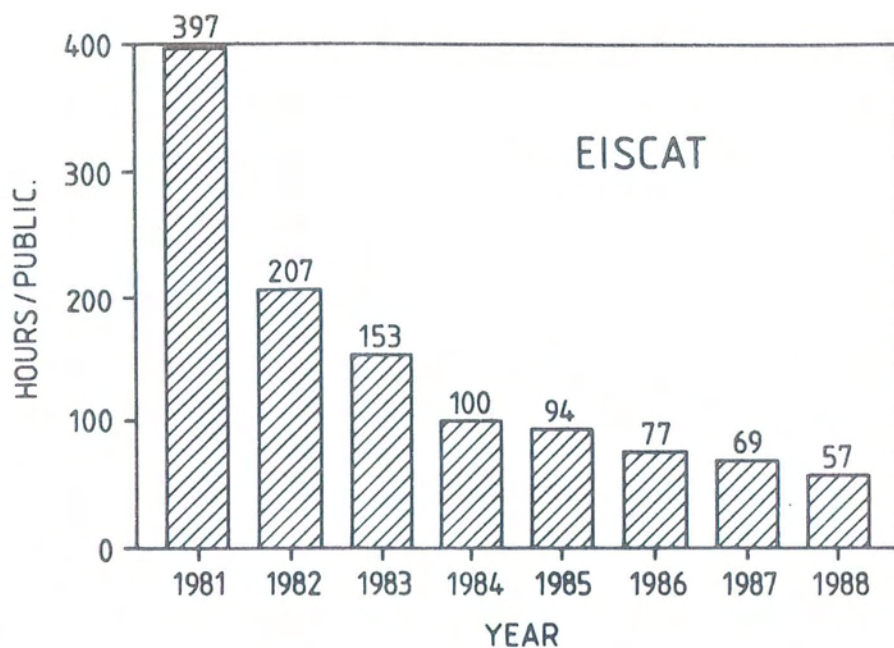


Fig. 6. The ratio of accumulated operating hours with data taking to the number of total publications.



Fig. 7. The EISCAT Council during the 31st meeting in May 1988 at the Max-Planck-Institut für Aeronomie in Katlenburg-Lindau, W.Germany.

First row (l.t.r.): T.B. Jones, K. Schlegel, C. La Hoz, L. Westgaard, J. Röttger, B. Hultqvist, W.J.G. Beynon, O. Havnes, G. Caudal. Second row (l.t.r.): A. Siivola, O. Ranta, A. Berroir, W.I. Axford, G. Preiß, M. Meinecke, P. Bauer, G. Wannberg, J. Gustavsson, B.R. Martin, P. Hagström.

EISCAT

TOTAL CAPITAL INVESTMENT IN MSEK (% OF TOTAL)

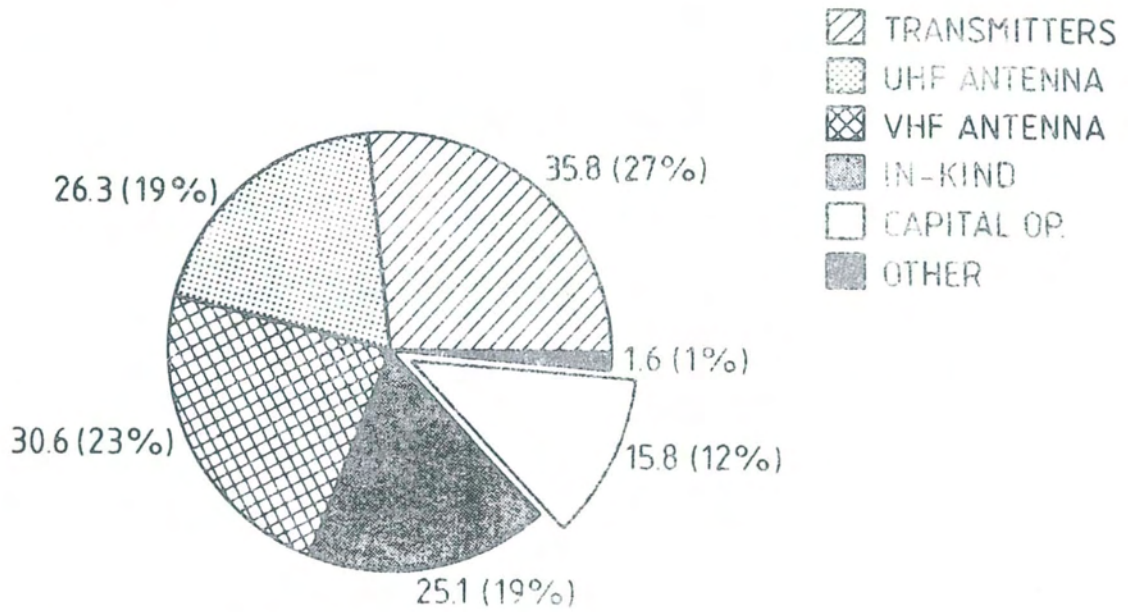


Fig. 8. The total capital investment.

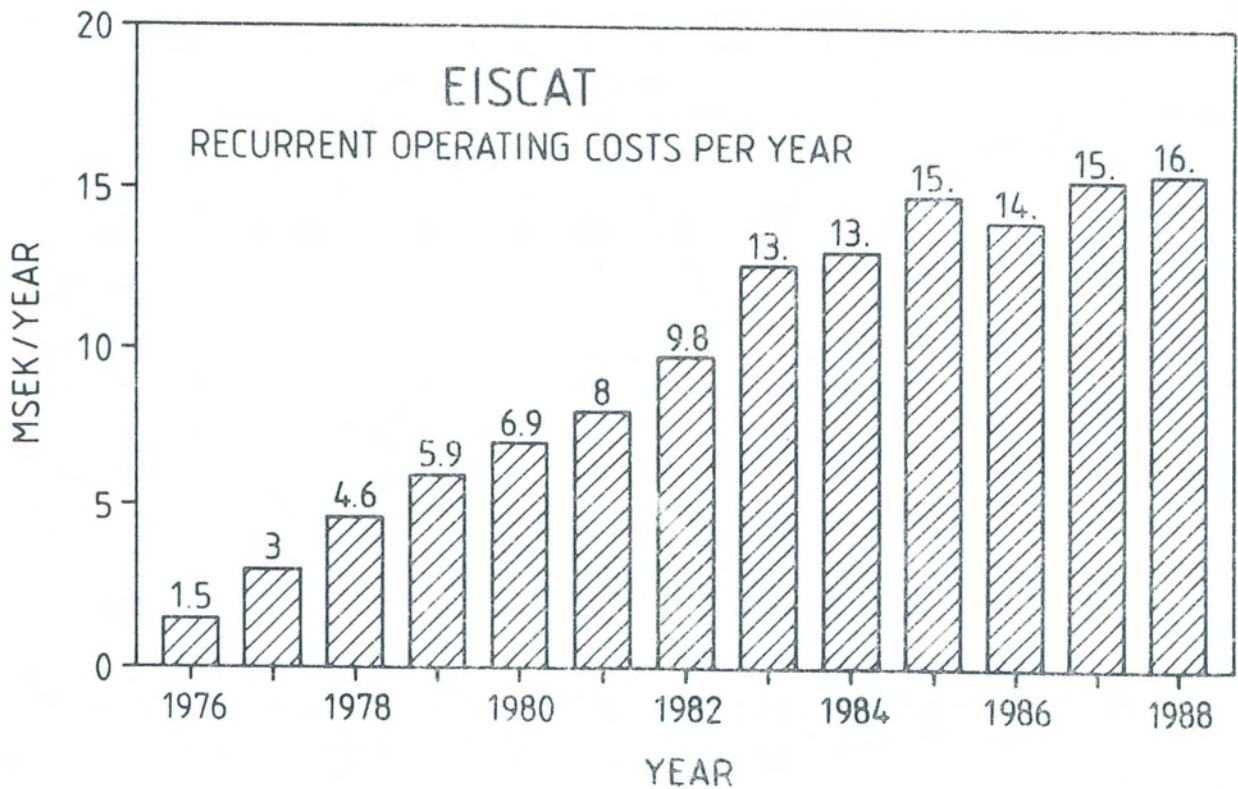


Fig. 9. Recurrent operating budget per year in million Swedish Crowns.

10% for Norway, 9% for Sweden and 5% for Finland, EISCAT needed about 5% of Special Programme time for experiment tests, part of the latter were also for experiments of staff scientists (see special section on page 14).

During all these experiment operations interesting science was achieved and several new phenomena were detected, such as for instance the extremely large ion convection velocities and anisotropic temperatures as well as coherent echoes from the E- and the D-region. This introduction should not aim to be a scientific review of all the achieved results, which would comprise an assessment of the value of the EISCAT operations. However, a straight measure can be applied here, namely the list of publications dealing with EISCAT results. The list of all the 68 publications in 1988 is found at the end of this Annual Report. It demonstrates numerically that the operations of EISCAT had been quite efficient. By the end of the year 1988 a total of more than 200 papers had been published in refereed journals or books. This number does not even include the numerous reports, theses and notes, published on EISCAT results. The development of the scientific and technical publications can be followed in the diagram of Figure 5. The significant increase proves to us that the operations were valuable, have attracted an extended community of scientists and can be extrapolated into a healthy use of EISCAT in the years to come.

Regarding the fact that the milestones of ten thousand operating hours and 200 publications had been passed in the year 1988, it is opportune to evaluate the development of the operating hours, operating costs and scientific publications in terms of EISCAT's efficiency. The comparison of these parameters may eventually allow extrapolation into the future developments. Although the values displayed in the accompanying diagrams cannot directly be transferred into practical applications, it is interesting and illustrative to notice the numbers and their trend over the years. In Figure 6 the accumulated operating hours per scientific publication is shown. Beginning with about 400 operating hours, which were needed to publish the first paper in 1981, the average number of accumulated experiment hours per publication has been reduced to about 60 in the year 1988.

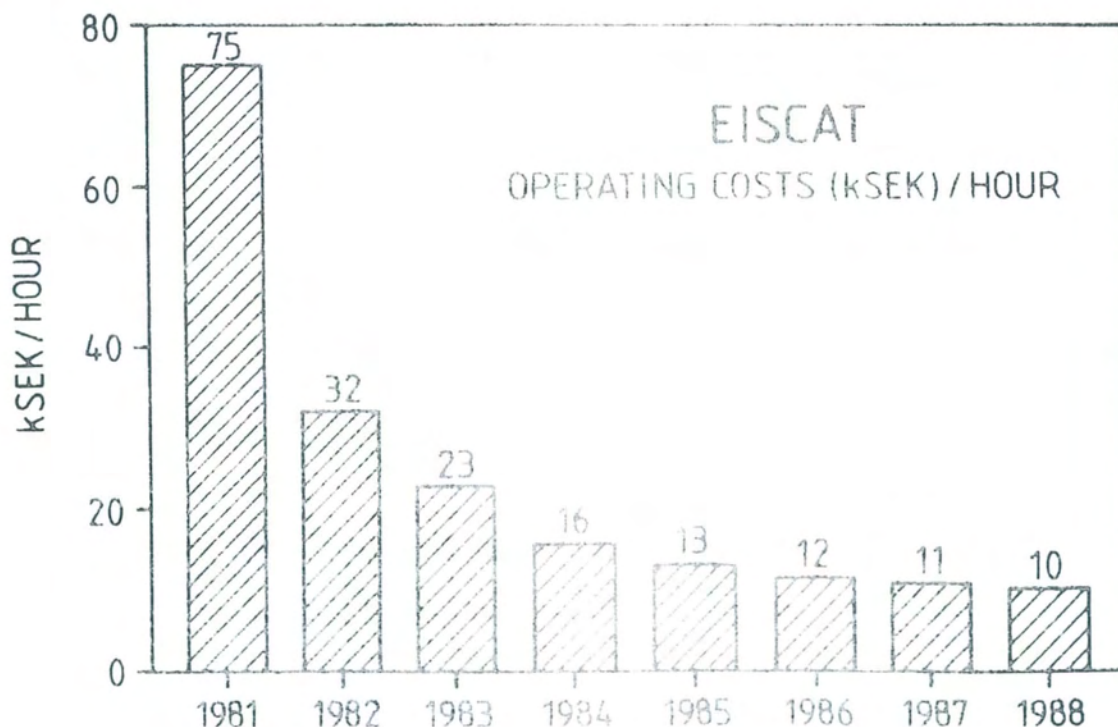


Fig. 10. Accumulated operating costs (in thousand Swedish Crowns) per accumulated operating time in hours.

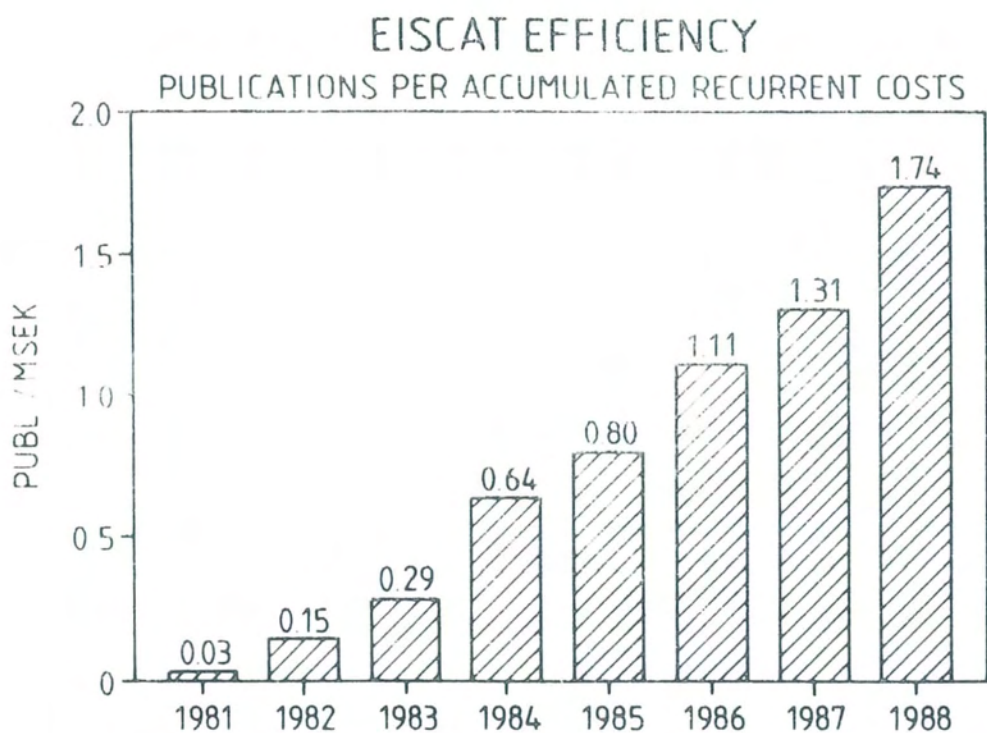


Fig. 11. The number of accumulated publications per accumulated recurrent operating costs.

It is also a vital requirement for a facility like EISCAT to obtain the necessary funding for the scientific operations as well as to have a perspective of excellent scientific interest, which is one of the bases for the continuity of funding. We appreciate very much the permanent support through the research councils in the associate countries, who are represented in the EISCAT Council (see Fig. 7). The associates have contributed over the years a significant amount of funds to EISCAT's investments, which are displayed in Figure 8, and have accumulated to 135 million Swedish Crowns. The total recurrent operating costs had accumulated to almost 130 million Swedish Crowns by the end of 1988. The yearly operating budget has stabilized around 16 million Crowns. The development of the recurrent operating costs since the beginning of EISCAT is displayed in Figure 9. The accumulated operating costs per experiment hour has reduced from 75000 Swedish Crowns in 1981 to about 10000 Crowns (Fig. 10).

A figure of merit of EISCAT is the number of publications per accumulated recurrent costs, which is displayed in Figure 11 as the "EISCAT Efficiency". This efficiency has notably increased by about a factor of 50 from 1981 to 1988. We also note the linear upward trend of this figure of merit, which can be regarded as very healthy and should point the way to a prosperous development into the next decade.

The scientific results, achieved with EISCAT data by numerous scientists from many countries, are summarised in the main section of this Annual report on pages 21 - 56. These selected highlights are compiled from contributions from all the EISCAT associate countries. We note with satisfaction that the quantity as well as the quality of the scientific outcome is further progressing. It is also well appreciated in this context that the use of experimental data from EISCAT is encouraging and yields significant results. The input of scientists to the EISCAT operation by means of designing for instance new experiment routines, coding schemes and analysis procedures as well as proposing and stimulating new instrument adaption and development is also a highly appreciated feature of the internati-

onal scientific collaboration within EISCAT. We also appreciate the keen attention paid to the operation of the EISCAT sites and Headquarters by the Administrative and Finance Committee during its spring meeting in Kiruna, by the Scientific Advisory Committee during its autumn meeting in Sodankylä as well as by the Council during its autumn meeting in Kiruna.

The personnel situation of EISCAT is stable. With usual fluctuations of very few staff members per year, we have 33 employees, whereof 8 are scientific (including directors), 14 engineering-technical, 5 computing, 4 administrative-secretarial and 2 caretaking. The major change was the leaving of the Head of Computer Operations, Walter Schmidt, who had served EISCAT efficiently for almost six years and was replaced by Stephan Buchert in August 1988.

My thanks and acknowledgements are again directed to the EISCAT staff members for their dedicated work, to the scientific users of EISCAT for their continuing and enthusiastic interest as well as to the EISCAT Council and Committees who guarantee the continuity of funding through the associates' research councils. Particular thanks are addressed to the members of the Scientific Advisory Committee, who submitted scientific input for this report, as well as to Dominique Fontaine, Kristian Schlegel and P.J.S. Williams, who revised certain parts of the scientific section of this Annual Report. I express also my acknowledgement to the EISCAT staff members, particularly Gurli Hultqvist for typing and editing, as well as Stephan Buchert, Peter Collis, Tony van Eyken, Cesar La Hoz and Gudmund Wannberg, who supported me efficiently in compiling, reviewing and finishing this Annual Report 1988.

Jürgen Röttger

OPERATIONS AND DATA ANALYSIS

Experimental Operation

In 1988 EISCAT operated active experiments for a total of 2546 hours. This figure divides into 1195 hours of common programs, 1281 hours of special programs of the associate countries, and 70 hours of special programs of EISCAT staff. Table 1 and Fig. 12-17 contain in detail various useful distributions of operation time.

The total of 2546 hours is higher than the target figure of 2000 hours by 546 hours. The CP operations exceeded its target of 1000 hours by 195 hours, and the SP operations exceeded its target of 1000 hours by 351 hours. The latter figure includes the 70 hours utilised by EISCAT staff.

The distribution of the old Common Programmes is reasonably close to the target of 40-20-40% for CP-1,2,3 respectively. This distribution does not take account of the number of hours employed by the new common programs CP-4 and CP-5 (Fig. 12). The new distribution of the common programs that takes account of the new common programs will take effect starting in 1989 according to a decision of the Scientific Advisory Committee.

The distribution of Special Programme experiments among the associate countries

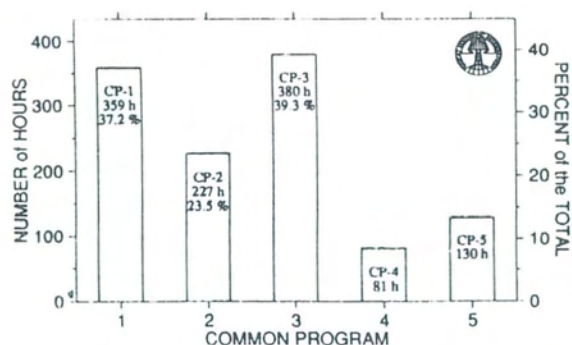


Fig. 12. Distribution of operational hours among the Common Programmes for 1988. Total number of hours is 1195.

continues the same trend as in previous years with the United Kingdom still above the goal of 25%, whereas France and Germany remain under the same goal (Fig. 14). The hours used by the associates show a sharp increase as compared to the previous year when a deficit of 258 hours occurred. This year France, Germany and the United Kingdom have all employed more than 300 hours

EISCAT OPERATIONS 1988

CP	1195 hrs
SP	1281
EI	70
TOTAL	2546

Distribution of Special Programmes

	1988 hrs	Acc. 1987 hrs	Acc. 1988 hrs	Acc. 1988 %
FI	46	241	287	4.88
FR	324	975	1299	22.10
GE	379	892	1271	21.63
NO	70	495	565	9.61
SW	117	395	512	8.71
UK	345	1309	1654	28.14
EI	70	219	289	3.60

Distribution of Common Programmes

CP-1	359hrs	37.2 %
CP-2	227	23.5
CP-3	380	39.3
CP-4	81	
CP-5	130	
UP-1	17	
UP-2	1	
TOTAL	1195.0	

Table 1. EISCAT operations for 1988. The abbreviations are: CP Common Programme; SP Special Programme; EI EISCAT; FI Finland; FR France; GE Germany; NO Norway; SW Sweden; UK United Kingdom.

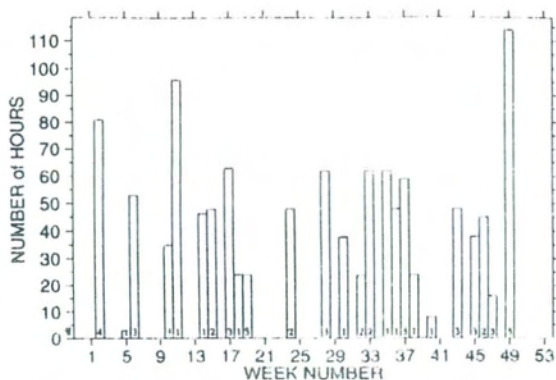


Fig. 13. Distribution of Common Programme operations per week for 1988.

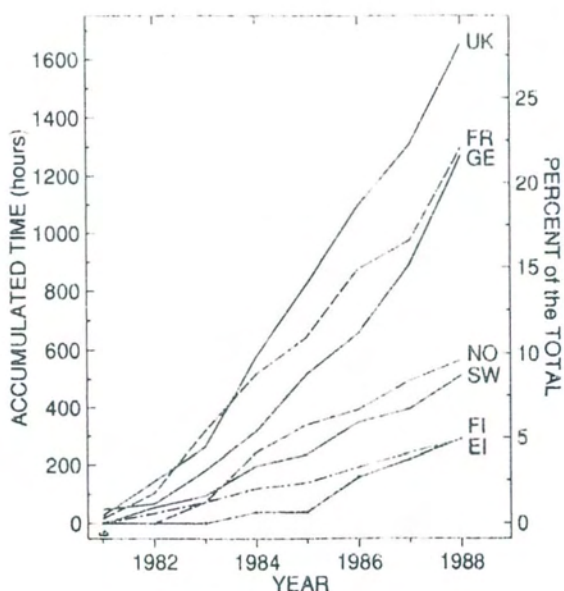


Fig. 14. Accumulated Special Programme operations for each Associate, shown as total number of hours and as percent of the total, for the years 1981 to 1988.

each as compared to the 250 hours allocation. This increase has resulted in a total excess of 281 hours of Special Programmes that becomes 351 hours when taking into account the hours employed by EISCAT staff (Fig. 13).

Operations of the VHF radar in 1988 amounted to a total of 277 hours that includes 32 hours employed by EISCAT staff (Fig. 17).

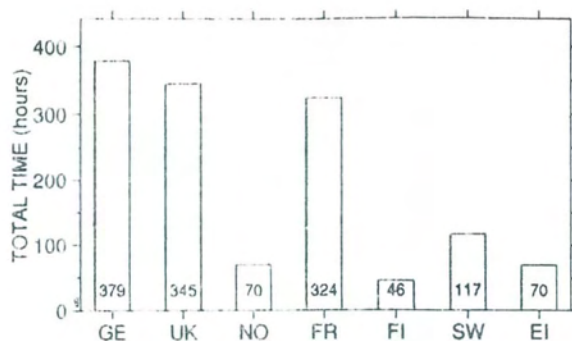


Fig. 15. Special Programme operations for 1988 according to Associate country. Total number of hours for Associates is 1281; for EISCAT staff 70.

Incoherent Scatter Data Analysis at EISCAT

Data analysis is the term used for deriving values for the basic ionospheric parameters from the incoherent scatter radar measurements. This procedure is implemented at EISCAT such that for most operations the raw radar data are able to be post-integrated and analysed directly from the computer memory during the course of experiments themselves, rather than at a later time from recorded data on tape. The latter option is of course available for analysis or re-analysis of older data, but is also sometimes needed due to unforeseen problems during experiment operation.

In principle all Common Programme data are analysed in close to real time. Rapid availability of the results has many benefits, both in monitoring the system performance and in having up-to-date knowledge of ionospheric characteristics. It is also possible to apply the same procedures to special experiments (provided that their design is not too unusual). In this way, the identification of special ionospheric conditions has been used as a launch criterion for sounding rocket experiments, for example.

Particular files are reserved on the EISCAT computer system for both the analysis programs themselves, as well as the integrated data and results of the analysis. These exist in parallel so that

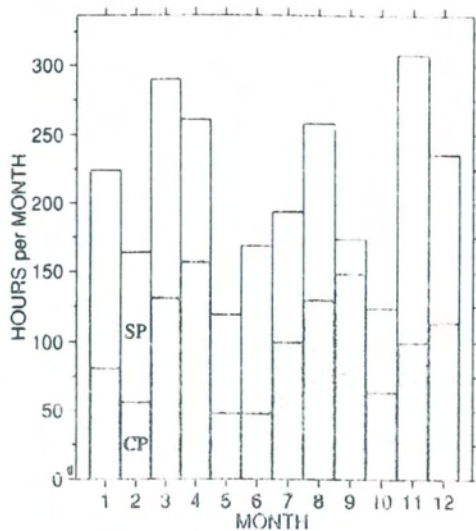


Fig. 16. Month-by-month distribution of CP and SP operations for 1988. Total number of hours is 2546.

analysis of common programs as well as of special experiments can be undertaken during busy operations periods.

Common Programme Data Analysis

Common Programmes CP-1, CP-2 and CP-3 were described in last year's Annual Report. The new common programs CP-4 and CP-5 were introduced in 1988. Each required special adaptations of the standard analysis. CP-4 was originally UK-POLA, a two-position beam swinging experiment looking at a low elevation far to the north, and differs from other Common Programmes in that it takes identical measurements on six channels. In the processing of these data, each of the six channels is analysed individually, as well as the average of them all. The results from combining all six channels are statistically the most accurate, but by including the results from the individual channels also, the possibility exists to examine the data for consistency among the channels.

CP-5 (originally a special French experiment) is a scanning CP-1-H pulse scheme, with pointing geometry taken from CP-3-F (but excluding the most extreme positions). The extra time gained

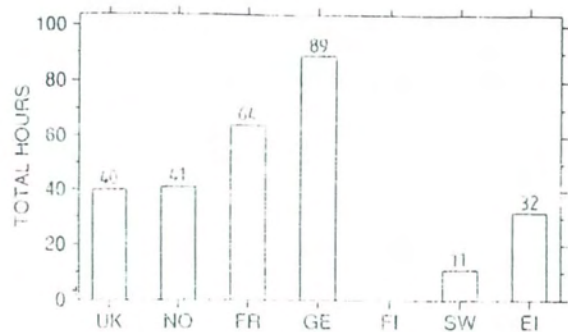


Fig. 17. Distribution of VHF experiment time among the Associates for 1988. Total number of hours is 277.

from omitting some of the CP-3 positions is spent in a longer dwell in the field-aligned position (10 minutes), during which time the remote sites are able to scan down to the E-region and back, allowing the possibility of neutral wind determinations. A special feature introduced into the CP-5 analysis (or rather, into the post-integration of the raw data), was to synchronise the Tromsø integration periods with the remote site scanning while the Tromsø beam was stationary in the field-aligned position.

A new version of CP-3 (version 'F') was introduced in 1988. The design of this experiment is very similar to CP-3-E, the only differences being in the radar duty cycle and post-detection filter widths. Common Programme 2 continued with version 'D', first run in November 1986 and Common Programme 1 remained as version 'H', also introduced at the end of 1986. An example of results from a continuous 4 day operation of CP-1-H from March 1988 is shown in Fig. 18.

World Day Operations

Besides providing the Associates with results from common programs, EISCAT also sends copies of results from Incoherent Scatter Coordinated Observation Days ("world days") to the NCAR radar data base in Boulder, USA. EISCAT operated on all 26 world days in 1988, and results from all these experiments have been sent to NCAR. This is

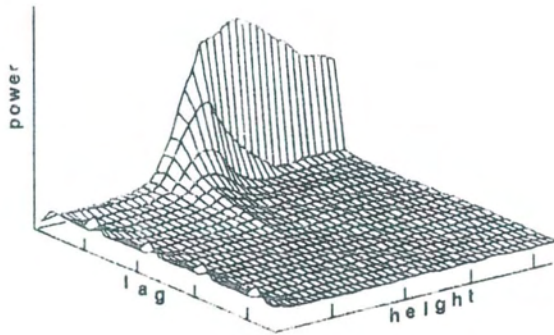


Fig. 19a. One raw GEN-11 data dump integrated for 20 minutes is shown. The real part of the ACF is plotted as a function of lag and height in arbitrary power scale. The data dump covers altitudes from 70 to 113 km and lag numbers from 0 to 21 with lag increment 2.222 ms. Due to range ambiguities lag 0 values appear low compared with other lags. The small distortions in other lags are most clearly seen as a ridge located at lag 5 for higher heights.

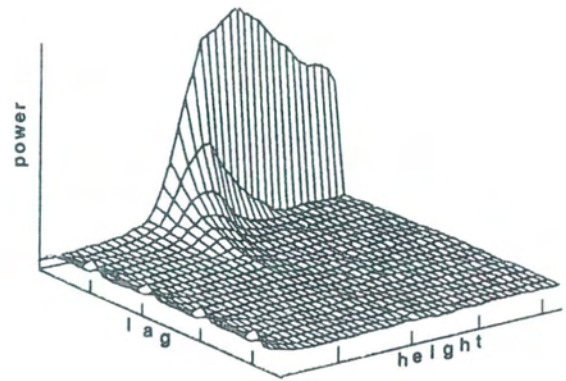


Fig. 19b. The same data dump after range ambiguity correction is shown. At each height the ACF has a clean exponential form as is expected for D-region plasma. Lag 0 fits well to this behaviour. Above about 100 km lag 1 disappears in contrast with the raw data and the ridge at lag 5 flattens. At the lowest heights there is still left a contribution from the ambiguities due to clutter from ground.

indicated by (3) in the remarks column of Table 2, which also gives additional information concerning analysis of Common Programme data from 1988.

New techniques in data analysis

a) Method of determination of electric fields

A method has been proposed to determine the perpendicular components of the ion velocity (and hence of the perpendicular electric field) from EISCAT tristatic measurements, in which an additional constraint on the parallel velocity is introduced in order to take into account the knowledge that the parallel ion velocity is small. This procedure removes some artificial features due to unfavourable tristatic geometries, in particular at the southernmost or northernmost positions of meridian scans. (Caudal and Blanc, 1988).

b) Range ambiguity corrections for GEN-11 experiments

GEN-11 is a commonly used experiment scheme for investigations of the lowest part of the ionosphere, between about 70 and 90 km altitude, and is also planned to be used as part of the VHF common program experiments from 1989. Although designed to suppress most potential noise contamination sources, the measurement algorithm itself produces ambiguities in the raw data. A scheme for correcting these ambiguities has recently been developed, Fig. 19 (Pollari, E. Turunen, Huuskonen, T. Turunen, The effect of range ambiguities on analysis of EISCAT VHF common mode experiment for D-region research).

Common Programmes in 1988

START Y-MM-DD HH	END MM-DD HH	EXPT	ANALYSIS COMPLETED YY-MM	TAPE MAILED YY-MM	TAPE NUMBER YYMMDD	APPROX HOURS T K S	REMARKS

1988							

88-01-12 09UT	01-16 09UT	CP-4-A	88-01	88-03	880112	88 85 85	2),3),5
88-02-09 11UT	02-11 15UT	CP-3-E	88-02	88-03	880112	48 47 47	2)
88-03-08 09UT	03-09 20UT	CP-3-E	88-03	88-07	880308	35 34 34	
88-03-16 09UT	03-20 09UT	CP-1-H	88-04	88-07	880308	96 94 96	3)
88-04-05 08UT	04-07 06UT	CP-1-H	88-04	88-07	880405	46 46 46	
88-04-11 08UT	04-13 08UT	CP-2-D	88-04	88-07	880405	48 48 48	3),5)
88-04-25 10UT	04-27 22UT	CP-3-F	88-11	88-11	880413	61 59 61	
88-05-03 08UT	05-04 08UT	CP-1-H	88-05	88-11	880503	24 23 24	
88-05-10 10UT	05-11 08UT	CP-3-F	88-11	88-11	880503	23 22 22	
88-06-13 08UT	06-15 08UT	CP-2-D	88-06	88-11	880503	48 48 48	3,5)
88-07-12 08UT	07-14 22UT	CP-3-F	88-07	88-12	880614	62 61 60	3)
88-07-26 08UT	07-27 22UT	CP-1-H	88-07	88-12	880726	38 38 38	
88-08-09 08UT	08-10 08UT	CP-2-D	88-08	88-12	880726	24 24 24	
88-08-16 08UT	08-18 22UT	CP-2-D	88-08	88-12	880816	65 65 65	5)
88-08-30 08UT	09-01 22UT	CP-1-H	88-09	88-12	880818	62 62 62	
88-09-06 08UT	09-07 22UT	CP-1-H	88-09	89-02	880906	38 38 38	
88-09-12 11UT	09-14 22UT	CP-3-F	88-09	89-02	880906	60 59 59	3)
88-09-20 08UT	09-21 08UT	CP-1-H	88-09	89-02	880906	0 24 24	
88-10-25 10UT	10-27 10UT	CP-3-F	89-01	89-02	881025	47 47 47	
88-10-27 15UT	10-27 23UT	CP-1-H	89-01	89-02	881025	7 7 7	
88-11-09 09UT	11-10 23UT	CP-3-F	88-11	89-02	881025	38 36 36	3)
88-11-15 09UT	11-17 07UT	CP-2-D	88-11	89-02	881115	39 39 39	
88-12-05 13UT	12-10 08UT	CP-5-A	89-02	89-03	881205114114114		3),5)

Table 2. EISCAT common program operations and data analysis overview for 1988. Approximate hours refer to available good data and the remarks are as follows: 2) Some data gaps due to low signal levels; 3) World day operation - results also sent to NCAR; 5) Results fill more than one 2400 feet tape at 1600 bpi.

THE EISCAT COMMON AND UNUSUAL PROGRAMMES

The Common Programme CP-1 uses a fixed transmitting antenna, pointing along the geomagnetic field direction. The 3-dimensional plasma velocity and anisotropy in other parameters are measured by means of the remote receiving stations in Kiruna and Sodankylä. The CP-1 experiment is capable to provide results with very good time resolution along a fixed ionospheric profile, and is suitable for the study of substorm phenomena and here particularly the aurora when conditions may change rapidly. On longer time scales, CP-1 measurements also allow studies of diurnal changes (eg. atmospheric tides) and seasonal variations. Eventually solar cycle variability will be able to be studied when sufficient data have been collected.

The Common Programme CP-2 is designed to obtain measurements from a small, rapid transmitter antenna scan. One aim of this is to identify wavelike phenomena with length- and time-scales comparable with, or larger than, the scan (few tens km and ten or more minutes). The present version consists of a scan of four antenna positions covered in six minutes. The first three measurements in the scan form a triangle from the transmitter vertical to the south to south-east, and the final direction is parallel to the geomagnetic fieldline. The remote site antennas are directed so that the 3-dimensional velocities in the E- and F-region can be measured.

The Common Programme CP-3 covers a 10 degree wide range of latitudes in a 17 position scan up to 74° N in a 30 minute cycle. The measurements are made in the magnetic meridian plane through Tromsø and Kiruna, and the remote site antennas in Kiruna and Sodankylä follow the transmitter beam in the F-region.

The Common Programme CP-4 covers the latitudes up to almost 80° N, corresponding to about 77° invariant latitude. This Common Programme is particularly suited to study the plasma convection pattern at very high latitudes.

The Common Programme CP-5 has been designed in order to suit the objectives of lower thermosphere coupling. It combines a latitudinal scanning of the ionosphere with a vertical sounding along the magnetic field line of Tromsø in the middle of the antenna scan. The main purpose of this experiment is to observe the dynamics of the neutral atmosphere while exploring simultaneously the electrodynamic environment.

Unusual Programmes had been developed, UP-1 for D-region observations, UP-2 for auroral arc and related studies and UP-3 for high resolution sporadic E-layer studies. These Unusual Programmes can be started at very short notice when suitable geophysical conditions exist.

Whereas these CP and UP experiments are run with the UHF radar, two Common Programmes CP-6 and CP-7 to observe the low and the high altitudes with the VHF radar are in preparation and a high latitude programme is planned.

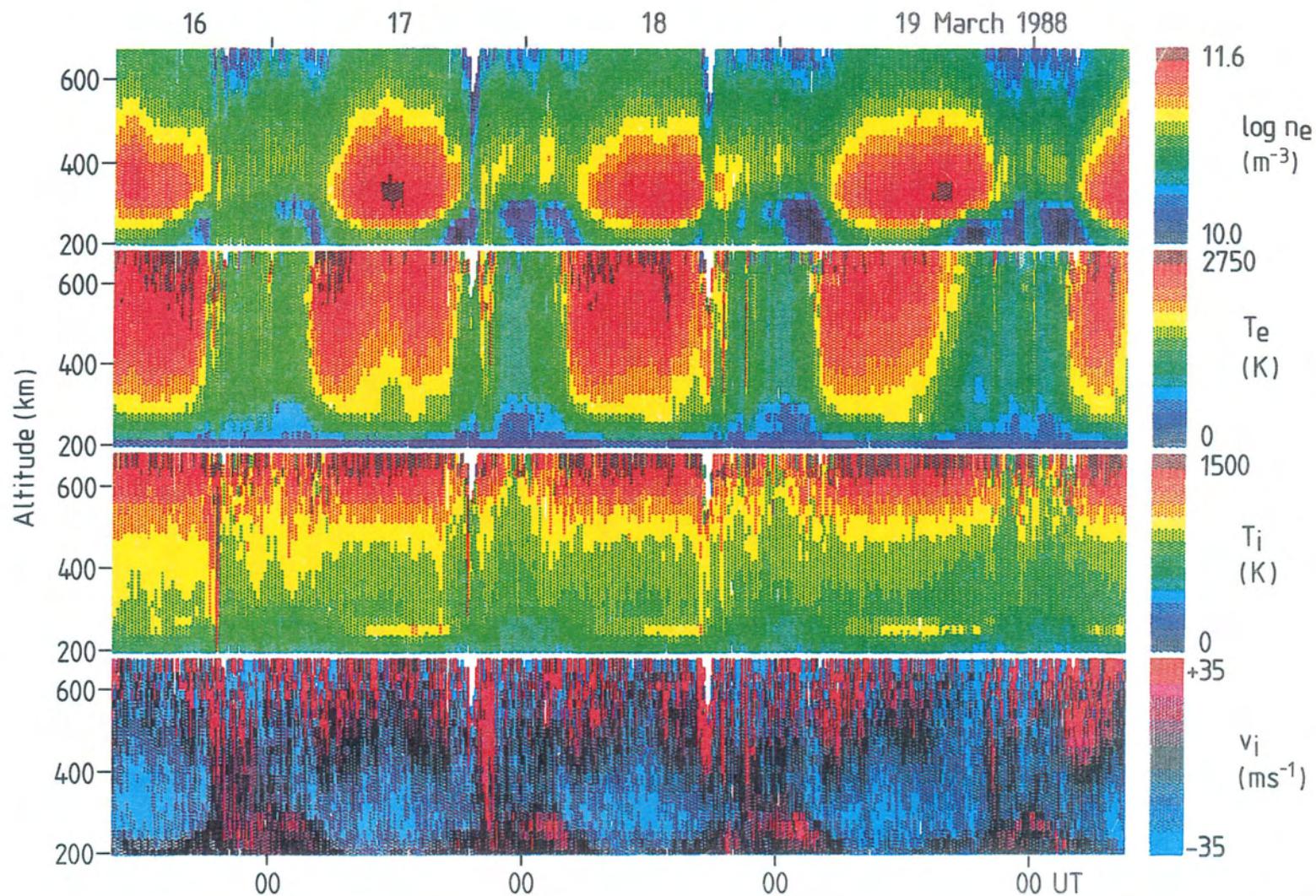


Fig. 18. Colour representation of long pulse results from an operation of Common Programme CP-1-H from 9 UT on 16 March to 9 UT on 20 March 1988. These results show the variations of (top to bottom) electron density ($\log n_e$), electron temperature (T_e), ion temperature (T_i) and line-of-sight ion drift velocity (v_i) between 135 and 600 km altitude. Experiment CP-1-H also provides multipulse measurements from E-region heights and two sets of power profiles in this scheme with the transmitting antenna pointed permanently along the geomagnetic field direction.

SCIENTIFIC RESEARCH

It has become a standard that the EISCAT Annual Reports contain a summary of the achieved scientific results. In the course of the years the scientific work has continuously increased, very new phenomena have been detected and the deepness of the scientific investigations has revealed an improved understanding of several of the observed phenomena. It becomes more and more taxing and complex to trace all the science which is coming out from EISCAT. This for instance is reflected in the increasing amount of published papers, which is displayed in the graph on page 9. The following pages should provide a comprehensive overview and explanation of the scientific results and of the ongoing work. As usual, results which were published in papers or reports are indicated in brackets by the names of the authors, followed by the numeral of the year (1988). Results achieved in 1988 and being prepared for publication are signified in brackets by the names of the co-investigators and the title of the research topic or manuscript, if available.

Observations of the D-region and the Mesosphere

The EISCAT UHF and VHF radars had been designed to study the D-region by means of incoherent scatter from the collision-dominated lower ionosphere. This allows to measure profiles of electron density and ion velocity. Under certain circumstances the ratio of collision frequency and temperature as well as the ratio of negative ion and electron density and the mean positive ion mass can be deduced. Early results of these investigations with the EISCAT radars are described in the Annual Reports of former years.

Incoherent scatter studies

Almost all of these first investigations were done with the well-known GEN-11

radar program, which applies the pulse-to-pulse method and Barker coding. The analyses of the acquired data rely on the application of the theory of collision-dominated incoherent scatter without being affected by the coherent echoes, which are discussed in the later paragraphs of this chapter on D-region and mesosphere studies with EISCAT.

Results of recent analyses of UHF radar data show good agreement of collision frequency and temperature with models as well as large ion masses at the mesopause altitude in summer (E. Turunen, Collis and T. Turunen, 1988). Further evidence for the existence of heavy positive ions at the summer arctic mesopause was found from other UHF radar observations (Collis, T. Turunen and E. Turunen, 1988). The ion mass can be used to deduce the Schmidt number, which is the ratio of kinematic viscosity to electron diffusion coefficient and is an indicator of the extension of the electron gas fluctuations to scales shorter than those of the neutral turbulence. At mesopause altitudes Schmidt numbers of about unity were found in winter, whereas they were increasing to about five in summer (C. Hall and Brekke, 1988). A persistent ledge of increasing negative ion to electron density ratio was found at about 80 km in winter (C. Hall, Devlin, Brekke and Hargreaves, 1988). Gravity wave observations in a bistatic UHF operation between Tromsø and Kiruna showed an apparent relation between the variability of the spectrum width and vertical velocity which could indicate that temperature and density are modified by vertical displacements due to gravity waves in the mesosphere (Hoppe and Hansen, 1988). Both UHF and VHF radars were used simultaneously, running cooperative programmes, for the first time to study the propagation of disturbances (Howarth, Hargreaves and Burns, Comparison between D-region disturbance velocities measured by EISCAT UHF and VHF and riometers).

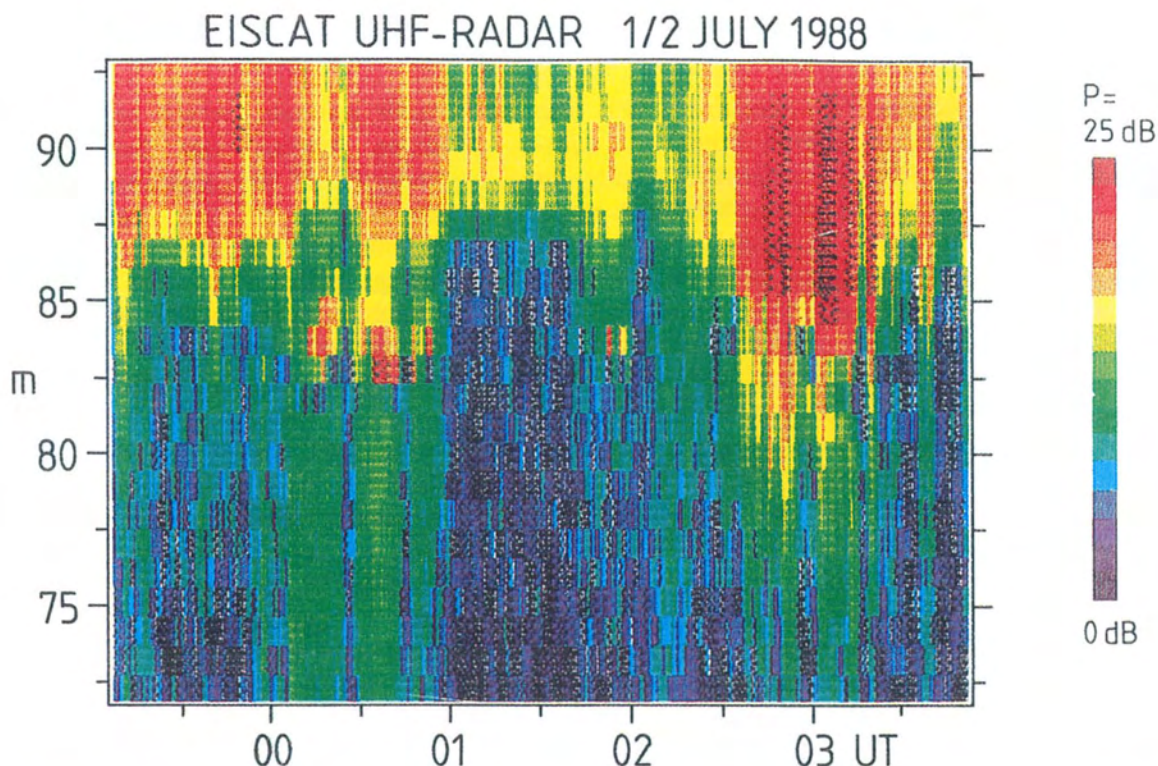


Fig. 20. Raw power plot of lower ionospheric echoes detected with the UHF radar. Displayed is the uncorrected and non-calibrated magnitude of the autocorrelation function at the pseudo-zero lag of the applied GEN-11 radar program. This raw power profile, which is not corrected for code-sidelobes, constitutes a first order estimate of the non-range adjusted electron density profile.

Polar Mesosphere Summer Echoes

In addition to the incoherent scatter echoes, which are analyzed to yield the mentioned standard parameters, strong coherent echoes were first detected with the VHF radar in summer 1987 and detailed studies were done in summer 1988 (see cover photo). Although such echoes were seen with 50 MHz radars at other locations many years earlier, their later detection with the EISCAT 224 MHz radar was surprising (Hoppe, Hall and Röttger, 1988). It was regarded as impossible that these coherent echoes, which were so far assumed to be caused by neutral air turbulence generating electron density irregularities, should be detectable at the short radar wavelengths of EISCAT.

It was even more surprising that such coherent echoes were now also detected with the UHF radar on the much shorter

wavelength of 32 cm. In Fig. 20 the raw power plot of these first events is shown. It is clearly noticeable that, besides the enhancements of incoherent scatter power due to particle precipitation extending over wide altitude ranges, strong echo power occurs occasionally from very localized altitudes around 85 km. Since at the same time the 46.9 MHz radar CUPRI (Cornell University Portable Radar Interferometer) was operated from Tromsø and detected similar kinds of echoes, we are convinced that these EISCAT UHF radar observations show real events (Röttger, Rietveld, La Hoz, T.Hall, Kelley and Swartz, Polar mesosphere summer echoes observed with the EISCAT 933 MHz radar and the CUPRI 46.9 MHz radar). Because of their unique features, we call these "coherent" echoes, which are seen on 46.9 MHz, 224 MHz and 933 MHz, the Polar Mesosphere Summer Echoes: "PMSE".

Scattering Mechanisms, Relations to Atmospheric Gravity Waves and Noctilucent Clouds

Detailed investigations of these echoes and their relation to electron density depletions, observed by rockets, were done during the MAC/SINE campaign in summer 1987 (Kelley, Ulwick, Inhester, Röttger and T. Hall: Comparison of rocket and radar data during the EISCAT-salvo of MAC/SINE). It is obvious that these strong PMSE cannot be caused by conventional incoherent scatter, and it also has to be excluded that electron density irregularities generated directly by clear air turbulence cause the scattering (Röttger, La Hoz, Kelley, Hoppe and C.Hall, 1988). One possibility was proposed earlier, namely that the irregular fluctuations in the electron gas are extending to much smaller scales than those in the neutral gas, if there are heavy cluster ions in the cold mesopause region proposed by Kelley, Farley and Röttger in 1987. Other possibilities have also been suggested that the recombination between heavy positive ions and electrons is faster in localized cold areas which causes irregularity structures and thus coherent scatter. Charge separation and accumulation could also happen in the presence of heavy cluster ions, vertical motions and electric fields (Röttger and La Hoz: The fine-structure of Doppler spectra of PMSE observed with the EISCAT 224 MHz radar). There is no doubt that these processes are related to the cold environment of the polar mesopause in summer, and the chosen name "PMSE" of these phenomena detected by the radars appears to be well justified. It is still an open question how these PMSE relate to the other well-known phenomena in the polar mesopause in summer, namely the noctilucent clouds, NLC, as well as how their relation is to atmospheric gravity waves and turbulence in the mesosphere. Concurrent observations of NLC and PMSE, which were done in a short campaign in August 1988, did not prove a relation between these two phenomena (Taylor, van Eyken, Rishbeth, G.Witt, N.Witt and Clilverd,

Simultaneous observations of noctilucent clouds and polar mesospheric radar echoes: Evidence for non-correlation). Relations of certain structures in PMSE power variations to vertical motions due to atmospheric gravity waves, however, was recently found (Williams, van Eyken, C.Hall and Röttger, Modulations in the PMSE and associated gravity waves).

Interferometry and Split-Beam Operation

Particular operations of EISCAT and other instrumentation took place in a special campaign PMSE88 in summer 1988 to study PMSE and to develop special radar programs, which allowed for the first time to apply the complementary code to the EISCAT radar, yielding a best altitude resolution of 150 meters (La Hoz, Röttger, Rietveld, Wannberg and Franke, The status and planned developments of EISCAT in mesosphere and D-region experiments). To study spatial structures for the first time also the spatial interferometry was applied making use of the two receiving antennas of the EISCAT VHF radar (La Hoz, Röttger and Franke, Spatial interferometer measurements with the EISCAT VHF radar) and also the frequency domain interferometry was implemented by transmitting on two frequency channels (Franke, La Hoz, Röttger and Liu, Frequency domain interferometry of PMSE). Also split-beam operations were done with the VHF radar to investigate inclination of structures, which showed slopes of a few degrees from horizontal (van Eyken, C.Hall and Williams, A determination of the orientation of a polar mesosphere summer echo layer using EISCAT as a dual beam radar). It is evident that these newly implemented techniques comprise a major step-forward in the VHF radar operation and have also substantially improved our understanding of the PMSE, although the reason for the generation of the electron density irregularities is still unknown.

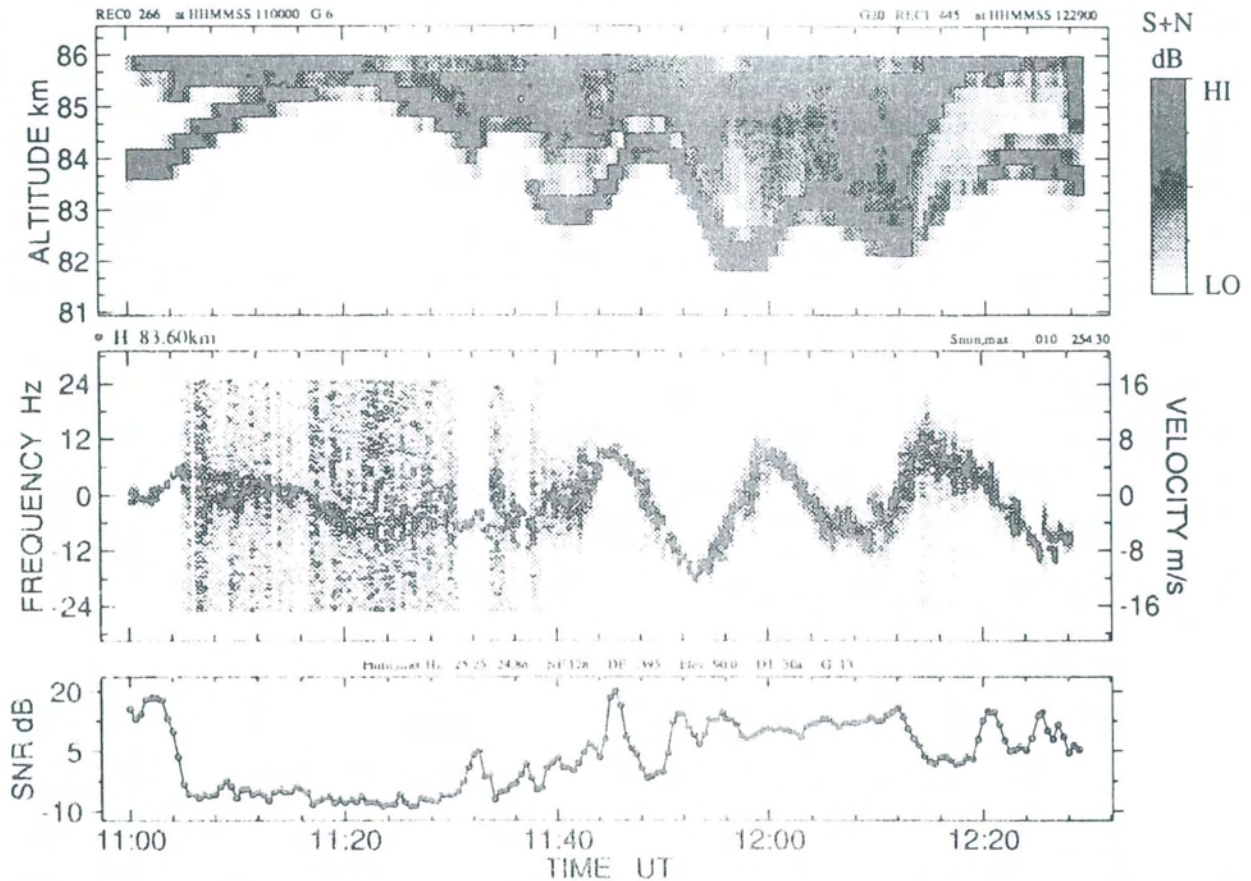


Fig. 21. Self-normalized height time intensity plot (upper panel) showing the spatial and temporal variations of PMSE, and the corresponding spectrogram at a fixed height (center panel) showing the variations of the vertical velocity deduced from the Doppler spectrum. In the lower panel the signal-to-noise ratio (SNR) is shown for the self-normalized spectrogram. (*each time slice is individually normalized to the maximum echo power in that interval).

Structure and Dynamics of PMSE

The high time- and altitude-resolution experiments, which were performed in 1988, have gained more detailed insight into the structure and dynamics of the PMSE. The cover diagram of this Annual Report shows an impressive example of the dynamical behaviour of the PMSE: One clearly notices the relatively thin structures of echo power, which are lifted upwards and downward. The simultaneously measured Doppler frequency is often consistent with this vertical motion. It is therefore concluded that the scattering entities which cause these echoes

could be considered as passive tracers of dynamical processes in the mesosphere (La Hoz, Röttger and Franke, Dynamic spectra of PMSE measured by EISCAT at 224 MHz; Hoppe, Fritts, Reid, Czechowsky, Ruster, C.Hall and Hansen, Multiple-frequency studies of the high-latitude summer mesosphere: Implication for scattering processes).

To support this suggestion, in Fig. 21 a wave event is shown of a case of a thin layer on the bottom of a very wide region of echo structures. A three-cycle oscillation with period of about 16 minutes is clearly seen, which is on top of a longer

period oscillation of about 40 minutes. The middle panel contains the dynamic spectra at a fixed altitude of 83.6 km which cuts approximately through the middle of the oscillating layer in the upper panel. We notice that the vertical velocity varies between -12 ms^{-1} and $+8 \text{ ms}^{-1}$ and the layer altitude varies accordingly by several kilometers. The altitude and velocity oscillations are exactly coherent and the velocity is lagging the altitude by a 90 degree phase difference. This example proves that a gravity wave with large amplitude was lifting an existing layer of passive scatterers (La Hoz, Röttger and Franke, Dynamic spectra of PMSE measured by EISCAT at 224 MHz).

It is also noted from the vertical advection of layers that the lifetime of particular scattering layers is at least several minutes. Spectra of the vertical velocities show prevalent periods of 20 minutes, and there is also evidence for Doppler shifting of gravity waves due to horizontal winds. The waves show surprisingly little vertical phase progression over 5-10 km. This could mean that the vertical wavelengths are very long, or perhaps that the waves are ducted in the mesopause region (Fritts, Hoppe et al., A study of vertical motions near the high latitude summer mesopause).

Another example of the intensity of PMSE corresponding to a maximum upward velocity was observed and explained to be due to adiabatic cooling during the upward lift by a large-amplitude gravity wave, which causes heavy ion clustering and consequently the suggested extension of the inertial subrange in the electron gas (Williams, van Eyken, C.Hall and Röttger, Modulations in the polar mesosphere summer echoes and associated atmospheric gravity waves).

Gravity Wave Breaking and Steepening

This relation of vertical velocity and echo power is not always as clear as described, but it in any case proves that gravity

waves play a relevant role in the variability of the PMSE. It is frequently assumed that gravity waves break into turbulence in the mesosphere and thereby deposit a major amount of momentum to achieve a geostrophical balance of the global wind system. The PMSE observations by EISCAT allow to investigate the gravity wave and turbulence dynamics in great detail to check this primary assumption. According to conventional theory of gravity wave instability and turbulence, PMSE should show widened Doppler spectra due to turbulence bursts in certain phases of the wave oscillations and the power also increase in those phases. These evidences can occasionally be proved by the EISCAT observations, as we for instance see in Fig. 21. It is noticed on the other hand that the spectrum, which frequently is extremely narrow (corresponding to velocity fluctuations of much less than one ms^{-1}), can suddenly widen as displayed by the burst of spectrum widening in Fig. 22 or the jump in frequency as displayed in Fig. 23. Taking this spectrum widening as an indication of enhanced velocity fluctuations due to turbulence, a clear relation to wave breaking cannot be seen in these data. It is also obvious that the existence of PMSE is not at all related to the occurrence of this turbulence burst. This supports our idea that the scattering process of PMSE and the originating electron density structures are not only related to neutral air turbulence (Röttger and La Hoz, Fine-structure of Doppler spectra and signal power characteristics of PMSE observed with the EISCAT 224 MHz radar). Support for this suggestion is given by other observations during the MAC/SINE campaign that apparently the Doppler spectrum width does not increase with the echo power (Hoppe et al., Multiple frequency studies of the high latitude summer mesosphere, Implications for scattering processes). Also the absolute reflectivity of PMSE cannot be explained by the conventional scattering mechanisms (Röttger and La Hoz, Fine structure of Doppler spectra of PMSE observed with the EISCAT VHF radar).

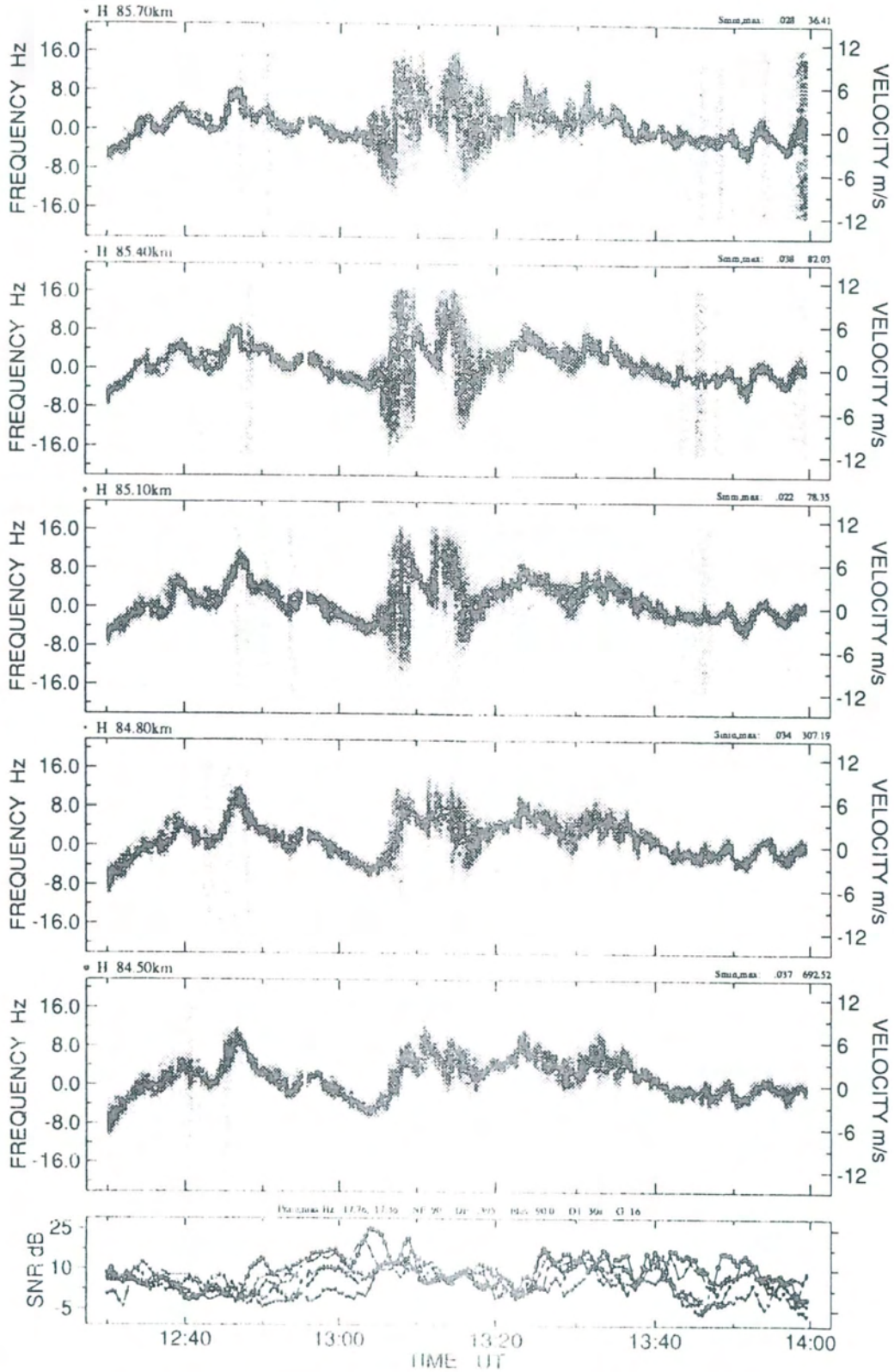


Fig. 22. Self-normalized spectrograms for the altitudes 84.5 km to 85.7 km, showing sudden bursts of spectrum widening in the upper altitudes. In the lower panel the corresponding SNR is drawn, which is used to self-normalize the spectrograms.

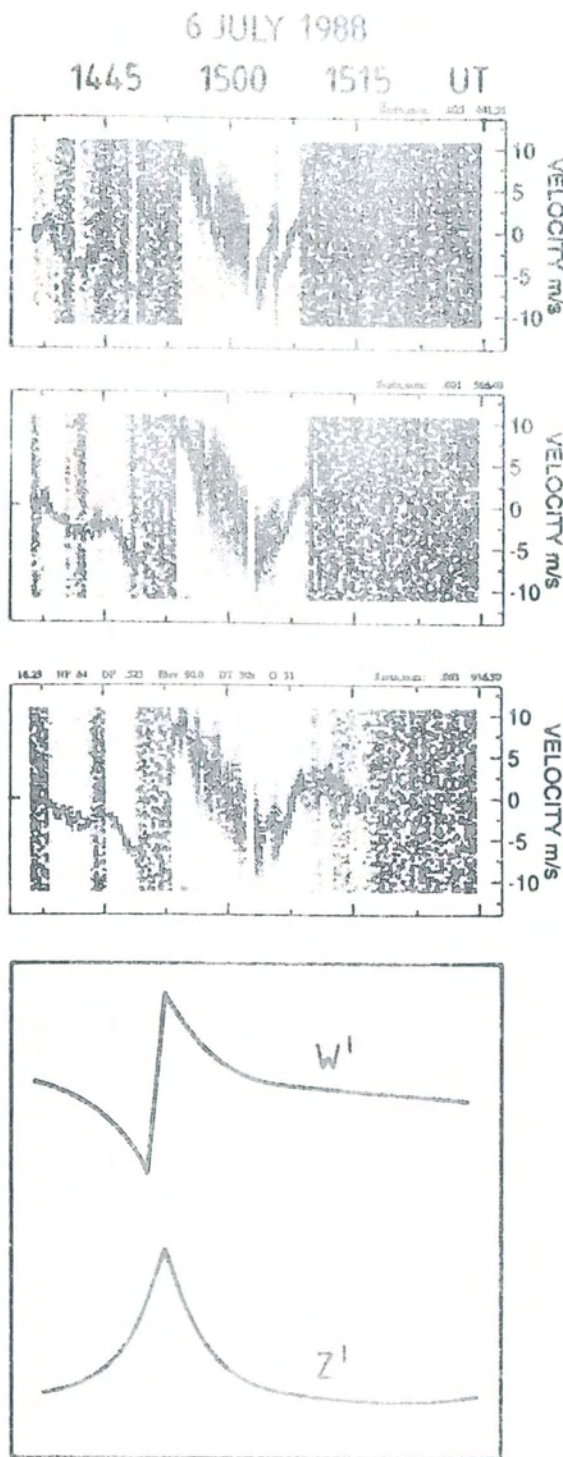


Fig. 23. Self-normalized spectrograms of altitudes 84.50 km, 84.80 km and 85.10 km, measured with an altitude resolution of 150 m. The frequency jump around 14.50 UT is due to a steepened gravity wave. Another jump is seen at 85.10 km around 15:08 UT. In the lower panels the corresponding model of velocity w' and vertical displacement z' is shown.

Further proof for the suggestion, that not only neutral turbulence is involved in the PMSE generation, is given by the observations of PMSE with the UHF radar on 933 MHz. In Fig. 24 a sample set of Doppler spectra, averaged over only 10 seconds, is shown. It is very evident, that these spectra are much narrower as well as much stronger than the spectra of incoherent scatter echoes (e.g., those in the lowest gate 82.6 km). These spectra indicate some enhancement of neutral air turbulence, but this is not sufficient to explain the high echo power on 933 MHz. In addition to searching for a new scattering mechanism, we have now also to be careful in the interpretation of incoherent scatter echoes from the D-region, which could occasionally be contaminated by these "coherent" PMSE on 224 MHz as well as on 933 MHz (Röttger, Rietveld, La Hoz, T.Hall, Kelley, Swartz, Polar mesosphere summer echoes observed with the EISCAT 933 MHz radar and the CUPRI 46.9 MHz radar).

The conventional "breaking of waves into turbulence" is not immediately exploitable by the EISCAT observations so far. Instead the oscillations seen during PMSE conditions are often non-sinusoidal and triangular shaped or sawtooth-like. These features are taken as an indication of gravity wave steepening and tilting, which was proved by model computations (see Fig. 23). This again shows that gravity wave breaking into turbulence is not as frequent an effect as may be needed to explain the PMSE by conventional turbulence theory. It also may have an implication on the supposition that gravity waves lose their energy and momentum in the mesosphere solely by breaking into turbulence. It is presumed that other effects, such as non-linear steepening, wave-wave interaction and other damping mechanisms have to be seriously considered (Röttger, La Hoz, Franke and Liu, Gravity wave steepening and tilting detected in high-resolution Doppler spectra of PMSE observed with the EISCAT 224 MHz radar).

EISCAT UHF RADAR
2 JULY 1988

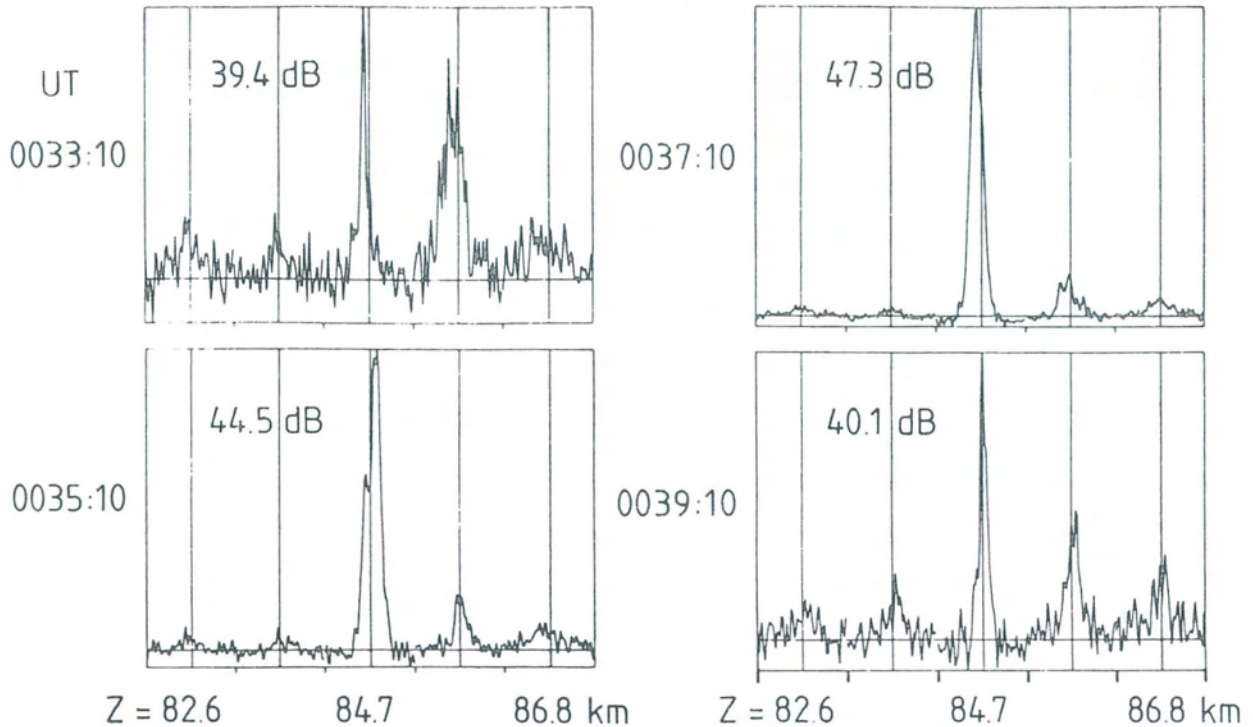


Fig. 24. Sample groups of 5 spectra measured within 10 sec integration time with the UHF radar between 82.6 km and 86.8 km. The strong and narrow spectra at 84.7 km are related to polar mesosphere summer echoes. The usual incoherent scatter is for instance seen in the range gate at 82.6 km.

Relation to Magnetic Disturbances

It was also suggested that the PMSE could be related to magnetic disturbances (Rishbeth, van Eyken, Lanchester, T. Turunen, Röttger, C. Hall and Hoppe, 1988). Although the mechanism behind such a relation is at present unknown, one could expect that the enhanced particle precipitation and electric fields and currents during magnetic storms should also affect the middle atmosphere and thus the polar mesosphere summer echoes.

Future Studies of the Polar Middle Atmosphere

EISCAT is at the most suitable location and has the most appropriate capabilities to study, simultaneously, the effects of coupling from the magnetosphere and ionosphere (above) and from the troposphere and middle atmosphere (below).

This coupling takes place uniquely in the high latitude mesosphere and two seasons of EISCAT investigations of PMSE, and the structure, dynamics and aeronomy of the region, have already allowed critical tests of the theories concerning gravity wave dissipation at mesospheric altitudes, demonstrated that conventional theories were much too elementary, allowed the proposal that PMSE echoes are mainly due to enhanced neutral air turbulence may be discounted and suggested a wealth of further possible mechanisms which will be investigated in future experiments. They have also demonstrated the superb capabilities of EISCAT's VHF radar, even at low power and duty cycle, and fostered the development of new observing techniques which capitalise on the system's unique features. One may confidently look forward to further exciting developments in this, previously unexpected, area.

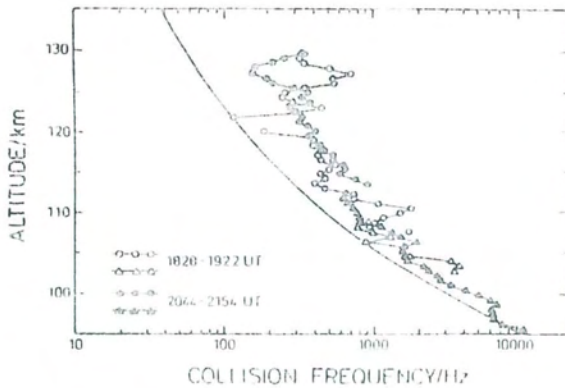


Fig. 25. Ion-neutral collision frequency determined from the spectral method (triangles) and from the new method (circles) compared with the MSIS 86 model (line) for 26 August 1985.

E-region Studies

The E-region above EISCAT is often disturbed by phenomena associated with the highly variable particle precipitation and electric field patterns found at auroral latitudes. Results of such studies are presented later in this report. It is also important to measure and understand the properties of the undisturbed, or average, ionosphere, and EISCAT continues to contribute in this area. Examples of such topics include ion-neutral collision frequency, layer phenomena and thermal and electrical properties.

Ion-neutral collision frequency

An alternative method for determining the ion-neutral collision frequency in the E-region has been developed. The method is based on observations of plasma drift caused by electric field and horizontal neutral wind. Height profiles of two ion velocity components are measured sequentially with vertical and eastward tilted beam directions, and electric field is obtained from the tristatic data. The two velocity components of the neutral wind can then be eliminated from the momentum equation and the collision frequency can be solved from the resulting cubic equation. The method is applicable at higher altitudes than the conventional

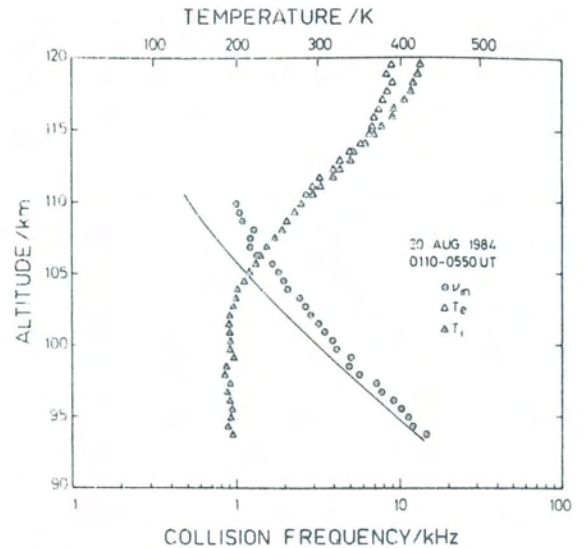


Fig. 26. Ion temperature (open triangles), electron temperature (filled triangles) and ion neutral collision frequency (circles) from a 280-min post-integration of EISCAT data, and MSIS-86 collision frequencies (line).

method using the spectral shape. Fig. 25 shows results obtained on 26 August 1985. The open and filled dots indicate collision frequencies for two different time periods, solved from the cubic equation, and the triangles are results given by the conventional spectral analysis. The continuous line is the MSIS 1986 model atmosphere. The results show a considerable disagreement with the model. A similar disagreement in August has been observed previously below 110 km using the conventional method, whereas in February, for instance, a better agreement has been found (Nygrén et al., A method for measuring ion-neutral collision frequency, using sequential ion velocity measurements in two directions).

Ion-neutral collision frequencies and ion and electron temperatures were studied in the altitude range of 94-120 km using high range resolution (600 m) EISCAT UHF radar measurements. The data base consisted of 100 hours of such measurements made in February, July and August 1984 and August 1985. The observed collision frequencies (at 94-110 km) agreed with other EISCAT results and indicated that the MSIS-86 model gives

correct collision frequencies in July but underestimates them in February and August. The temperature observations (below 110 km) agreed with the MSIS-86 model in general but the observed event-to-event variation was larger than that predicted by the model. At 110-120 km the ion temperature was found to exceed the electron temperature. Fig. 26 shows an example of the best results (20 August 1984). Their good quality is evident and the statistical errors of the results are small, as determined from the scatter of points in the profiles. The collision frequencies deduced from the MSIS-86 model (solid line) are smaller than the observed ones, especially above 100 km, (A. Huuskonen, High resolution observations of the collision frequency and temperatures with the EISCAT UHF radar).

Sporadic E-layers

Studies of sporadic E-layers continued using the purpose-written GEN-6B programme. On 12 July 1987 the afternoon wave of the semidiurnal atmospheric tide was observed to generate a descending Es layer. Oscillations in the inferred neutral wind were observed and the short-term changes in the velocity profiles were closely linked with the rise and fall of the layer and with its fading, reappearing and eventual disappearance, destroyed apparently by a strong upward motion, Fig. 27 (Lanchester et al., Wave activity, F1-layer disturbance and a sporadic E layer over EISCAT).

Although sporadic E-layers are very narrow in altitude extent, they are usually intense enough to be detected by general-purpose experiments such as the common programs. Several summertime events in common program data have been observed to descend in altitude in response to the semi-diurnal tide and to disappear rapidly upwards with the onset of electric field activity. Layer formation was shown to be more consistent with the altitude variation of the zonal component rather than the meridional component of

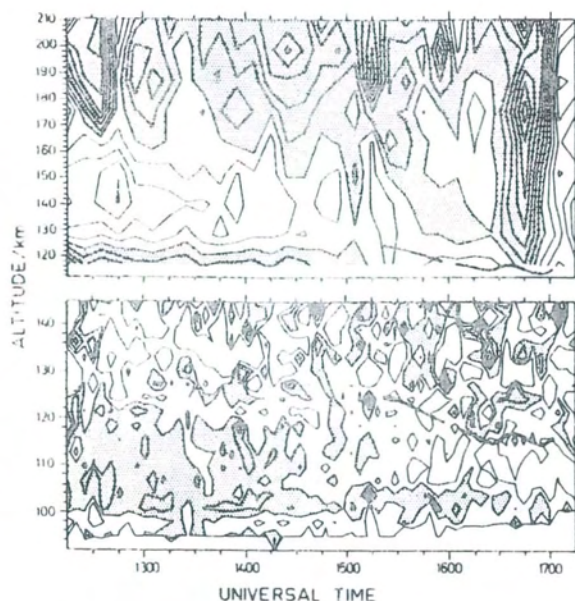


Fig. 27. Contours of field-aligned ion velocity from long pulse (top) and multipulse (bottom) measurements, vs height and time, July 12, 1987. The shaded regions indicate downward velocities. The thick curves mark the position of the sporadic E-layer: within the region of upward velocity and below a velocity null.

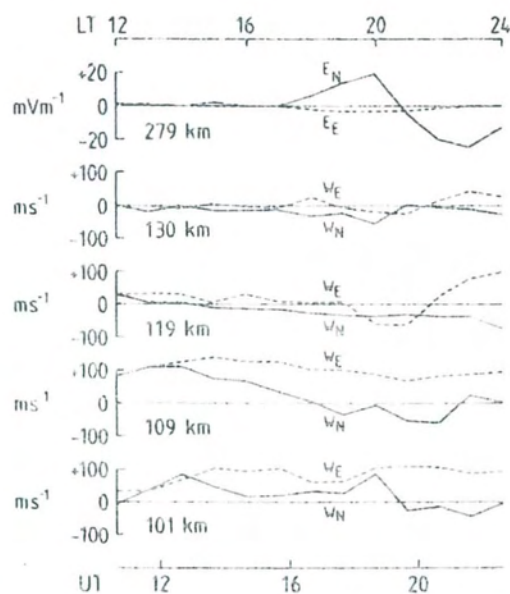


Fig. 28. Electric fields and neutral winds on the afternoon of 16 June 1987, from CP-1-H data. A sporadic E-layer descended from 116 to 112 km between 14 and 16 UT, with eastward winds below it and still air above it. It disappeared rapidly upwards after 16 UT as the electric field increased.

the horizontal neutral wind, Fig. 28 (Collis, Multi-experiment studies of summertime sporadic E-layers using EISCAT).

Another example of a sporadic E-layer detected in common program data was found to correlate with a simultaneous sudden sodium layer observed by lidar on Andøya. An explanation in terms of formation by the action of a long-period gravity wave in the presence of initially low concentrations of metallic atoms and ions has been developed. The mechanism proposed depends on vertical neutral motion associated with the gravity wave and is thus distinctly different from the usual explanation of sporadic E-layers in

terms of a shear in horizontal winds, which in any case would be extremely ineffective at such low altitudes at high latitude. (Kirkwood and Collis, Gravity wave generation of simultaneous auroral sporadic E-layers and sudden sodium layers).

Enhanced electron density layers below 100 km altitude.

Some layers of electron density in the lowest part of the ionosphere are considerably broader than typical sporadic E-layers. Their enigma is that they are narrower than would be produced by normal solar radiation or typical particle

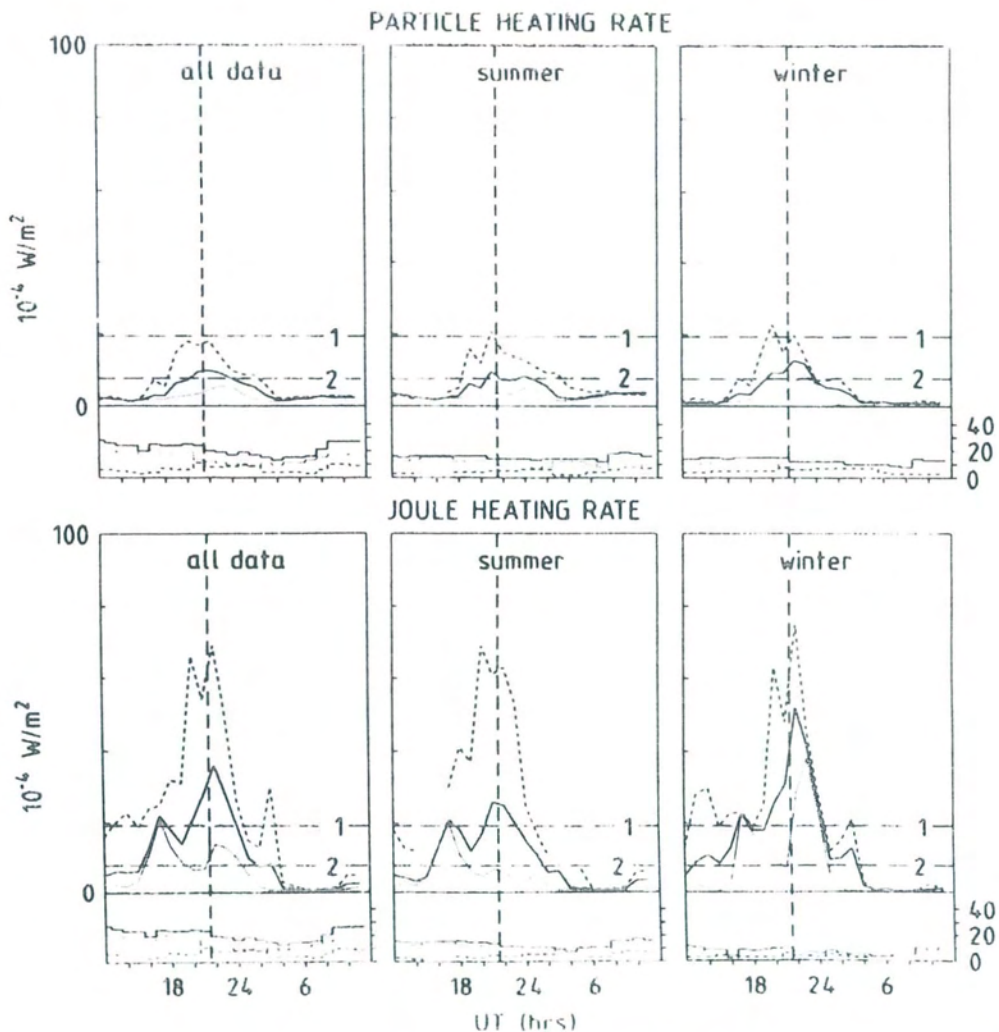


Fig. 29. Averaged values of the particle and the Joule heating rates versus time. The dashed curves correspond to high, the dotted curves to low activity, and the full lines characterize an average of both. The vertical dashed line indicates the local magnetic midnight. In the lower part of each panel the number of samples is plotted.

precipitation, and often narrower than would be produced by mono-energetic particle precipitation (Collis and Kirkwood, Discrete layers of D-region ionisation in the high-latitude ionosphere). One subset of these layers occurs during winter daytime and persists for many hours. In some cases the inferred ion temperature in the layer is lower than expected, indicating that the assumption of a mixture of NO^+ and O_2^+ ions in the data analysis is incorrect and that some ions of mass heavier than 30.5 amu are present.

Ionospheric conductivities

From the observations of two coordinated experiments (18 October 1983 and 30 August 1983) between the two radars EISCAT and STARE, the ionospheric height-integrated Hall conductivities have been derived by two methods: (i) from EISCAT electron density measurement associated with a model of neutral atmosphere, (ii) from STARE electric field measurements combined with ground-based magnetic field observations. The comparison shows that the conductivities deduced from EISCAT, with the standard assumption of identical

electron and ion temperatures, are underestimated for high electric fields. A better agreement is found for electron temperatures greater than ion temperatures in the E-region, following the statistical model developed by Nielsen and Schlegel in 1983. This increase of electron temperature is suggested to result from the heating produced by short-scale waves in the E-region. (Nielsen, Senior and Lühr, 1988).

Electron energy budget in the auroral ionosphere

Both the solar illumination and the auroral precipitation of magnetospheric electrons act as sources of ionization and of heating for ionospheric electrons. The heating rate at each altitude in the ionosphere was theoretically computed by using a program for electron vertical transport developed by Strickland and Oran in 1978 and adjusted by Lilensten, Kofman and Wisenberg. This energy input is progressively degraded in the ionosphere due to cooling processes by elastic and inelastic collisions and transported by thermal conduction. Simultaneous observations of approximately conjugated vertical profiles of iono-

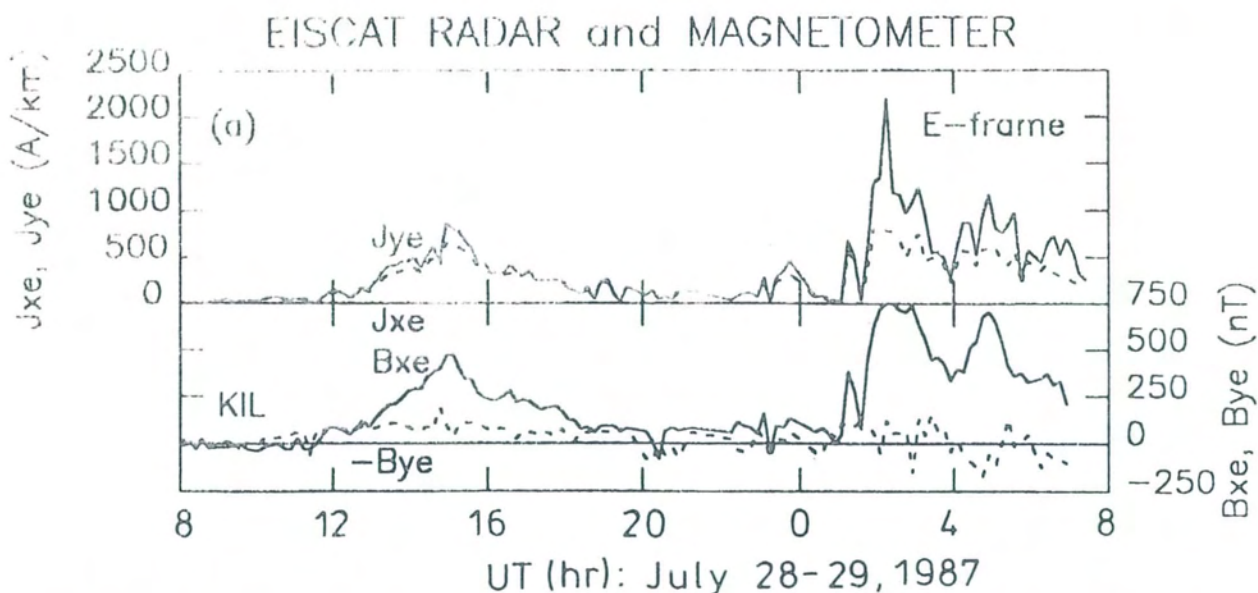


Fig. 30. Correlation between the ionospheric current and the magnetic field variations on the ground of the station Kilpisjärvi of the EISCAT magnetometer cross in the E-frame. J_{ye} is the Hall current, J_{xe} the Pedersen current.

MARCH 23 1988 ERRRIS DATA

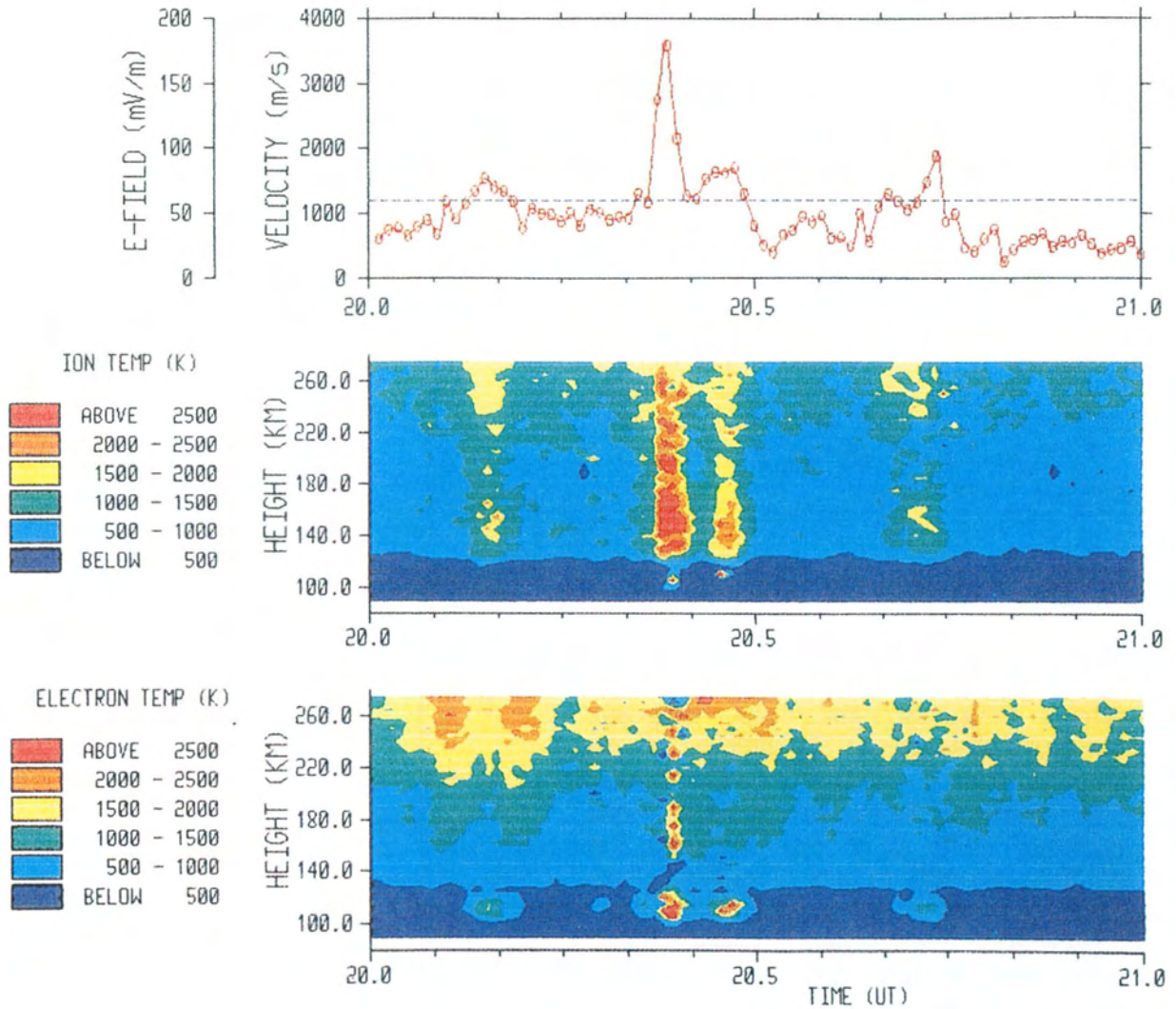


Fig. 31. Electric field, ion temperature, electron temperature and $\underline{E} \times \underline{B}$ drift versus time measured by EISCAT on 21 March 1988 during the ERRRIS campaign.

spheric parameters by EISCAT and of precipitation fluxes at the top of the ionosphere by the Viking satellite permit to test the theoretical computations against observations and to analyse the role of the heating, cooling and thermal conduction in the energy budget for ionospheric electrons (Lilensten, Fontaine, Kofman, Lathuillère and Eliasson).

Momentum and heat input into the auroral E-region

A statistical study of the Joule heating, the particle heating and the Lorentz-force

have been performed using CP-1 data from 21 experiments between February 1985 and December 1986. The Joule heating has been calculated using the electron density in the E-region and the vector of the electric field, the particle heating from the electron density and the electron temperature, and the Lorentz force from the current vector. All these parameters are provided by EISCAT, only the neutral density (from MSIS 86) and the magnetic field (from IGRF 85) have been taken from models. The three quantities in question have been calculated for the height range 90-170 km and then integrated in order to obtain height-

integrated values. These were averaged over the time of the day, separately for summer and winter, and for high ($K_p \geq 3$) and low ($K_p < 3$) activity. Fig. 29 shows the results for particle and Joule heating rates. Generally the average Joule heating rates are twice as high as the average particle heating rates, both quantities exhibit their maximum around magnetic midnight. The Joule heating rates show also a second maximum in the afternoon. The knowledge of average values of these quantities is important for quantitative energy balance and gravity wave calculations. (Natorf, Schlegel and Wernik, Momentum and heat input into the high latitude ionosphere derived from EISCAT measurements.)

E-region currents

Quantitative correlation studies have been made of the relationship between ionospheric currents and the magnetic variation observed at 7 stations of the EISCAT magnetometer cross. The current was estimated from the F-region drift velocity vector ($\underline{E} \times \underline{B}$ drift) and the electron density in the E-region, both obtained from CP-1 experiments. Two coordinate systems called B- and E-frame were used in this study. The B-frame represents the ordinary geomagnetic coordinates where the geomagnetic north and east are taken as x- and y-axis. In the E-frame, the direction of the horizontal electric field is parallel to the x-axis, so that the Hall current always flows in the positive y-direction and the Pedersen current in the positive x-direction. The results show that the correlation is highest in the E-frame between the Hall current and the northward, and lowest for the Pedersen current and the eastward component of the magnetic field. This is documented in Fig. 30. The contribution of the Hall current to the magnetic field variation on the ground is $0.48 \text{ nT}\cdot\text{km}\cdot\text{A}^{-1}$, the contribution of the Pedersen current only $0.16 \text{ nT}\cdot\text{km}\cdot\text{A}^{-1}$. Both values apply when the center of the current is above the radar station. With the help of the

EISCAT magnetometer cross it was possible to localize the maximum of the current quite accurately in latitude and also to infer some latitudinal and longitudinal structure. (Araki, Schlegel and Lühr, Geomagnetic effects of the Hall and Pedersen current flowing in the auroral ionosphere.)

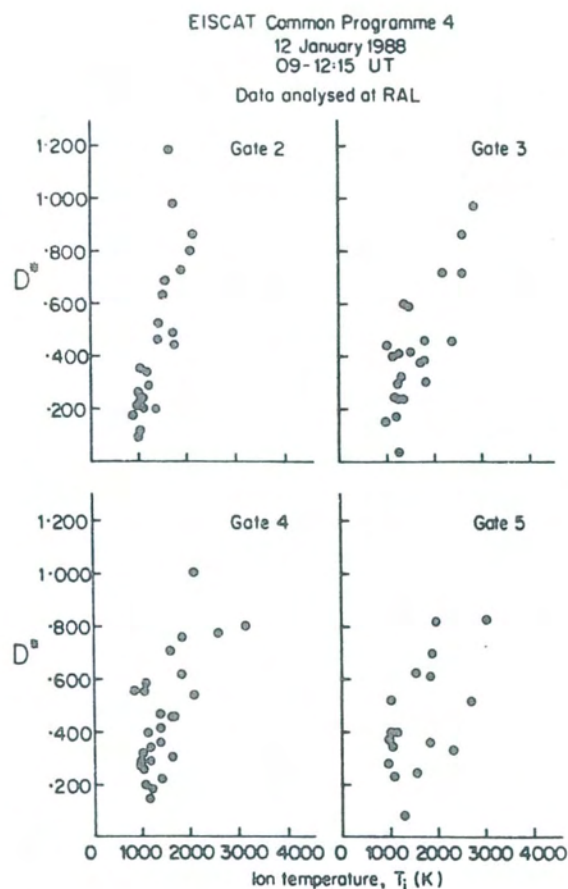


Fig. 32. Common Programme 4 observations of non-Maxwellian ion velocity distribution functions, which determine the ion temperatures. The fitted distribution function shape distortion parameter, D^* , is shown as a function of true ion temperature for the strong flow period shown in Fig. 43. The D^* -values show that the distribution function varies between Maxwellian ($D^*=0$) and the threshold of a toroidal form ($D^*=1.25$).

Ionospheric dynamics

From the use of CP-1 data the studies of the ionospheric conductivities have continued. A close relationship between the electron energy input and the Hall-to-Pedersen conductance ratio has been demonstrated. A study is in progress on the relationship between the ionospheric current densities and the electric and magnetic field fluctuations. Coordinated EISCAT-neutral E-region wind measurements and partial reflection drift measurements have been performed from which general agreement is found with respect to direction, while the magnitudes of the winds from the EISCAT measurements are larger than those derived from the E-region drift experiment (Brekke et al.).

E- and F-region Irregularities

Elevated E-region electron temperatures by wave heating

Heating of the electron gas in the high latitude E-region by unstable plasma waves caused by the modified two stream (Farley-Buneman) plasma instability has been studied with EISCAT.

During the ERRRIS (E-region rocket and radar instability study) rocket campaign EISCAT observations have been coordinated with rocket launches aimed at the in-situ investigations of the above mentioned instability. Using the alternating code technique very high quality data have been collected with EISCAT during March and April 1988, showing several cases of elevated E-region electron temperature up to more than 1000 K (Fig. 31). These enhancements can be quantitatively interpreted with current models of the wave heating process. (Hägström, Jones, Robinson, Schlegel, Interpretation of enhanced electron temperatures measured in the auroral E-region during the ERRRIS campaign.)

The electron temperature behaviour in the high latitude E-region has also been reviewed in general. The average picture

that emerges suggests that the electron temperature response is correlated with the electric field amplitude and inversely correlated with the ambient electron density. Higher resolution studies also show that departures from this average picture may be of great importance. As the electron temperature profile itself can vary, the magnitude of the temperatures can change substantially on a scale of a minute or less, and the correlations with the electric fields may be blurred. From the theoretical point of view, the proposed arguments favour the plasma wave heating as a probable explanation for the observations (Saint-Maurice, Kofman and Kluzek).

Non-Maxwellian ion velocity distributions

The study of non-Maxwellian plasma effects with EISCAT has been continued in 1988. It turned out that these effects are much more important and occur more frequently than previously assumed. This has been shown by model predictions (Farmer et al. 1988). The major problem to solve is the analysis of EISCAT data in the presence of such distributions. Former algorithms have been based on the evaluation of a triple integral at each step of the fitting procedure which requires considerable computer time and is thus unsuitable for the processing of large amounts of data (Moorcroft and Schlegel, 1988.)

A new algorithm using a series expansion avoids these difficulties since several of the required quantities need only be computed once for a given radar geometry (Suvanto, 1988). The routine has proven to be suitable to fit large amounts of EISCAT data (Fig. 32). It was further shown that the analysis must be restricted to 1-dimensional ion temperatures for aspect angles less than about 30°, 3-dimensional temperature estimates show large errors in this case (Fig. 33). The ion temperature and composition can be derived without errors and assumptions about the velocity distribution function of the ions only at an aspect angle of 54.7°.

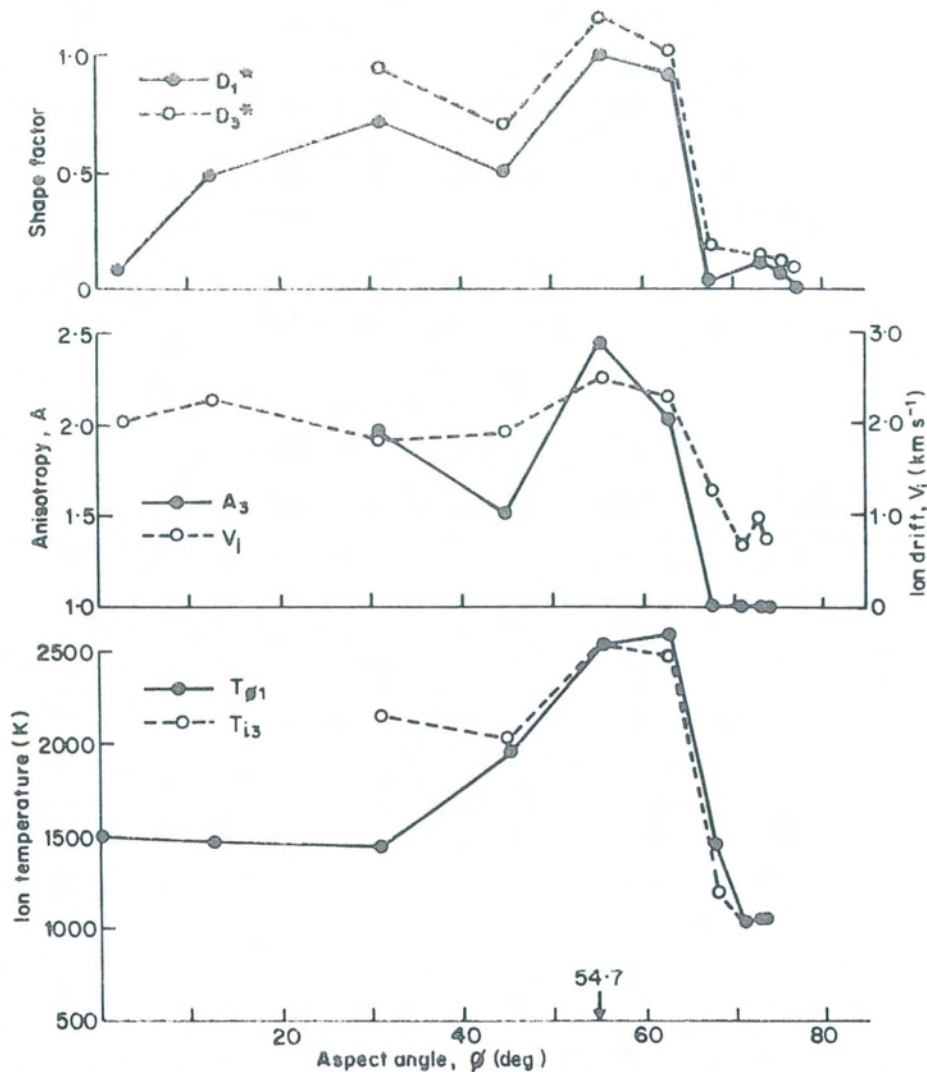


Fig. 33. Non-Maxwellian analysis of Common Programme 3 observations at 1300-1320 UT on 27 August 1986, covering a range of aspect angles ϕ . For aspect angles less than 63° , the ion drift v_i is roughly constant, but the shape distortion functions from 1- and 3-dimensional analysis (D_1^* and D_3^* , respectively) and the corresponding temperatures $T_{\phi 1}$, T_{i3} , as well as the ion temperature anisotropy $A_3 = T_{\perp}/T_{\parallel}$, determined from the 3-dimensional fit show a marked aspect angle dependence.

The observed features of the velocity distribution are remarkably close to predictions made by Monte-Carlo simulations which allow for more than one ion-neutral interaction mechanism. (Lockwood and Winser, 1988, Lockwood et al., 1988.)

A considerable source of error in the correct interpretation of the measured spectra is the uncertainty of the ion composition. The range of electric fields (given as D' , the ratio of the ion-neutral differential velocity to the neutral thermal velocity) where the assumption of a bi-

Maxwellian ion distribution is good enough to provide reliable measurements of T_e , n_e and the ion temperature anisotropy, is a function of the principal ion population and the direction of the radar beam relative to the magnetic field (Fig. 34). If two ion species have to be taken into account, the usual assumption of the same temperature for both species breaks down, since the two species do not have the same ion temperature anisotropy. One main conclusion is that the validity domain of the standard analysis as a function of D' and the aspect angle, is smaller for a mixture of ions than for a

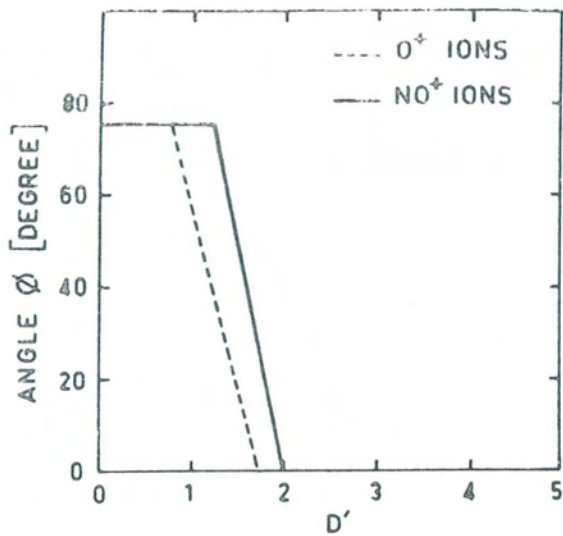


Fig. 34 Validity domain of a bi-Maxwellian velocity distribution for different ion species.

single ion plasma. It was also shown that the ion composition cannot be well estimated as soon as D' is greater than about 0.5 (corresponding to an electric field of 20 mV/m) for measurements along the magnetic field line (Hubert and Lathuillère).

Another important aspect of the non-Maxwellian effects is the influence of collisions. All the EISCAT studies made so far in this field are based on the limit of a zero collision rate. Using a relaxation collision model the effects of a non-zero ratio of ion-neutral collision frequency to ion gyro frequency have been investigated. It turned out that the incoherent scatter spectra are asymmetric in this case, thus leading to an uncertainty in the line of sight velocity estimate. Model calculations show that the true line of sight velocity and the estimate performed in the usual way by a fit to a symmetrical spectrum can differ considerably. The difference depends on the collision frequency, the electric field magnitude, the T_e/T_i ratio and the aspect angle. Fig. 35 shows an example (Cooper and Kohl, The simulation of asymmetric Thompson scatter spectra from a relaxation collision model.)

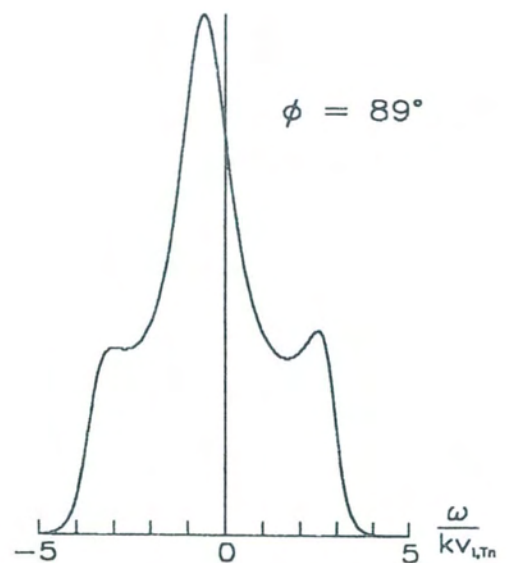
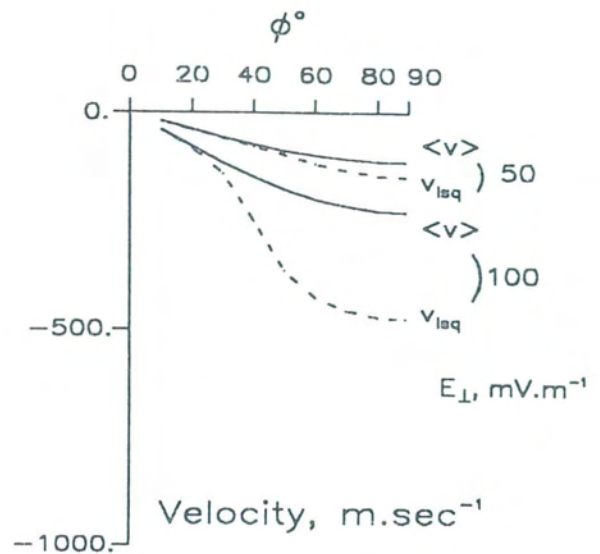


Fig. 35. Upper panel: The difference between the true line of sight velocity $\langle v \rangle$ and the velocity v_{lsq} , fitted in the usual way to a symmetrical spectrum as a function of aspect angle ϕ for electric fields of 50 and 100 mV/m. Lower panel: Example of an asymmetric spectrum in the presence of a 100 mV/m electric field. In both cases a ratio of collision frequency to gyro frequency of 0.1 was assumed.

F-region irregularities, Gyro-line, Plasma line

The morphology of F-region irregularities and the nature of their production mechanism have been examined from coordinated observations between EISCAT and EDIA, the HF radar based in France covering the southward part of the EISCAT meridian scans. During night hours, EDIA continuously detected small-scale irregularities in the F-region. Their location was not correlated with any large-scale horizontal density gradients measured by EISCAT at 350 km altitude, but with strong north-south gradients at 150/200 km altitude, indicating the equatorward boundary of particle precipitation. The examination of the different mechanisms of F-region irregularity production suggests that structured precipitation may be an important source of irregularities with scale lengths of about 100 m, which could cascade to small-scale irregularities by the universal drift mode. (Bourdillon and Fontaine, 1988.)

In June 1988 the first gyro line observations with the EISCAT VHF radar were made. The gyro line (also called "resonance line" and "whistler line" in the literature) corresponds to the electrostatic wave mode to $\approx \Omega \cos \alpha$ known to be present in the weakly magnetized ionospheric plasma (Ω is the electron gyro frequency and α is the angle between the direction of the wave vector and the magnetic field). The gyro line is very weak - even weaker than the plasma line - but the frequency offset is only marginally dependent on electron density and temperature so that the position of the line can be easily predicted and long integration times can be applied in the measurement. Favourable conditions for observing the line are obtained by looking with the VHF radar at a low elevation to the north. Fig. 36 shows gyro line returns from a 300 μ s pulse in the altitude region 100-200 km, detected at elevation angles of 30° and 45°. The experiment used a filter bank of 12.5 kHz filters. The figure shows the returns in two adjacent filters

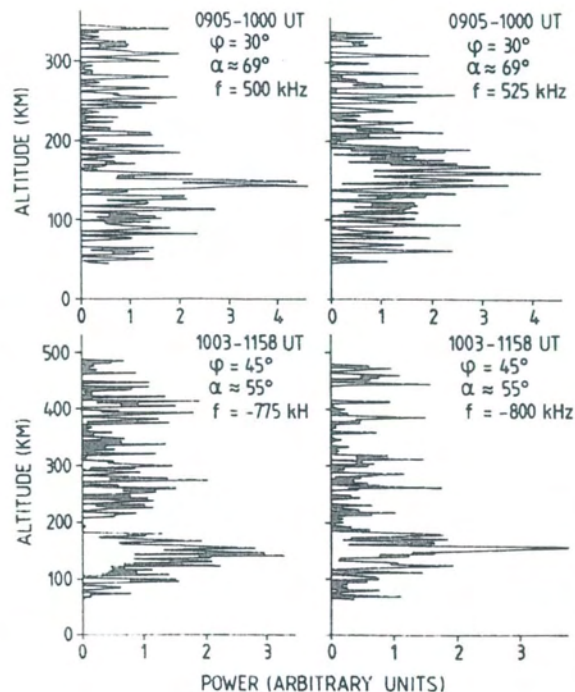


Fig. 36. Gyro line returns from a 300 μ s pulse measured on June 8, 1988 with the VHF radar at elevation angles of 30° and 45°. α is the aspect angle, f the frequency offset of the receiving filters.

with offsets of +500 and +525 kHz (upshifted line) and -775 and -800 kHz (downshifted line) for the 30° and 45° elevations, respectively. The transmitted peak power was 1.5 MW. The strong dependence of the gyro line offset on the magnetic field strength and direction can be used to map the geomagnetic field. The enhancement of the line in the presence of nonthermal electrons gives information of the intensity and energy distribution of electrons in a new energy regime. In the absence of nonthermal electrons the width of the gyro line is a sensitive measure of the electron temperature (Björnå, Hansen, Esjeholm).

Measurements of natural plasma lines started in 1987 with the EISCAT PLASMA-D experiment were continued in the summer season 1988. This experiment uses the CCD spectrum analyzer for the plasma line measurement and the

correlator for ion line ACFs. The observations have been used by Trondsen (1988) to estimate the UHF system constant. From a series of measurements an average value of $(1.18 \pm 0.05) \cdot 10^{19} \text{ m}^{-5} \text{ s}^{-1}$ was found which is in excellent agreement with the value in current use. The PLASMA-D data are also used to determine the ion composition in the F region by the method introduced by Björnå and Kirkwood (1988). A similar method can be applied to derive the ion-neutral collision frequency in the lower E-region. When the measured plasma line offset is incorporated in the least squares fitting procedure for the ion line ACF, the temperature/collision frequency ambiguity can be resolved. No assumption on the electron-to-ion temperature ratio is needed. Fig. 37 shows the altitude profile of ion-neutral collision frequency derived

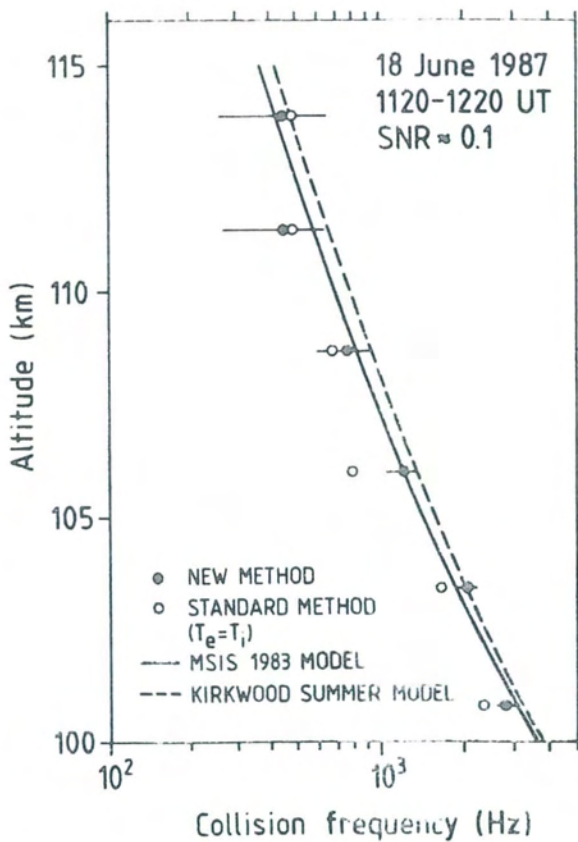


Fig. 37. Ion neutral collision frequency profile obtained with the ion line/plasma line method in comparison with values from models and from the standard analysis.

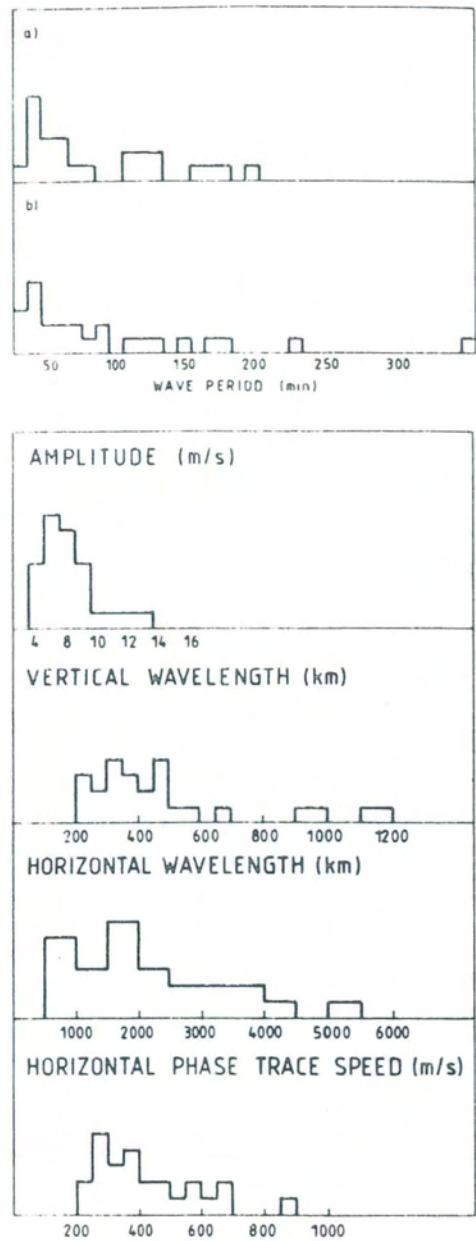


Fig. 38. Distribution of the parameters of the analyzed gravity waves. In the upper panel a) denotes the periods of the waves as they are observed, b) the Doppler-shifted periods.

by this method (solid circles) compared with values derived by the standard method assuming that the temperature ratio is unity (open circles), with MSIS 1983 model values (solid curve), and with the Kirkwood summer model (dashed curve) used by EISCAT (Björnå, Hansen, Fredriksen, Trondsen).

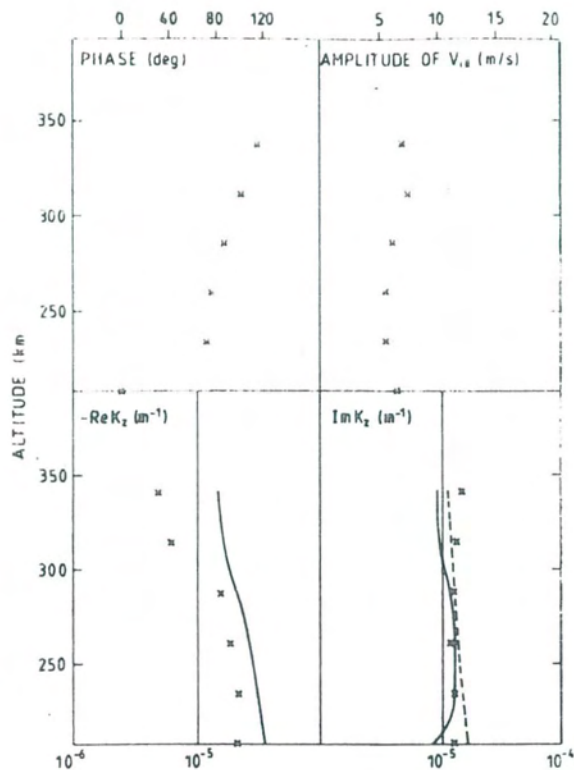


Fig. 39. Analysis of a single wave event on the 22 May 1985 between 07 and 09 UT. The crosses denote the experimental results, the full line the result calculated from Clarks dispersion relation. The dashed line characterizes the dissipation term $(2 \text{ scale height})^{-1}$.

TIDs and gravity waves

Wave-like fluctuations in the line of sight ion velocity measured with CP-1 have been interpreted in terms of gravity waves. The data were first screened for such wave-like events and these were then fitted to a sine wave $A \cdot \sin(\omega t + \theta)$. A , θ are height dependent quantities depending on the parameters of a true gravity wave, the vertical (complex) and horizontal wave number, the frequency and the phase, obtained from the linearized ion momentum and ion continuity equations. Also the meridional component of the neutral wind (estimated from EISCAT data) was taken into account. This method has the advantage that it

does not assume any dispersion relation of the waves. Data from 16 CP-1 experiments from November 1984 to December 1985 have been used. Fig. 38 shows the distributions of parameters of the analyzed waves. The fitted parameters have also been compared with corresponding results obtained from a dispersion relation for planar waves taking thermal conduction, viscosity and ion drag into account. Fig. 39 summarizes this comparison for one single wave in terms of phase, amplitude and the complex vertical wave number, all as a function of altitude. In general the agreement between theoretical and experimental results is satisfactory. (Natorf, Schlegel and Wernik, Incoherent scatter observations of TIDs in the auroral zone.)

In another study, travelling ionospheric disturbances (TID) behaviour was investigated using CP-2 data. With the help of the maximum entropy method the wave periods have been calculated for a three hour data window which was moved through the whole 24 hours data set in steps of 6 minutes. The resulting sonogram, Fig. 40 shows an example, exhibits traces of all occurring TIDs. These sonograms have been used to select certain TID events which have then been studied in more detail, particularly with respect to the propagation direction of the waves. For this purpose six phase trace speeds were calculated from the corresponding CP-2 data at one particular altitude and all four positions. These velocities can be fitted to give the horizontal k -vector of the waves. (Mauelshagen and Schlegel, Propagation direction of TIDs in the auroral zone.)

Energy and momentum can be transferred from the auroral ionosphere to the mid- and low-latitude thermosphere by the generation, propagation and dissipation of atmospheric gravity waves.

A very good example was observed by EISCAT during the first Worldwide Atmospheric Gravity-Wave Study in 1985. The source in the auroral zone was identified with a Westward Travelling

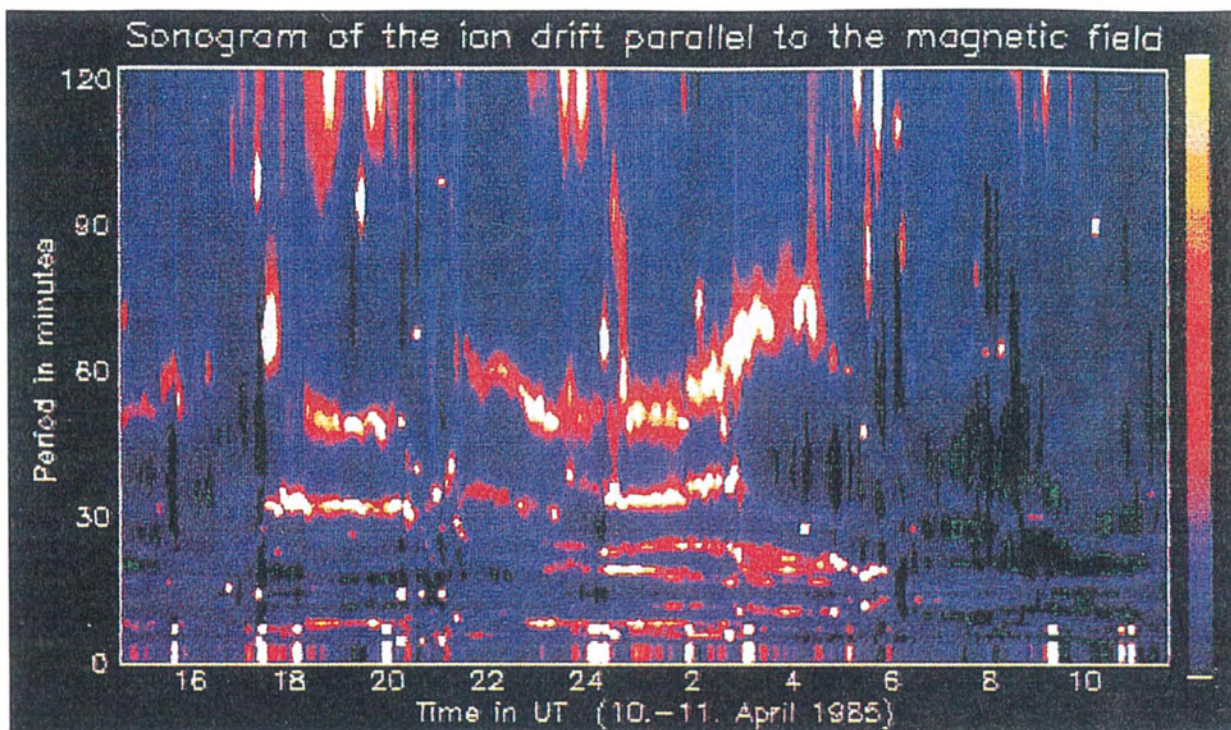


Fig. 40. Sonogram of travelling ionospheric disturbances.

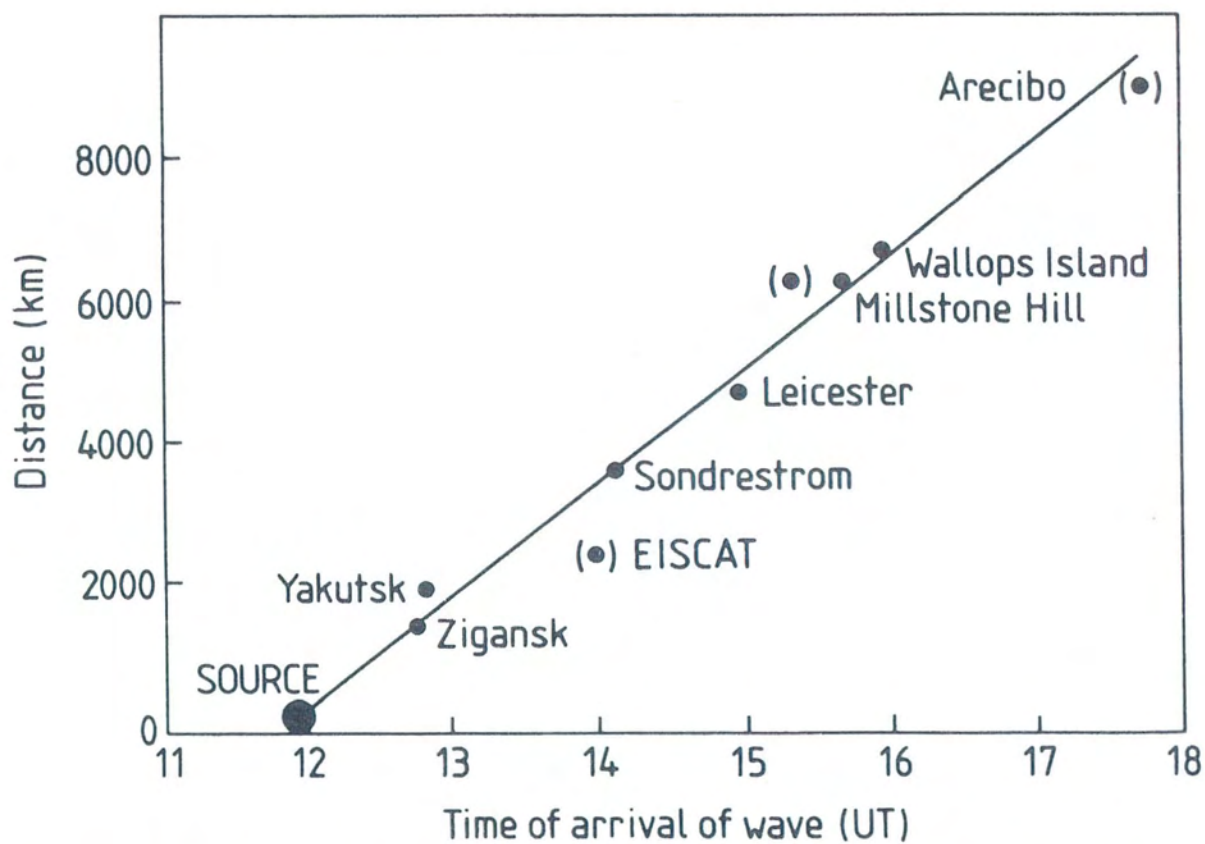


Fig. 41. Time of arrival on October 18, 1985 of a gravity wave with a period in the range of 50-80 minutes, plotted against distance from the proposed source.

Surge, observed at the conjugate point by the Dynamics Explorer satellite. The wave generated was observed close to the source by ionosondes at Ziganak and Yakutsk, and at greater distances by the incoherent-scatter radars at EISCAT, Sondrestrom and Millstone Hill, by an HF-Doppler radar in the UK, and by an ionosonde at Wallops Island. The vertical wavelengths determined at EISCAT and Sondrestrom were in good agreement (370 km) and the derived values of horizontal wavelength (1640 km) and phase velocity (430 ms^{-1}) were consistent with the measurements of the HF-Doppler radar, and also with the time-of-travel of the wave from the source to the different stations, Fig. 41 (Williams, Observation of atmospheric gravity waves with incoherent scatter radar).

Ionosphere-Thermosphere Coupling

The flow of energy and momentum from the magnetosphere to the auroral ionosphere in turn affects the neutral thermosphere. The momentum of the convecting ionosphere is transferred to the neutral atmosphere, while on a local scale energy and momentum inputs due to Joule and particle heating and Lorentz forcing can generate atmospheric gravity waves.

The coupling between the ionised and neutral components of the upper atmosphere has been monitored directly by using EISCAT in conjunction with Fabry-Perot interferometers operated at Kiruna and Kilpisjärvi by University College London, and on Svalbard by the University of Alaska. The results demonstrated that methods for deriving thermospheric winds from incoherent scatter data alone can have larger than expected errors at high latitudes and must be used with caution.

At the same time the measurements made by FPIs are complicated by the fact that on many days the wind pattern at EISCAT latitudes has large variations on a scale smaller than the horizontal field of view of the interferometer so that the

usual monostatic FPI techniques cannot be used to give reliable neutral winds.

However, some comparisons have been attempted, and the initial results indicate that the used estimate of the O-O^+ collision frequency may be too large by a factor of about 3 (Winser et al., 1988; Farmer et al., Ion-neutral dynamics: Comparing Fabry-Perot measurements of neutral winds with those derived from radar observations).

High latitude ionospheric modelling

The coupling between ionosphere and thermosphere is also the subject of advanced modelling work carried out at University College London and at the University of Sheffield. Plasma densities observed by EISCAT have been compared with the predictions of the coupled model.

Two approaches have been used. In the first, the convection pattern and its variations are matched to data from EISCAT and other radars and then used to model plasma densities. This approach has been successful, even under conditions when the convection pattern is changing rapidly with time, provided the convection pattern is known with some degree of confidence (Quegan et al., 1988).

The other approach has been to average statistically the large dataset accrued by EISCAT and compare these average values with predictions from the numerical model run to "steady-state" in the diurnal sense with fixed input conditions. This approach has verified the value of the model as it accurately predicts the average levels of ionisation and the gross features of the diurnal variations in both summer and winter for moderate-to-high solar activity levels. There are differences between predicted and measured height profiles of ionisation - particularly in the variations in the F-region peak height - but these may be minor "tuning" differences.

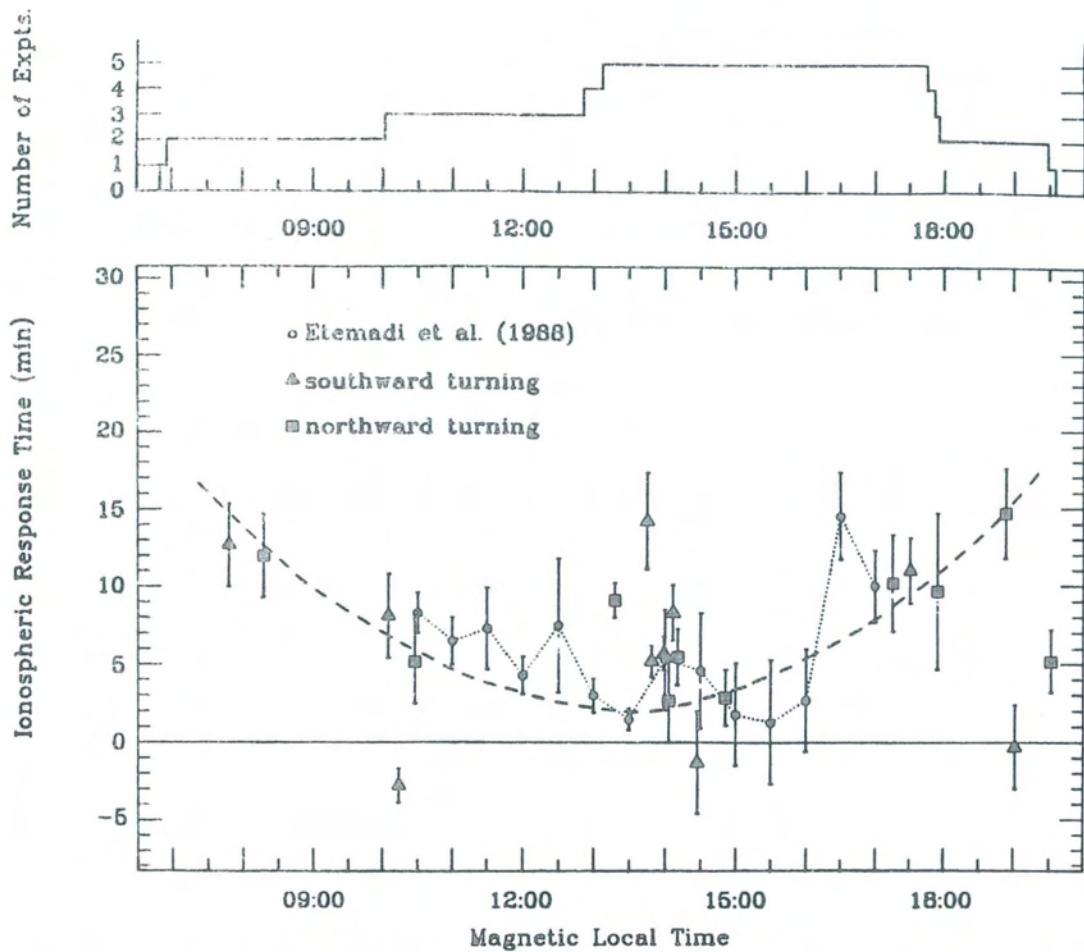


Fig. 42. Ionospheric response times (the delay between a change in the interplanetary magnetic field observed by AMPTE impinging upon the magnetopause and the response in ionospheric flows observed by EISCAT) as a function of the Magnetic Local Time of the EISCAT observations. The results are shown from the statistical study by Etemadi et al. (1988) and from the case-by-case survey of Todd et al. (1988). The dashed line shows model predictions from the model developed by Lockwood et al. in 1986. After Lockwood and Cowley (1988).

The Excitation of Ionospheric Convection

Momentum transfer across the magnetosphere

Further work is continuing, extending the comparison to much lower solar activity levels, where the EISCAT database is much larger (Farmer et al., Comparing numerical simulations of the high latitude ionosphere to an empirical mean model based on EISCAT data). The coupled model has also been used to predict the occurrence of non-Maxwellian plasma driven by supersonic ion flows at the longitude of EISCAT (Farmer et al., 1988).

One of the least-understood and controversial interactions in the solar-terrestrial chain is the transfer of mass and momentum across the Earth's magnetosphere. The exploitation of the unique dataset obtained by EISCAT while the AMPTE-UKS and -IRM satellites were in the solar wind has given important new insights into the mechanisms involved. A statistical survey (Etemadi et al., 1988) and case studies (Todd et al., 1988) have demonstrated that the flow of ionospheric

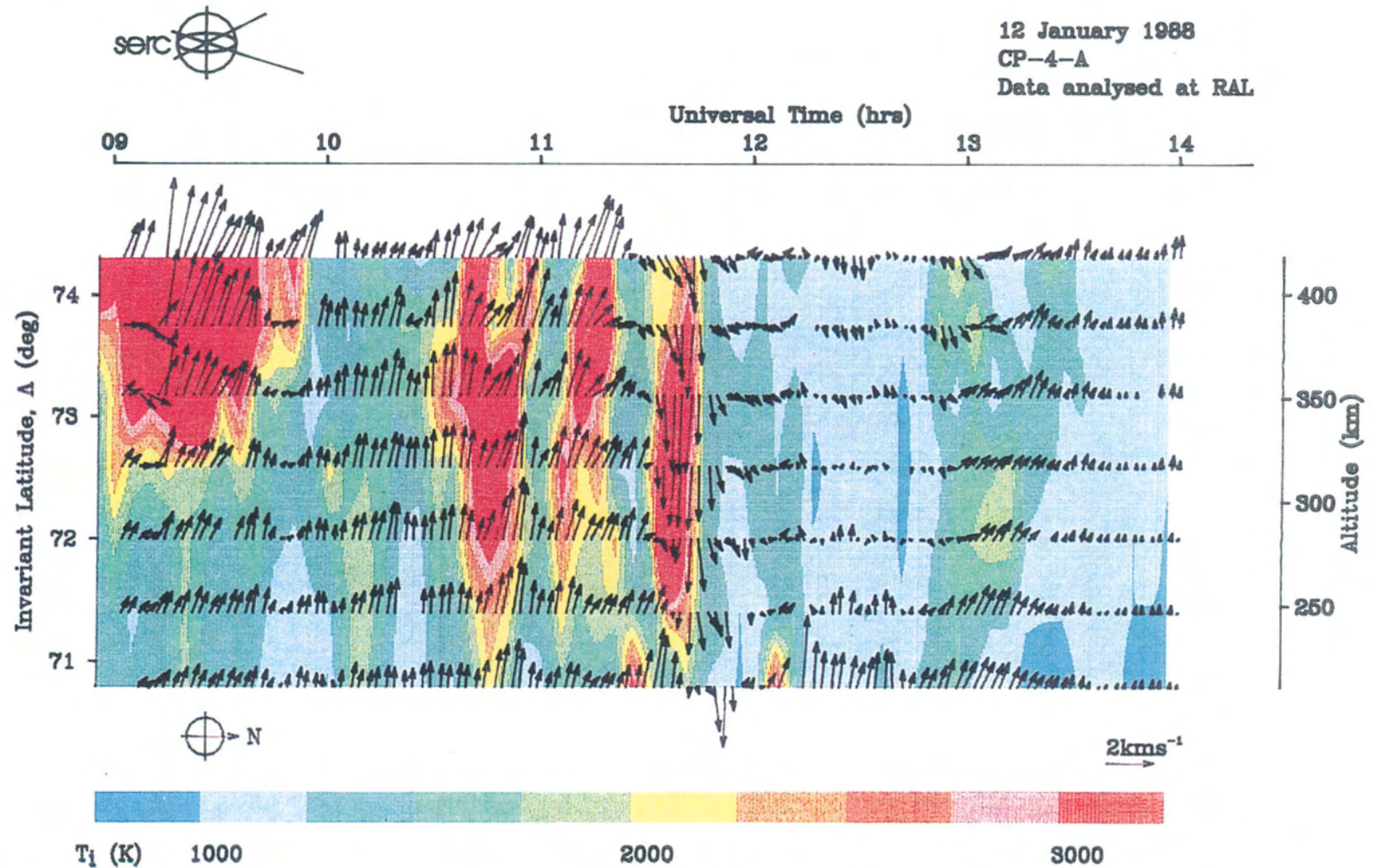


Fig. 43. EISCAT Common Programme 4 data showing plasma flows (in "electric field" format, i.e. with northward flow pointing to the right) superposed on colour contours of ion temperature. Bursts of exceptionally fast flow before 11:30 are found to correlate well with transient dayside aurora and pulses of southward IMF. Comparison with optical data from Spitzbergen shows that the dramatic slowing of the flow around

11:45 UT occurs on open field lines, well inside the polar cap, showing that open field lines only impart momentum to the ionosphere in a narrow region immediately poleward of the cleft (Lockwood and Cowley, 1988). The large ion drifts also drive the non-thermal ion velocity distribution distortions shown in Fig. 32 (Lockwood et al.).

plasma, observed in both the auroral oval and polar cap by EISCAT, responds very rapidly to changes in the north-south component of the Interplanetary Magnetic Field as observed by AMPTE (Figures 42 and 43). The response time of a few minutes could be observed because of the uniquely high time resolution of the EISCAT flow data and the ideal location of the AMPTE satellites. This discovery requires a completely new concept of the

excitation of ionospheric convection to be adopted and shows that the transfer of momentum across the magnetopause, and subsequently to the ionosphere, is restricted to a narrow region immediately poleward of the cleft (Lockwood and Freeman, Recent ionospheric observations relating to solar wind-magnetosphere, Figure 44). This model explains many otherwise anomalous features of field-aligned currents and convection patterns and agrees with the "driven" and "storage" responses of the magnetosphere as deduced from magnetic activity.

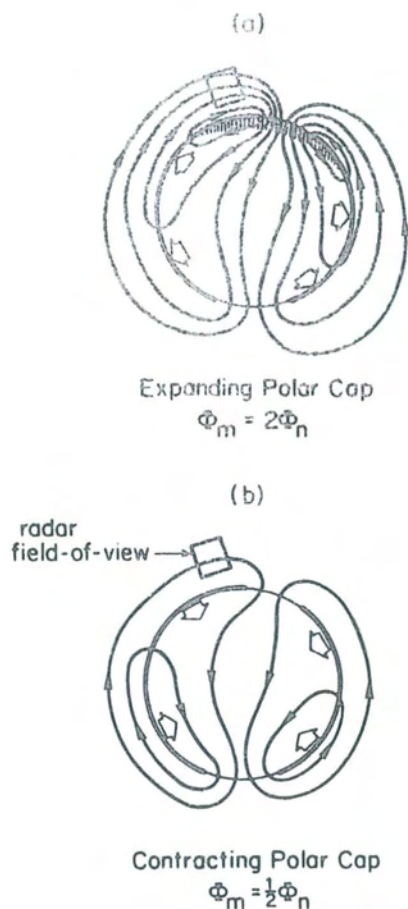


Fig. 44. Schematic of plasma convection patterns for (a) expanding and (b) contracting polar caps of the same area. This model explains the observed rapid response of dayside convection to changes in the IMF (Fig. 42), and also requires that open field lines only impart momentum in the narrow "smile" region (shaded poleward of the cleft: this has also been demonstrated to be the case using EISCAT data (Fig. 43). From Lockwood and Freeman, Lockwood and Cowley (1988) and Lockwood et al.

Furthermore, the transfer of momentum at the magnetopause has been shown to proceed in a series of bursts, each associated with a "midday auroral breakup" event. These transient arcs and arc fragments have been observed in both 630 nm and 557.7 nm auroral emissions to the north of EISCAT by meridian-scanning photometers and all-sky TV cameras operated on Spitzbergen by the Universities of Oslo and Tokyo. The coordinated EISCAT, optical and magnetometer observations show these events to be fully consistent with the expected signatures of Flux Transfer Events (FTEs) and are in excellent accord with recent theoretical considerations of FTE generation (Sandholt, Lockwood, Oguti, Cowley, Freeman, Egeland, Lybekk and Willis, Midday auroral breakup events and related energy and momentum transfer from the magnetosheath, Figures 45 and 46). In addition the arcs and the other features of the putative FTE signature are found to move east or west initially, under the influence of the magnetic tension resulting from the B_y component of the IMF, before being pulled slowly anti-sunward by the solar wind flow. The EISCAT data provide the first measurement of the potential applied across the magnetosphere by each event and it is found to be surprisingly large (at least 30-80 kV). Indeed, if these dramatic events prove to be typical, FTEs must be the dominant driving mechanism for convection in the ionosphere and magnetosphere.

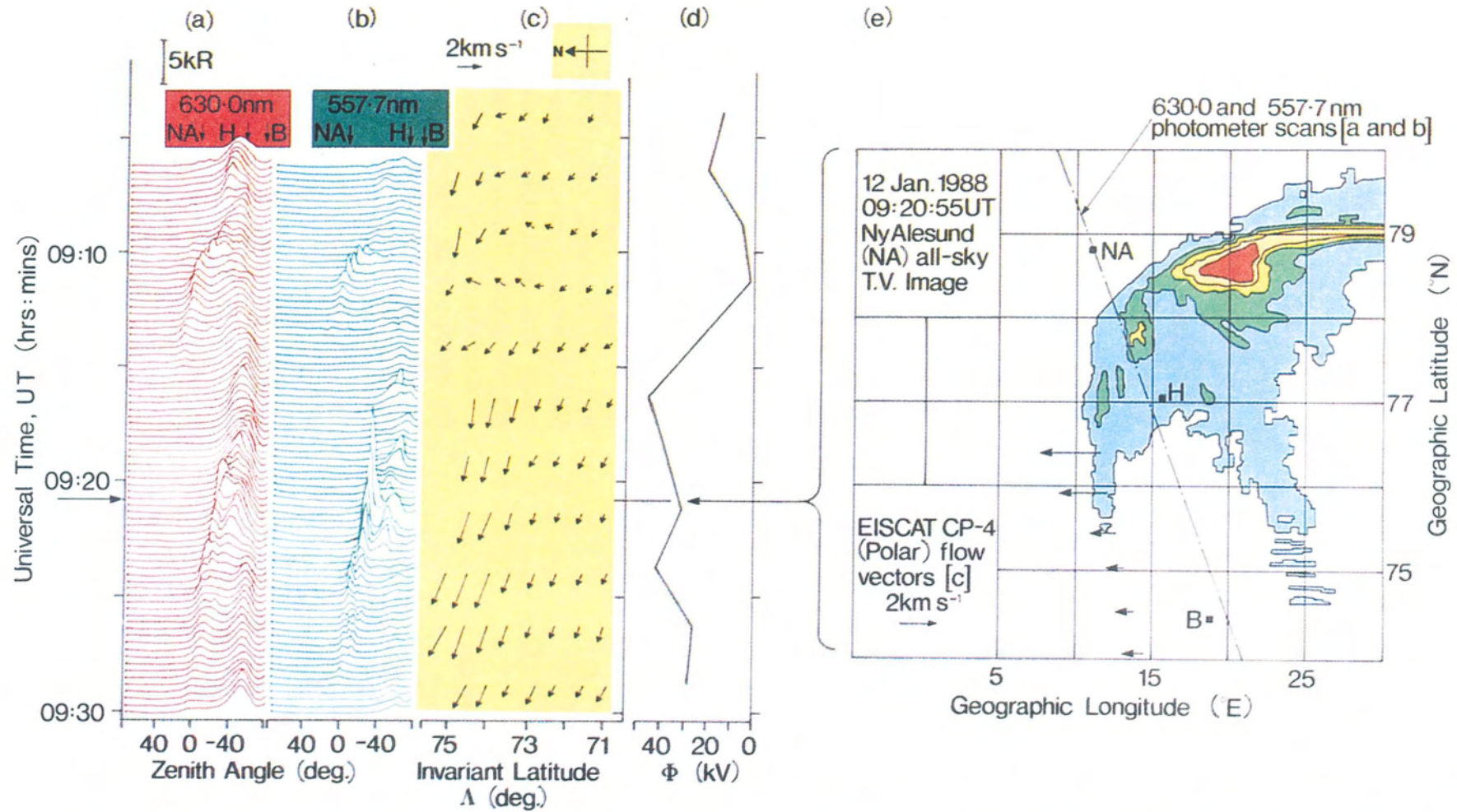


Fig. 45. Combined EISCAT observations (c and d) with meridian scans by photometers observing at 630 and 557.7 nm (a and b) and an all sky TV camera at Ny Ålesund, Spitzbergen. The midday auroral breakup events around 09:10 and 09:20 UT are found to be moved westward by the magnetic tension of the B_y component of the IMF, then poleward into the polar cap by solar wind flow. Combined with magnetometer records, these

observations prove momentum is transferred from the solar wind to the ionosphere in transient bursts (each giving a potential which must exceed the $\Phi=20-60$ kV applied across the radar field of view panel d) and that each event is fully consistent with the predicted signature of flux transfer events. (Lockwood et al.; Sandholt et al.).

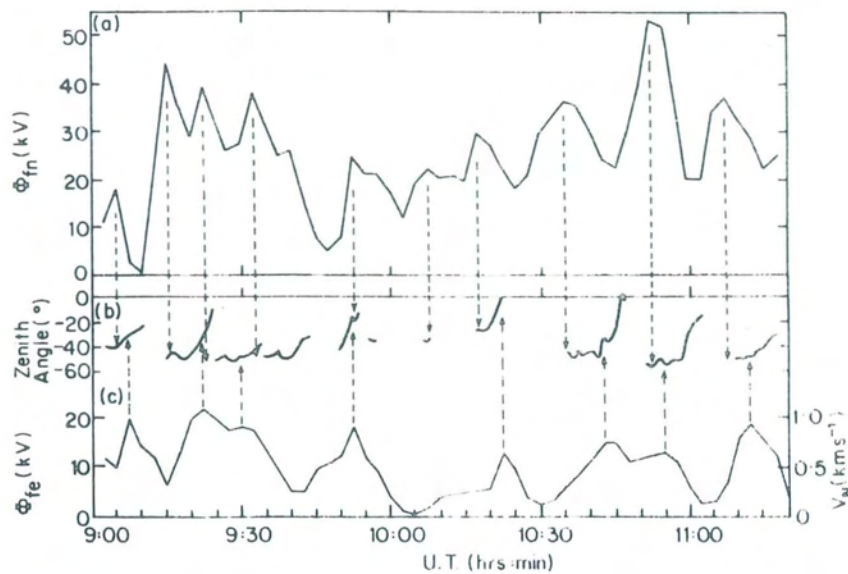


Fig. 46. Potential across the (a) meridional (ϕ_{fm}) and (c) zonal (ϕ_{fe}) dimensions of the EISCAT field of view as a function of time on 12 January 1988 (see Fig. 43). Panel (b) shows the zenith angles of dayside breakup arcs, observed at 630nm with $>3kR$ at Ny Ålesund. The dotted lines demonstrate that every peak in ϕ_{fm} is associated with the onset of a dayside auroral event which only occur when IMF B_z is southward. Combined with magnetometer data, the radar observations show the minimum total potential in an event is 40-80 kV. The data also show events are fully consistent with the predicted ionospheric signatures of Flux Transfer Events, which must now be considered to be the dominant mechanism for driving ionospheric convection. (Lockwood et al.).

Polar/auroral convection and cross polar cap potential drop

EISCAT electric field and conductivity data, obtained during the GISMOS campaign in January 1984, were included in a large data base (with electric field, conductivity and currents observed by radars and spacecraft, and ground-based magnetic field measurements), and combined with statistical models of electric field and conductivity in order to map the instantaneous large-scale electric potential pattern in auroral and polar regions, by using a technique developed by Richmond and Kamide (1988). In particular, the total cross polar cap potential drop deduced from the resulting global potential pattern agrees well with independent estimates from solar wind data. (Richmond, Kamide, Ahn, Akasofu, Alcayde, Blanc, de la Beaujardiere, Evans, Foster, Friis-Christensen, Fuller-Rowell, Holt, Knipp, Kroehl, Lepping, Pellinen, Senior and Zaitsev, 1988).

The potential due to viscous interaction on the flanks of the magnetotail during quiet periods has also been quantified for the first time by ground-based observations. The convection polar-cap boundary remained within the field of view for two hours and the potential drop corresponding to the flow into the polar cap across this segment near dawn was found to be only 7 kV. The flow patterns are consistent with ISEE3 observations of viscous-like interaction in the far tail (Lockwood et al., 1988). The EISCAT observations were taken as part of the June 1987 GISMOS campaign and the rapid contraction of the polar cap observed by EISCAT was used to define a substorm which was studied using simultaneous data from the Söndreström and Millstone Hill incoherent scatter radars, the Goose Bay, STARE and SABRE coherent radars, a wide network of magnetometers and images from NASA's Dynamics Explorer 1 satellite. The substorm was shown to be consistent with the moving neutral-line theory of

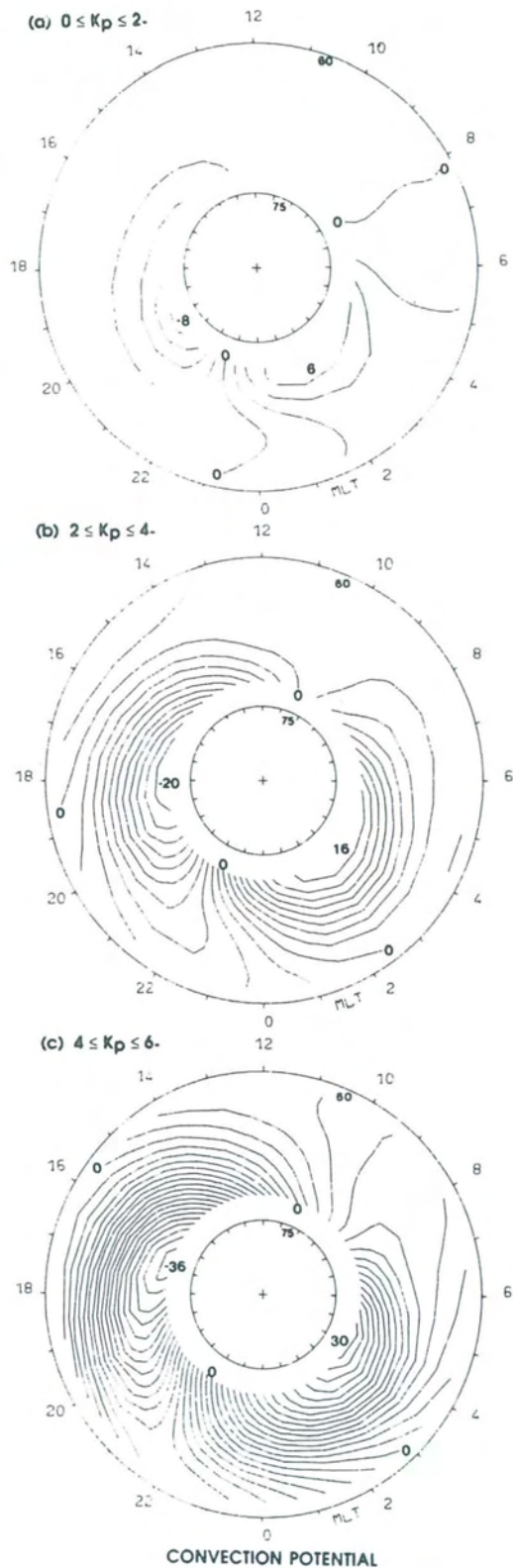


Fig. 47. Empirical models of high latitude convection potential derived from EISCAT CP-3 tristatic data. The three panels are drawn for quiet, normal and disturbed magnetic conditions.

substorms (Clauer, Kelly, Lockwood, Robinson, Ruohoniemi, de la Beaujardiere and Hakkinen, June 1987 GISMOS experiment: preliminary report on high-time resolution multi-radar measurements).

Empirical statistical models of the convection electric field and of the electrostatic potential have been constructed on the basis of more than three years of EISCAT tristatic observations from 61° to 73° invariant latitude with the Common Program CP-3. The statistics, organized as a function of the magnetic activity index K_p as illustrated in Fig. 47, provide a quantitative evaluation of the observed increases with magnetic activity of the cross polar cap potential drop, of the longitudinal and latitudinal extensions of the convection cells, of the rotation of the potential pattern relative to the noon-midnight meridian, and of the electric field penetration toward mid-latitudes. Finally, the statistical electric fields computed from EISCAT observations agree well with those of Millstone Hill and Chatanika radars, with slight differences due to the different geographic locations of the three radars. (Senior, Fontaine, Caudal, Alcayde and Fontanari, Convection electric fields and electrostatic potential over 61° - 72° invariant latitude observed with the European incoherent scatter facility 2., Statistical results).

Convection penetration towards middle and low latitudes

As well as driving the neutral atmosphere in the polar caps and auroral zones, magnetospheric electric fields can have a global effect by direct penetration to lower latitudes. The Gismos campaign of January 1984 gave the opportunity of examining the electrical coupling between the high, middle and low latitude ionospheres from observations of interplanetary and high-latitude ground-based magnetic fields and of F-region plasma drift measurements by incoherent scatter radars at several latitudes and longitudes including EISCAT. This data set shows that the global convection models repro-

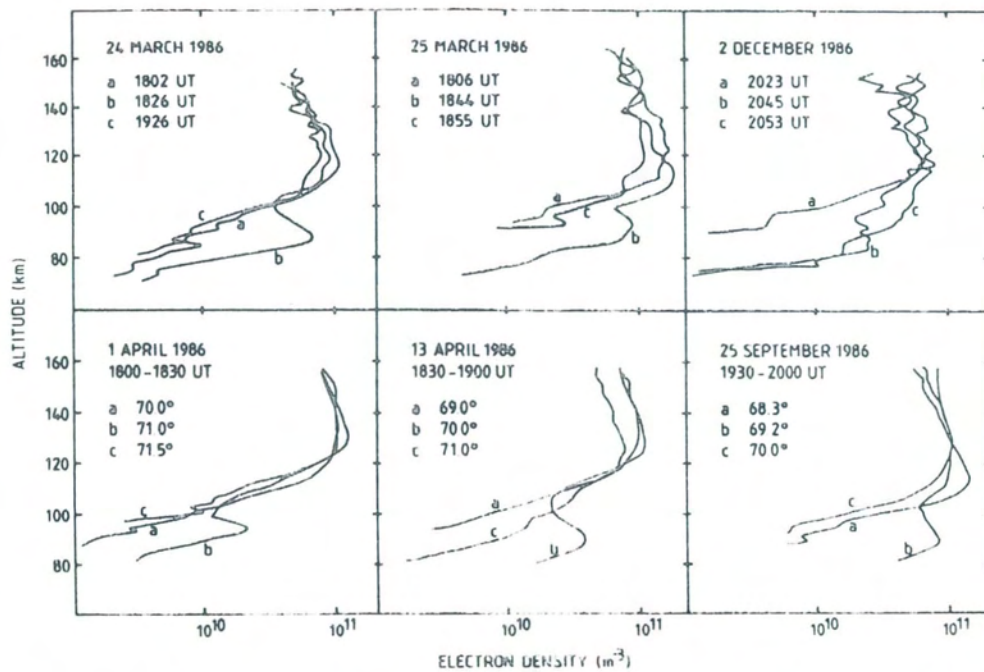


Fig. 48. E-region electron density profiles measured by EISCAT during the growth phases of 6 different substorms. The lower layer, peaking at about 90 km altitude appears to result from energetic electron precipitation from the outer edge of the radiation belts (Kirkwood and Eliasson).

duce roughly the main characteristics of middle and low latitude electric fields associated with variations of the cross polar cap potential drop. However, substantial disagreements between observations and theoretical models may appear, and could be due to the action of the disturbance dynamo effects on middle and low latitude electric fields (Fejer, Kelley, Senior, de la Beaujardiere, Holt, Tepley, Burnside, Abdu, Sobral, Woodman, Kamide, Lepping, Low and mid-latitude ionospheric electric fields during the January 1984 GISMOS campaign).

Auroral Signatures of Magnetospheric Substorms

Auroral electrodynamics during substorms

During the lifetime of the Viking satellite a number of auroral substorms were observed both by the satellite and by the EISCAT radar. Two studies have been made of the most active substorm phases. The first concentrated on ionospheric

conductivities, which were found to be substantially higher than previously assumed in the active aurora leading the substorm expansion. This study also found evidence that currents in the highly-conducting zones were largely driven by the neutral wind (Kirkwood et al., 1988).

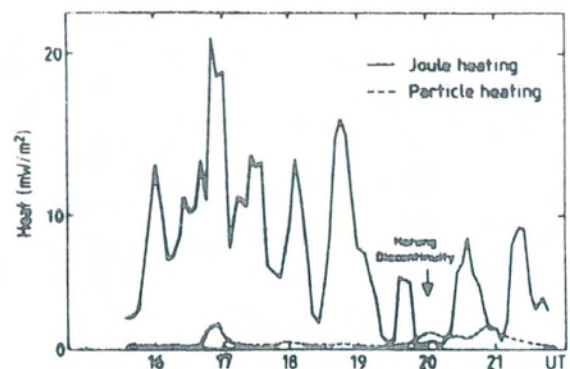


Fig. 49. Total particle heating and Joule heating as measured by EISCAT on 18 October 1985.

The second study was concerned with the spectra of the precipitating particles associated with the different substorm features. Good agreement was found between particle flux-energy spectra derived from EISCAT electron density profiles and direct measurements by the Viking satellite during intervals of diffuse precipitation in the substorm growth phase and after the substorm onset. EISCAT electron density profiles associated with the active auroral arcs leading the substorm expansion were found to give flux-energy spectra which are consistent with earlier satellite measurements in similar auroral situations but which also give better estimates of high-energy precipitation (>10 keV) than previously published (Kirkwood, Eliasson, Opgenoorth, Pellinen-Wannberg, A study of auroral electron acceleration using the EISCAT radar and the Viking satellite).

A third topic studied was that of precipitation in the substorm growth phase using EISCAT electron density profiles and Viking particle measurements. It was shown that the zone of equatorward-drifting energetic electron precipitation, which is often seen in the evening sector 1-2 hours before substorm onset, is due to electrons precipitated from the outer edge of the radiation belt. Precipitation occurs close to the isotropy boundary for >10 keV electrons (i.e. where the particle pitch-angle distribution changes from trapped to isotropic) and probably results from a decrease in the radius of curvature of the magnetic field-lines threading the boundary so that the electron gyro-radii become comparable to the radius of curvature. The study also suggests that this boundary may be important in controlling the occurrence of field-aligned acceleration and the triggering of substorms (Kirkwood and Eliasson, Energetic particle precipitation in the substorm growth phase measured by EISCAT and Viking).

EISCAT was used as an ideal facility for monitoring the ionosphere during a substorm, allowing an estimate of the integrated Joule heating and heating due

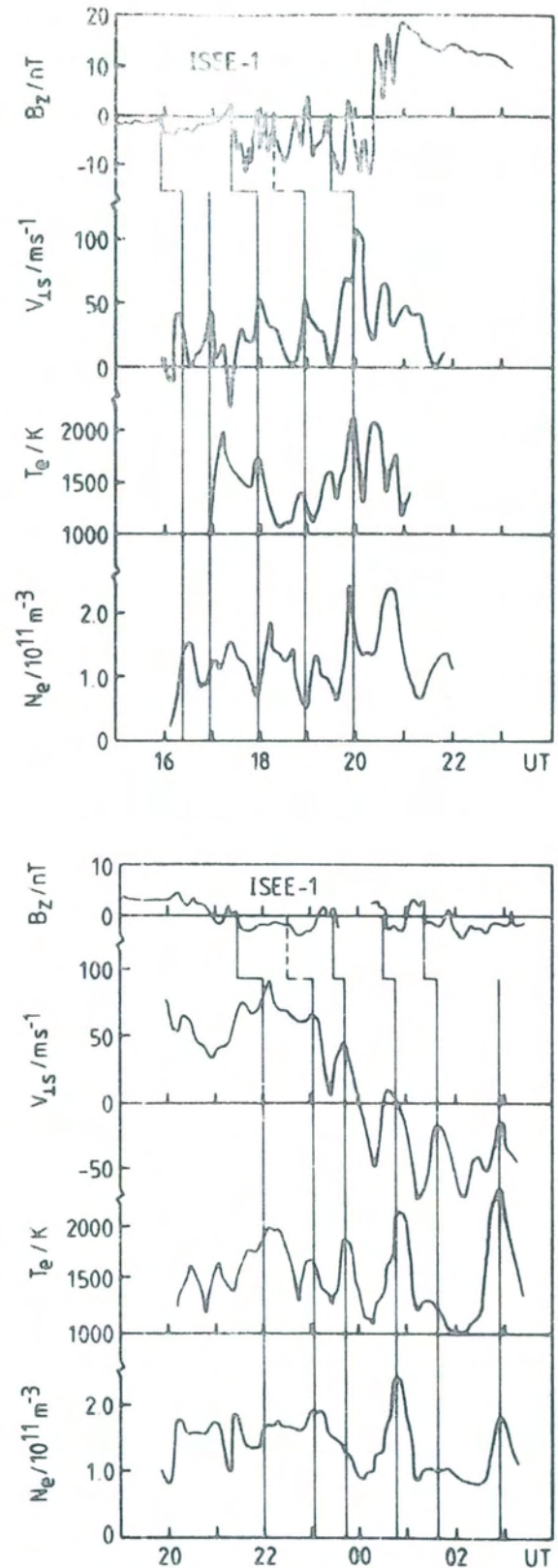


Fig. 50. Satellite measurements of the IMF inside the bowshock compared with EISCAT measurements of the NS field perpendicular plasma velocity, T_e at 306 km and N_e at 160 km (a) 13 October 1985 (b) 15/16 October 1985.

to particle precipitation. This confirmed earlier reports that Joule heating was an order-of-magnitude greater than particle heating, and represents the main channel of energy transfer from the geomagnetic tail to the ionosphere. An important result followed a study of the time variation of Joule heating during a substorm. The average value of Joule heating often remained significantly high over a period longer than shown by the particle precipitation or by magnetic disturbances. This suggested that traditional means of monitoring substorms, using magnetometers, riometers and auroral observations, give only a selective picture of the whole phenomenon, related to the precipitation of electrons with energies above 1 keV. EISCAT measurements provide a more complete and continuous picture, giving full consideration to the precipitation of particles with less than 1 keV energy (which are responsible for Pedersen conductivity) and the variations in electric field (Williams et al., Fig. 49).

Substorm control by the interplanetary magnetic field (IMF)

EISCAT often measures short bursts of a westward electric field (southward plasma flow) coinciding with soft-particle precipitation. The neutral-line model of a substorm provides a natural basis for interpreting these data. In this picture, two sources of flow are anticipated in the nighttime auroral zones, one directly driven by the IMF B_z with a delay time of 15-20 min and associated with dayside reconnection, and the other appearing typically an hour after southward turnings of the IMF and associated with rapid tail reconnection. The resulting pattern of ionospheric flow often shows a quasi-periodic variation with periods of about one hour. In two cases, in which concurrent IMF data was available, it appears that the periodicity was inherent in IMF B_z , but this was not expressed unmodified in the auroral zone because of the presence of the two sources of flow which depend on IMF B_z in different ways (Williams et al., Fig. 50).

The analysis of over 200 hours of data from the EISCAT/Viking coordination is still a major source of interest. After a number of studies concentrating on substorm onset and expansion (especially westward travelling surges, see previous annual report) attention has now been paid to the transition of the magnetosphere from a quiet to a disturbed state, when the interplanetary magnetic field changes its direction. Two cases with quite similar characteristic features have been studied in detail. In both cases a quiet time convection system had developed during an extended period of northward directed interplanetary magnetic field. Typical for such a situation, when the projection of the magnetospheric convection on the ionosphere often displays a four cell pattern, is the formation of an auroral arc, extending over the polar cap from the midnight to the dayside prenoon portion of the auroral oval, the so-called trans-polar arc (TPA). In some cases this phenomenon has also

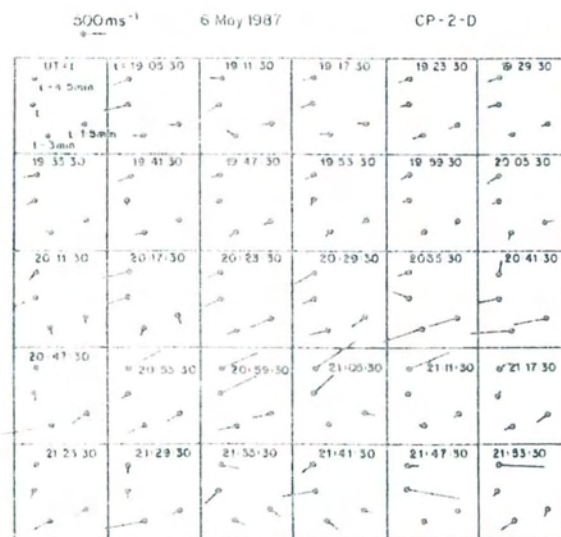


Fig. 51. Tristatic field perpendicular convection velocities on 6 May 1987. Major ion upflow events were observed along the Tromsø field line commencing at 21:00 and 21:47 UT. It can be seen that these times correspond to the passage of a convection shear over the beam and high ion temperatures and the resulting upflows were observed in the wake of the moving shear in both cases (Winser et al.).

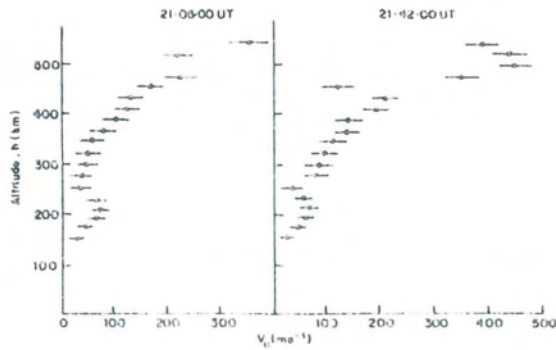


Fig. 52. Observed profiles of field-aligned plasma velocity on 6 May 1987, made using Common Programme 2. The plasma fluxes exceed 10^{13} ions $m^{-2}s^{-1}$ and are therefore more than an order of magnitude greater than the "classical polar wind". The terms in the field-aligned momentum balance equation could be studied individually using these data.

been called Theta-aurora, for the striking similarity of the auroral oval and its central trans-polar arc as seen in high altitude satellite images with the Greek capital letter Θ .

In both cases the imager onboard the Viking satellite observed a fading and subsequent disappearance of such trans-polar arcs only a few minutes after the interplanetary magnetic field direction changed from northward to southward. This disappearance of the trans-polar arc obviously indicated the formation of a different magnetospheric convection system. In both cases Viking also observed a simultaneous considerable increase of auroral emissions at the nightside footprint of the fading trans-polar arc, which was associated with disturbances in the ionospheric magnetic and electric field, as monitored by a network of magnetometers and EISCAT, respectively. At first glance these disturbances do not appear as indicators of a substorm type release of magnetospheric energy, but might be caused by other

processes following the reformation of the magnetosphere in response to changed conditions in the interplanetary magnetic field (Pellinen, Koskinen, Pulkinen, Murphree, Rostoker, Opgenoorth, Satellite and ground-based observations of a fading trans-polar arc).

Other coordinated studies, involving EISCAT, Viking, several ground-based instrument networks, the auroral sounding rocket AURELD-Vip, the AFGL-Airborne-Observatory, and the DMSP-F7 satellite have also been pursued. A complicated auroral situation in a generally disturbed magnetosphere could be analysed and understood in detail with the help of this uniquely complete dataset from various regions in the ionosphere-magnetosphere system. (Block et al., Conjugate Viking-Airborne Observatory and simultaneous DMSP and ground-based observations of aurora).

Pulsations associated with substorms

IPDP (Intervals of Pulsations of Diminishing Periods) type plasma wave events are a well-known signature of magnetospheric substorms. The characteristic feature of these events is an upward sweep of the frequency from about 0.1-0.2 to 1-2 Hz during the event which may last for 0.2-2 h. Several different theories have been proposed to explain the frequency shift in IPDP. It has been evident that it is produced by the radial $\underline{E} \times \underline{B}$ drift of the source of the magnetospheric ULF ion cyclotron waves, especially in the late evening-to-midnight sector. However, until now, no direct E-field measurements have been presented to test this suggestion. Kangas et al. (1988) have analysed EISCAT measurements during a typical IPDP event on 4 December 1986. It appears that the $\underline{E} \times \underline{B}$ drift explains the frequency drift in this IPDP quite well.

EISCAT UHF1 1986-12-13 1757UT

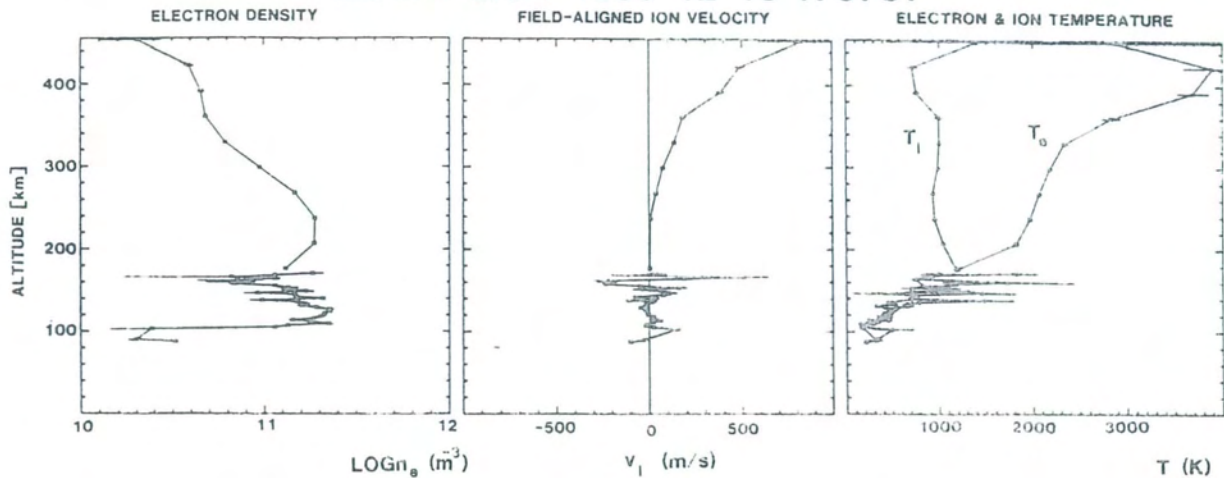


Fig. 53. Altitude profiles of electron density, field-aligned ion velocity (positive outward), electron and ion temperature as derived from the received EISCAT radar signal. The field-aligned ion velocity reaches large values of over 600 ms^{-1} in the upper F-region. At the same time the electron temperature increases by about 1500 K in the F-region during this minute-long event.

Field-aligned acceleration processes

By comparison of EISCAT-CP-1-F/UHF1 and VIKING data the typical behaviour of the ionosphere - as measured by EISCAT - during the occurrence of ion beams - as measured by VIKING was studied. For the investigation of energy fluxes, particle fluxes and field-aligned currents under different ionospheric conditions, electron energy spectra were calculated from EISCAT electron density profiles. By comparison with VIKING spectra, new information about the potential difference between the satellite and the ionosphere and about the acceleration mechanism of the precipitating electrons can be obtained. Further, the energy-balance for F2-layer ions and electrons was investigated for times of high ion temperatures, as measured in CP-1-F-mode. In a case study for 4 April 1986, the observed ion temperatures could be explained by a resonant-charge-model. (Glatthor, Investigation of ionosphere-magnetosphere-coupling by means of EISCAT and VIKING data).

Plasma upflows and topside ionosphere

The influence of non-thermal plasma on field-aligned dynamics has been studied, particularly within high latitude troughs or in the vicinity of the putative signatures of flux transfer events. When ion-neutral frictional heating is intense in the F region, the increase in plasma pressure provides an upward force which is increased by the hydrodynamic mirror force caused by the anisotropy in the ion velocity distribution. On one occasion a moving convection shear caused an upward velocity as high as 500 m/s along the Tromsø field line during CP-2 observations (Fig. 52). A careful examination of the data indicated the various factors involved in the upward acceleration. To overcome the gravitational force and the drag caused by ion-neutral collisions it was necessary for Joule heating to cause an upwelling of the neutral atmosphere which in turn carried the ions to a height where the increased plasma pressure could cause further acceleration without the inhibition of ion-neutral collisions (Jones et al., 1988).

Such upflows allow the high-latitude ionosphere to be a major supplier of plasma to the magnetosphere and offer a

possible source for some of the ionospheric ions observed in the wake of an FTE by AMPTE-UKS and -IRM (Lockwood et al., 1988).

Enhanced F-region electron temperatures have been observed in association with extremely large outward field-aligned flows of the bulk ion population in the F-region. Fig. 53 shows an example of such an ion outflow event. These ion flows are observed during auroral activity and are most common within auroral arcs, however they are not particularly well correlated with diffuse aurora. Strong electron temperature enhancements in the F region are observed in connection with almost all ion outflow events. However, high electron temperatures are not always an indicator for strong ion outflow events. The ions (mainly O^+) may reach field-aligned outward velocities of more than 500 ms^{-1} and the calculated ion fluxes usually reach $10^{13} \text{ m}^{-2}\text{s}^{-1}$. If one assumes a 100 km broad auroral zone, where ion outflows occur during 50 % of the time, auroral activity will result in an estimated total ion outflow of about 10^{25} ions s^{-1} to the magnetosphere. This value might even be an underestimation because the magnitudes of the ion flows are observed to increase steadily at higher altitudes. Thus the observed ion outflows from the ionosphere might constitute a major source for the magnetospheric ion population of heavier ions (Wahlund and Opgenoorth, EISCAT observations of strong ion outflows from the F-region ionosphere during auroral activity: Preliminary results).

Specific campaigns with the VHF radar were devoted to the study of the vertical distribution and transport of the ions O^+ and H^+ in the topside ionosphere. In July-August 1988, it was possible to measure the electron density up to about 1200 km and to determine the relative composition of O^+ and H^+ . Up to the highest observed altitudes, the O^+ ions remain dominant and exhibit large variations in the vertical velocity. A study was started to compute vertical velocity of the H^+ ions from these observations, which should permit the

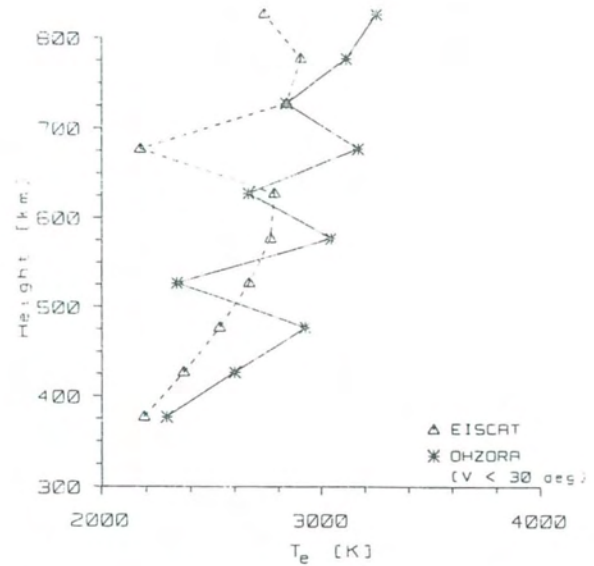


Fig. 54. Average electron temperature in the topside ionosphere measured with EISCAT and with a T_e -probe onboard the Japanese satellite OHZORA.

determination of polar wind characteristics (Wu Jian, Blanc, Alcayde, Kofman).

The electron temperatures above 350 km measured by EISCAT and with a T_e -probe onboard the high inclination Japanese satellite OHZORA have been compared. Since there were only a few cases when EISCAT was operating during a satellite pass above Tromsø, a statistical approach was used averaging EISCAT-CP-3 data and the satellite T_e -values obtained when OHZORA was in the vicinity of EISCAT ($50^\circ \leq \text{LAT} \leq 75^\circ$, $0^\circ \leq \text{LONG} < 45^\circ$) during the time period July 1984 to June 1985. This data base comprised about 30000 EISCAT T_e -values (with $\text{SNR} > 2\%$) and 10000 satellite T_e -values distributed in 50 km wide altitude bins centered at 10 heights between 375 and 825 km. Fig. 54 shows the corresponding T_e -profiles. Although the satellite data (and also the EISCAT data above 650 km) show considerable scatter, the agreement of the average T_e is quite good below about 650 km. Above this limit the EISCAT data are very unreliable since the averages are calculated from less than 10 samples.

A clear K_p - as well as a solar zenith angle dependence of the topside T_e -values was also found. (Schlegel and Oyama, 1988).

Artificial Modifications of the Ionosphere

UHF Radar Diagnostics and Chirp

A successful test at EISCAT of the chirp synthesizer on loan from the Arecibo observatory was described in the Annual Report of 1986. A similar device is now being completed at EISCAT (see Annual Report 1987). The tests, conducted in May of 1986, showed the advantages, particularly enhanced detectability, that this instrument gives in measuring photo-electron enhanced plasma waves in the natural ionosphere. In August of the same year a campaign was carried out in cooperation with the Heating facility of the Max-Planck-Institut für Aeronomie, just a few hundred meters from the EISCAT site in Tromsø. The aim of the campaign was to measure the plasma effects that result from RF overdense heating of the ionosphere with substantial improvements of range and spectral resolution. An interesting program for the UHF EISCAT radar was developed for this campaign with the ability to measure chirped and non-chirped channels simultaneously. Two channels were dedicated to chirped up and down shifted plasma lines covering a one MHz band at 8.7 kHz resolution each. Three non-chirped channels were dedicated to two additional plasma lines (up and down shifted) and the ion line that employed a one millisecond pulse to obtain good frequency resolution. Another channel made measurements of the background parameters of the ionosphere, whereas the last channel was a high range resolution power profile that could be tuned to the ion line or any of the plasma lines.

After several days of observations with negative results some surprising measurements were made. These are the excitation of plasma waves at frequencies

shifted from the known resonant bands by some 200-300 kHz and often showing multiple line structures (see Fig. 55).

Attempts to explain this effect have succeeded only partially. Close analysis and scrutiny of the data reveals a remarkable self-consistency among the various channels and in the spatial and temporal behaviour of the signals. Because of this and because efforts to identify any spurious effects have failed, the view has been taken that the observed effects are real. Thus far we know of no physical process capable of explaining the shifted lines. The possibility of resonant enhancements due to electron beams created by the heater has been discarded due to the requirement of extremely mono-energetic beams needed to explain the rather small altitude extent of the enhancements.

In addition, a non-thermal enhancement of the ion line power profile was observed to occur above the peak of the F layer at an altitude where the local plasma frequency was in resonance with the heater frequency of 4.02 MHz. This top-side enhancement has been tentatively explained by leakage of a fraction of the heater power to altitudes beyond the reflecting layer due to coupling to X-mode waves. These waves couple to the plasma again at the second resonant altitude and excite an unidentified plasma instability that accounts for the observed enhancements. The conspicuous absence of the natural plasma line enhanced by photo-electrons and the plasma line enhanced by the heater transmitter was also notable (Isham, Kofman, Hagfors, Nordling and La Hoz).

VHF Observations during Heating

A number of new surprising phenomena, observed with the VHF system, have been reported in the Annual Report of 1986. Three Heating campaigns were performed in 1988 and the following results were again obtained with the VHF.

SP-TH-CHIRP-7B-T 17/AUG/86

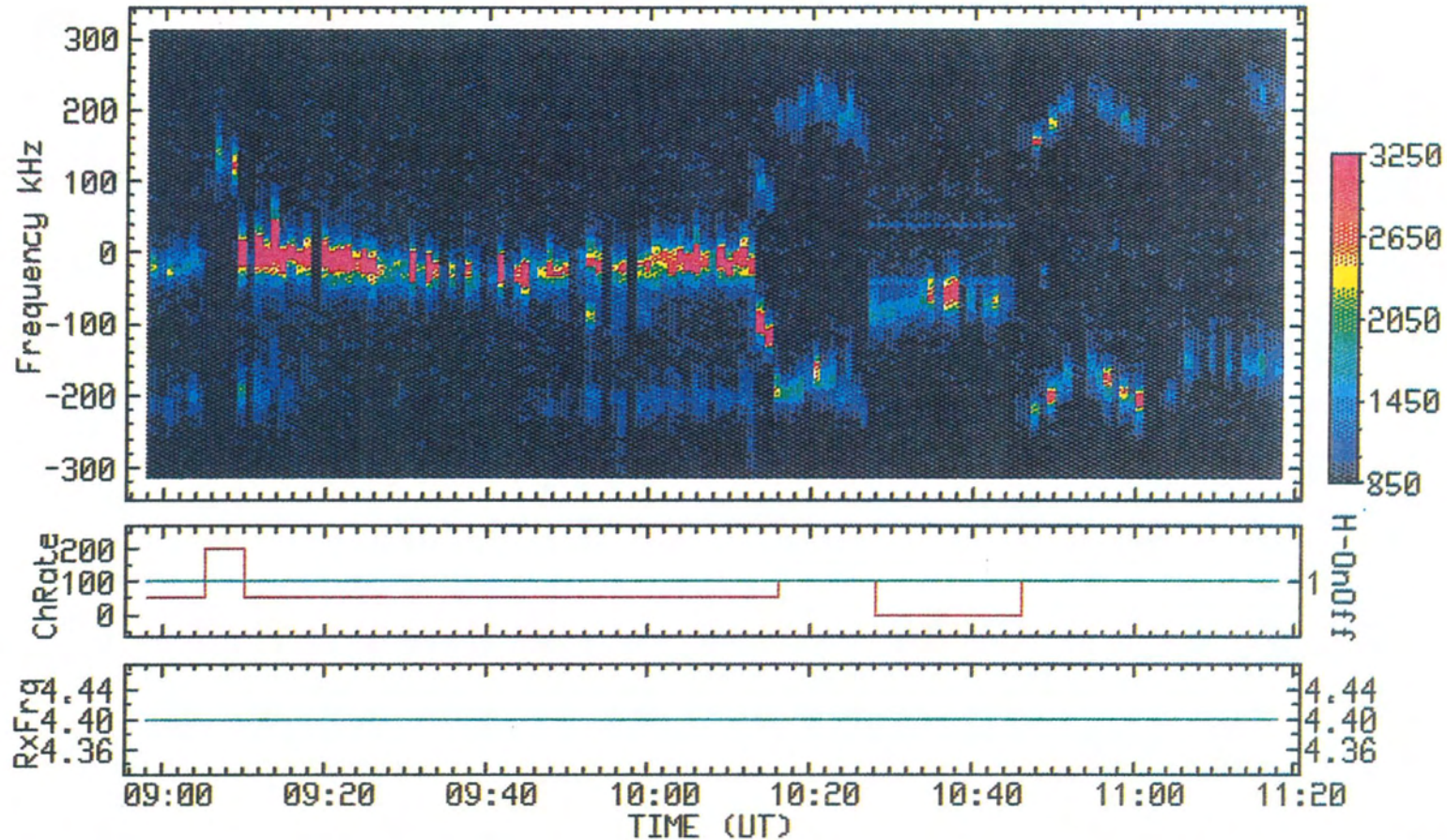


Fig. 55. Chirp-observations of the plasma line performed with the EISCAT UHF radar during ionospheric modifications in Heating experiments. The 0 kHz-frequency in the spectral plot (upper panel) corresponds to an offset of 4.402 kHz of the EISCAT receiver from the EISCAT transmitter frequency (lower panel) matching the Heater transmitter frequency. During the

experiment the Heater was transmitting continuously (middle panel, green line), while the EISCAT frequencies were linearly varied ("chirped") around the center frequencies with a rate given in the middle panel by the red line (in $100 \text{ Hz}\cdot\text{km}^{-1}$). This allows to determine the altitude of the plasma line enhancement with an accuracy of a few hundred meters.

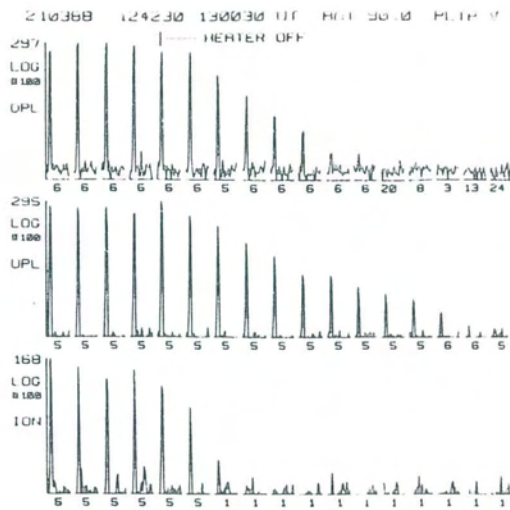


Fig. 56. Decay of the downshifted and upshifted plasma line (DPL and UPL) and ion line (ION) after heater switch-off. The individual power profiles were measured in 1 ms intervals.

Fig. 56 shows power profile sequences of the downshifted and upshifted plasma line, as well as of the ion line obtained from single radar pulses which were transmitted at time intervals of 1 ms. Every spike in the U profiles indicates the altitude region where the heater excited parametric instabilities. The aim of this experiment was to investigate the decay of the plasma and ion lines with very high time resolution, when the heater was off. As expected, the excitation decreased exponentially with different time scales: The ion line decreased fastest. This is in agreement with the theory of strong Landau damping of the ion wave. The plasma line should be only damped by electron collisions. With this assumption the collision number, ν_e , can be estimated from the measured decay time. The results are $\nu_e=1000 \text{ s}^{-1}$ for the downshifted plasma line and $\nu_e=500 \text{ s}^{-1}$ for the upshifted plasma line in agreement with theoretical calculations. However, the different decay times between upshifted and downshifted lines indicate, that other processes may be involved, e. g. the propagation of Langmuir waves.

Fig. 57 shows a similar experiment, studying the decay of the lines when the heater is on. The time interval between

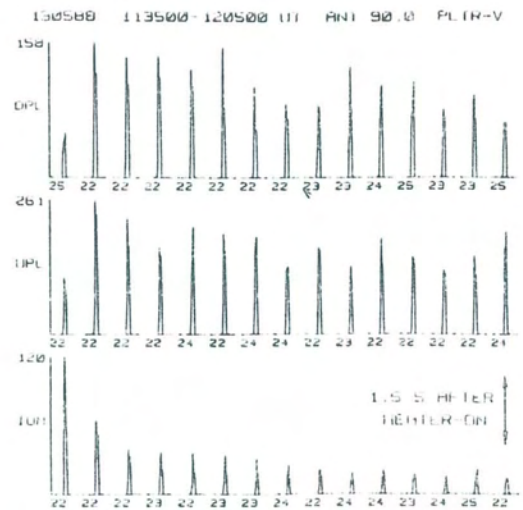


Fig. 57. Power profile sequences as in Fig. 56, but in 100 ms intervals. After the heater switch on a strong decay of the ion line within a second is seen, but not of the plasma lines.

concurrent power profiles had been increased to 100 ms. In this case the ion and plasma waves should be closely coupled and their intensities should be tightly correlated. Surprisingly the ion line decreased by about 10 dB in 1.5 s, while the plasma line intensities remained almost constant. This result also differs from observations with the Arecibo Observatory heater, where the "overshoot" after the heater switch-on is seen particularly strong in the plasma lines.

Another interesting effect is seen within about 100 ms after the heater switch-on: the altitude of the excited region increased by about 1-2 kilometers. This was observed in Arecibo, too. An explanation is not yet known.

The pulse repetition rate of the experiment shown in Fig. 58 was 4 ms. Here the excitation was observed over a larger altitude range of about 40 km. During the that time strong geomagnetic disturbances were recorded. Obviously the ionosphere was so distorted, that the conditions for the excitation of the lines (implied by the dispersion relation) were fulfilled over almost the whole sampled altitude ranges. In other words, irregularities at frequencies close to the heater frequency were

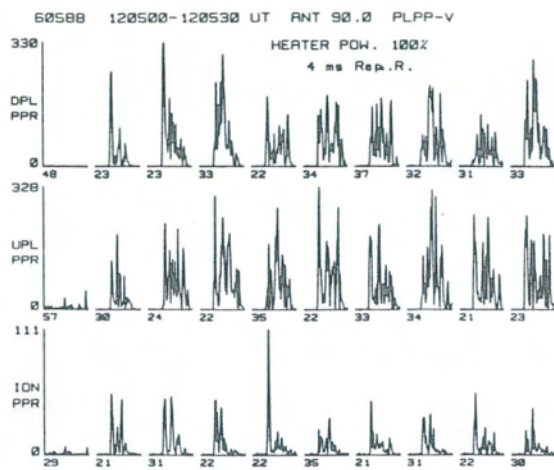


Fig. 58. Line excitation over about 40 km altitude range is observed during an ionospheric storm.

apparently present at a large altitude range. Similar results had been reported in 1986.

Fig. 59 shows a spectrum of the upshifted plasma line. About 25 kHz above the line another small unexplainable line appears.

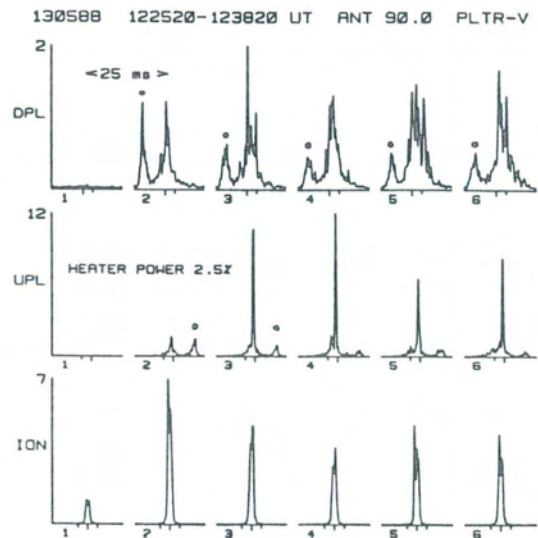


Fig. 59. Spectra of plasma and ion lines in 25 ms intervals after heater switch-on. Unexpected lines appeared, which are shifted by more than the heater frequency with respect to the radar frequency (marked by *).

Similar features have been seen at Arecibo (Djuth, private communication). They may be related to the multiple lines observed with the chirped UHF system, which are discussed in the previous chapter (Kohl).

TECHNICAL EVOLUTION AND ADAPTION OF THE SYSTEM AND INSTRUMENTATION

The Scientific Advisory Committee discusses regularly the status and the evolution of the system and the facilities and defines a list of priority. The Scientific Advisory Committee has laid out a list of evolutionary and revolutionary developments of the EISCAT system, which contains the following items: System improvement using advanced technology and advanced signal processing techniques, VHF beam steering capability, extended capabilities of EISCAT for investigations of the mesosphere, stratosphere and the troposphere, multiple beam capabilities at

the remote sites, new facilities for plasma physics research, array processors for fast computations and new mass storage media for data archiving.

It was earlier recommended that advanced coding techniques and signal processing would improve the system in such a way that observations would be possible in so far not accessible regions and with so far unprecedented data quality. Promising developments in these directions have been started, e.g. the use of new codes, the improvement of the system noise by

Muffin Prototype	
<i>MULTI</i> channel Finite impulse response <i>FILTER</i> and <i>INTEGRATOR</i>	
INPUT:	present ADC: 2 x 8 bit per channel 8 channels $2.3 \cdot 10^6$ samples/sec delay line input 16 bit/32 bit Real, Imaginary
DECODING:	max. code length 8 kbit, 2 delay lines 256 start addresses per channel 32 bit lag profiles real and imaginary parts processed in parallel
INTEGRATING:	2 x 32 bit sixteen 16 bit integration counters
ACCUMULATING:	2 x 16 k x 32 bit
SCALING:	max. 32 bit
OUTPUT:	buffer memory size: 2 x 16 k x 16 bit or 2 x 8 k x 32 bit
DATA FLOW:	ADC → MUFFIN → Correlator → DMA

Table 3. Technical parameters of the MUFFIN preprocessor.

new receiver components and the design of an integrator-decoder to enhance the capabilities of the present correlators.

In the last year's Annual Report brief descriptions were given on the work which is being performed on new instrument adaption for alternating and complementary codes, the CPU synchronization, the chirp synthesizer as well as on related software improvements.

The efficient and flexible signal processing capabilities will be enhanced by the MUFFIN project, which entered the testing phase during the year. The main parameters of this integrator-decoder device are summarized in Table 3. The operational tests and implementation of this processor into the system are expected in the following year.

1988 will be remembered as the year when EISCAT was confronted with the problem of how to survive the almost explosive growth of two-way radio services in the 900 MHz frequency range. Safeguarding the continued operation of the system and adapting the receivers to cope with the drastic changes in the RF environment suddenly became matters of top priority, and much of the time and manpower available for technical developments had to be invested in projects directly targeted at improving the UHF receivers. The activation of the two-way services will have far-reaching consequences for EISCAT and its users, and we have therefore devoted most of this summary to an overview of the issue.

The NMT 900 situation

Some years ago, the 935-942.5 MHz band began to be used by the base stations of the cellular telephone service (NMT 900) in metropolitan areas in southern Scandinavia (see Fig. 2 on page 6). Enquiries to the Nordic telecommunications administrations confirmed that a rapid pan-Nordic expansion of NMT 900 was in progress, and that the first base stations in areas close to the EISCAT sites would begin

operation in early 1988. It was soon realized that our existing UHF receivers were going to be incapable of handling the strong NMT signals without severe deterioration of linearity and noise temperature that would seriously affect all measurements. Immediate remedial action was thus necessary.

A great number of administrative actions followed. These have been adequately reported elsewhere, and it is sufficient to note here that EISCAT now enjoys a very good cooperation with the Finnish, Norwegian and Swedish frequency planners. One extremely valuable result of this cooperation is that for the time being, all NMT 900 base stations in the immediate vicinity of the EISCAT sites are transmitting above 939 MHz, thus avoiding direct co-channel interference with all our UHF ion line channels.

The UHF receivers

Most of the information content of an incoherent scatter signal is conveyed by the detailed form of its power spectrum. In order not to distort the physical information, all operations performed by the receiver on the signal must be strictly linear. Linearity can normally only be maintained over a certain range of input amplitudes, termed the "linear dynamic range" or, for convenience simply "dynamic range", but for the receiver to work properly in a real life situation, the dynamic range must be at least as great as the span between the strongest undesired signal in the band and a weak IS signal. This is not always easily accomplished.

When the UHF receiver was designed in the late 1970's, the primary goal seems to have been to build a receiver exhibiting the lowest system noise temperature then possible. Its RF bandwidth was fixed at 30 MHz, which is necessary and sufficient to enable plasma line measurements even under conditions of high electron density. Assuming a system noise temperature of 30 Kelvin, the total power due to thermal noise in this band at the receiver

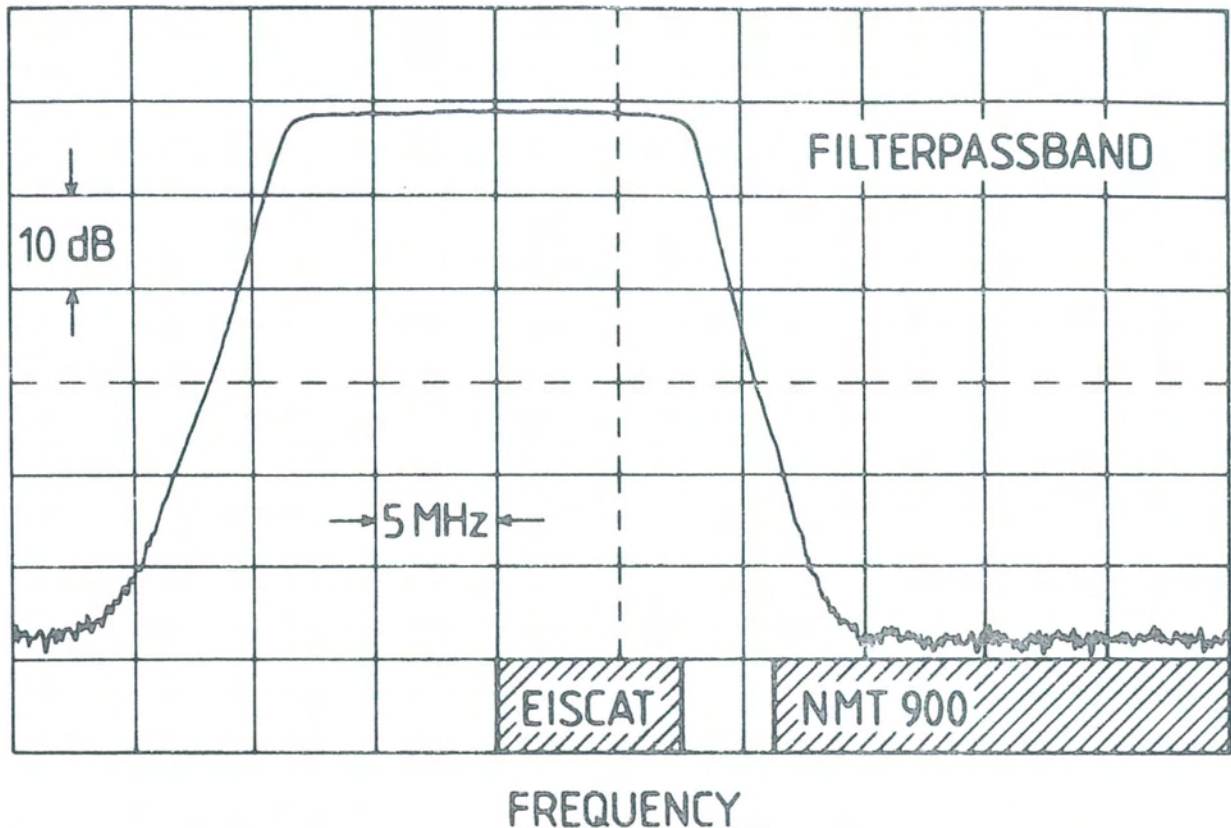


Fig. 60. Passband of the EISCAT intermediate frequency (IF) filter.

input is about $1.2 \cdot 10^{-11}$ W (-109 dBm). The power added by even a very strong incoherent scatter signal is totally negligible in comparison, so the gain distribution and power handling of the first generation receiver were laid out based on the noise power. The system noise temperature finally achieved with the first generation receivers was 50-60 K, which was considered acceptable at the time. The dynamic range of this noise-optimized design turned out to be well over 30 dB, which was totally adequate in the absence of interference.

Problems introduced by the NMT 900 system

The NMT 900 base stations in Kiruna and Sodankylä have been set up so that their antennas are in direct view of the EISCAT receiver antennas and at roughly

equal distances of 8 km. Pointing the EISCAT antennas directly towards a base would theoretically result in a power of $7.4 \cdot 10^{-6}$ watt (-21.3 dBm) per carrier being delivered to the receiver. This level exceeds the dynamic range of the old receiver by over 50 dB.

A more realistic situation is one where EISCAT is looking in an arbitrary direction far from the line of sight to the NMT base. In this case, we benefit from a suppression of the NMT carrier power by the sidelobe-to-peak ratio of the EISCAT antenna, i.e. about -50 dB. But after this attenuation, the signal level is still quite a few dB above the dynamic range of the receiver, and several amplifier stages will then be driven into partial or full compression by the NMT signal. The system noise level will increase and (worst of all) the IS spectra on all channels will become distorted.

As soon as the NMT base station in Kiruna was started (in March 1988), measurements of the carrier power levels were made. The measured values at antenna pointing directions used in CP1 and CP3 were within a few dB of the theoretically predicted ones, which confirmed that we really had a serious problem, which must be solved before reliable operation could resume.

System changes and results

Before any systematic improvements could be attempted, emergency action was necessary to keep the remote sites in operation. As a fast expedient, narrow-band filters were installed ahead of, and inside, the first intermediate frequency (IF) amplifier to prevent the NMT signals from saturating it. After fitting the filters, only F0-F4 could pass the first IF, but most ion line observations could still proceed normally, as there are rarely more than two channels used at the remote sites.

A critical review of the operating bandwidth requirements and the techniques available for overload prevention was now performed. It was found that bandpass filtering would be mandatory to prevent the NMT carriers from saturating the receiver "back end", and that this filtering would restrict the useable frequency range to below 937.0 MHz. The resulting loss of RF bandwidth could be partially recovered by a downward frequency shift of the transmitter band. We were advised by Varian and SRI experts that our UHF klystron could be tuned down by as much as 2 MHz, thus putting the transmitter band at 927.0-934.5 MHz. Based on this knowledge, a set of new IF bandpass filters were ordered to specifications that attempt to retain as much bandwidth as possible, while offering at least 35 dB of attenuation at frequencies corresponding to the NMT 900 RF band (>939 MHz). The passband of one of the new filters is shown in Fig. 55*. It is evident that as long as one uses transmitter frequencies at the low end of the shifted transmitter band, full plasma line measurements are

* Fig. 60.

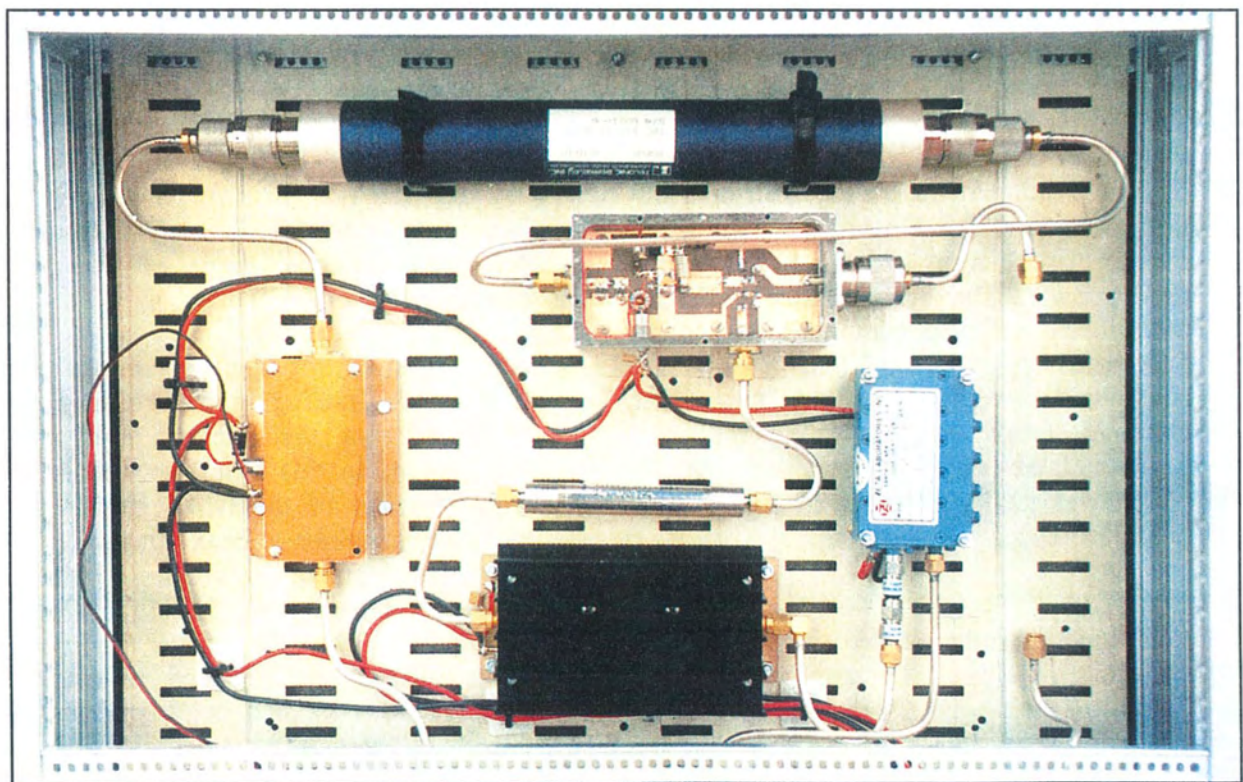


Fig. 61. New first mixer unit.

still possible for plasma frequencies of up to 7.5 MHz.

Attention was next directed towards the first mixer. The mixers used previously were not too well suited to operation under strong signal conditions, since they were designed for a relatively low local oscillator power level and had built-in IF amplifiers which could not be protected by bandpass filtering. Bench tests showed that the intermodulation performance of these units was poor at the signal levels to be expected from the NMT systems, so it was decided to design a replacement mixer, based on a high-power doubly balanced diode ring unit, coupled to a very low gain impedance matching amplifier.

The diode ring is specified to operate at a local oscillator power level of +23 dBm (200 mW), which is a factor of twenty more than in the old mixer. The new unit can tolerate input signals several hundred times stronger than the old mixer for the same amount of unwanted intermodulation. A completed mixer unit is shown in

Fig. 61. These mixers are now installed at both remote sites, and Tromsø will receive a similar unit shortly. With the new mixers, operation can proceed to within less than ten degrees off the line of sight to an NMT base.

In April 1988 new front end amplifiers, similar to the ones used at the remote sites (although uncooled) were installed in the Tromsø UHF receiver, thus providing electrically identical front ends at all sites. An attempt was made to provide calibration noise injection through the waveguide couplers in the manner used at the remotes, but an impedance mismatch problem peculiar to the Tromsø polariser (which has the transmitter permanently attached to one port) made the calibration level highly frequency dependent, and we were forced to revert to the old technique of injecting noise through a coaxial coupler. The system noise temperature nevertheless dropped substantially and is now nominally 95 Kelvin.

The EISCAT Facilities (December 1988)

Parameters of the EISCAT UHF system:

<u>Transmitter (Tromsø only):</u>	
Peak transmitted power	1.6 MW
Maximum duty cycle	12.5%
Operating frequencies	(929.5+0.5n) MHz, (n<15) n=0-15
Pulse widths	1-19999 µs
Risetime	0.1 µs
Maximum waveform repetition rate	1000 Hz
Modulations	on-off, phase-flip (0°/180°), frequency- step
<u>Antennas at all sites (Tromsø, Kiruna, Sodankylä):</u>	
Location and height of the UHF antennas above sea level (MSL), (Datum ED-1950):	
Tromsø site (Ramfjordmoen): (transmitter-receiver)	69°35'11.239" N 19°13'38.746" E h = 86.5 m
Kiruna site: (receiver)	67°51'38.373" N 20°26'06.806" E h = 417.9 m
Sodankylä site: (receiver)	67°21'49.266" N 26°37'37.497" E h = 197.3 m
Frequency band	933 ± 10 MHz
Rotation axes	Azimuth/Elevation
Azimuth angle range	540°
Elevation angle range	95° (0°-95°)
Lowest elevation permitted (transm.)	16° (5° within certain limited azimuth sectors)
Maximum rate of angular motion	1.3°/sec (each axis)
Diameter of main reflector	32.00 m
Feed system	Cassegrain
Diameter of subreflector	4.58 m
Focal length	11.01 m
Polarization	arbitrarily selectable, circular usually transmitted
Gain (calculated)	48.1 dB
Aperture efficiency (calculated)	0.651
Noise contribution (measured)	20-21 K
Half-power beamwidth	0.6°
Speed of mechanical movement, azimuth and elevation	80°/min
Fresnel zone limit:	6.37 km
Rayleigh distance:	1.59 km

Receivers:

Type of frontend	Cooled GaAsFET amplifier (Kiruna and Sodankylä)
System temperature	Uncooled GaAsFET (Tromsø) -35 K (Kir., Sod.) -95 K (Tromsø)
Number of IF channels	8 at each site
IF filter bandwidths	1.2 and 8.0 MHz
Detector	phase-coherent demodulator yielding quadrature components
Post-detection filters	12.5, 25.0, 50.0, 100. 0, 250.0 kHz 1MHz, 2MHz (all selectable)

Parameters of the EISCAT VHF system (Tromsø only):

<u>Transmitter:</u>	
Peak transmitted power	1.5 MW
Maximum duty cycle	4.5%
Operating frequencies	(222.4+0.2n) MHz, (n=5, 6, 7, 8)
Pulse widths	1-1000 µs
Risetime	0.1 µs
Maximum waveform repetition rate	1000 Hz
Modulations	on-off, phase-flip, frequency step
<u>Antenna</u>	
Location	69°35'11.9408" N 19°13'13.2300" E h = 85.3 m (reference point centre of elevation axis)
Frequency band	224 ± 1.25 MHz
Parabolic cylinder	2 panels for transmission, independently movable
Height of each panel	40 m
Width of each panel	30 m
Total width	120 m
Feed system	128 crossed dipoles (32 per panel)
Plane of mechanical motion	0.5° west of north
Speed of motion	5.0° min ⁻¹
Mechanical motion limits	30°-45° north to 70°-90° south of zenith
Effective aperture (on-axis)	3250 m ²
Beamwidth (on-axis)-vertical	1.7°
-transverse	0.6°
Gain	46 dBi

Off-axis phase steerability	21.3° in steps of 1.25°
Polarization	circular
Plane of mechanical movement	0.5°, measured 0.55° ±0.05° west of north
Operational modes	I: Combined mode, all elements aligned, physical area 5520 m ² . II: Split beam mode, element 1+2 and 3+4 pairwise aligned, structure behaves as two independent anten- nae, each of physical area 2400 m ² .
Effective area, broadside, mode I	3250 m ²
circular polarization:	3330 +240 m ²
horizontal polarization:	2890 ±210 m ²
vertical polarization:	2890 ±210 m ²
Polarization	Mode I: (i) Right- and left hand circular, possibility for polarization flipping from pulse to pulse (ii) Linear at + 45° with respect to vertical Mode II: Lefthand circular (transmission) Mode I: 0.6° east/west 1.7° north/south Mode II: 1.2° east/west 1.7° north/south
Beamwidths, broadside (calculated)	21.3° east and west of transit plane, steps approximately 1.2°
Beam steering by phasing	30° south to 60° north of zenith 5°/min
Range of mechanical movement	
Speed of mechanical movement	
Receiver:	solid state (gain >50 dB)
Frontend amplifiers	-250K
System temperature	8
Number of frequency channels	1.2, 8.0, 18.0 MHz
IF filter bandwidths	phase-coherent de modulator
Detector	selectable from 12.5 to 100 kHz in octave steps.
Post-detection filters	

PUBLICATIONS

Publications (Journals, Books) 1988

- Björnå, N. and S. Kirkwood,
Derivation of ion composition from a combined ion line/plasma line incoherent scatter experiment,
J. Geophys. Res., **93**, 5787-5793, 1988.
- Bourdillon, A. and D. Fontaine,
EDIA-EISCAT comparison between small-scale F region irregularities and large-scale electron density structures at sub-auroral latitudes,
J. Atm. Terr. Phys., **50**, 523-536, 1988.
- Brekke, A. and C.M. Hall,
Auroral ionospheric quiet summer time conductances,
Ann. Geophys., **6**, 361-376, 1988.
- Buchert, S. and C. La Hoz,
Extreme ionospheric effects in the presence of high electric fields,
Nature, **333**, 438-440, 1988.
- Buchert, S., W. Baumjohann, G. Haerendel, C. La Hoz and H. Lühr,
Magnetometer and incoherent scatter observations of an intense Ps 6 pulsation event,
J. Atm. Terr. Phys., **50**, 357-367, 1988.
- Caudal, G. and M. Blanc,
Using a constraint on the parallel velocity when determining electric fields with EISCAT,
J. Atm. Terr. Phys., **50**, 383-388, 1988.
- Collis, P.N. and I. Häggström,
Plasma convection and auroral precipitation processes associated with the main ionospheric trough at high latitudes,
J. Atm. Terr. Phys., **50**, 389-404, 1988.
- Collis, P.N., T. Turunen and E. Turunen,
Evidence of heavy positive ions at the summer Arctic mesopause from EISCAT UHF incoherent scatter radar,
Geophys. Res. Lett., **15**, 148-151, 1988.
- Etemadi, A., S.W.H. Cowley, M. Lockwood, B.J.I. Bromage, D.M. Willis and H. Lühr,
The dependence of high-latitude ionospheric flows on the north-south component of the IMF: A high time-resolution correlation analysis using EISCAT POLAR and AMPTE UK-S and IRM data,
Planet. Space Sci., **36**, 471-498, 1988.
- Farmer, A.D., M. Lockwood, T.J. Fuller-Rowell, K. Suvanto and U.P. Lovhaug,
Model predictions of the occurrence of non Maxwellian plasmas, and analysis of their effects on EISCAT data,
J. Atm. Terr. Phys., **50**, 487-499, 1988.
- Figueroa, D. and R. Hernández,
Collisional transfer rates for momentum and energy exchange in the case of relative drifts between ions and their parent neutral gas,
J. Atm. Terr. Phys., **50**, 447-454, 1988.
- Hall, C.M. and A. Brekke,
High Schmidt numbers in the mesopause region from 224 MHz incoherent backscatter,
Geophys. Res. Lett., **15**, 561-564, 1988.
- Hall, C.M., T. Devlin, A. Brekke and J.K. Hargreaves,
Negative ion to electron number density ratios from EISCAT mesospheric spectra,
Physica Scripta, **37**, 413-418, 1988.
- Hargreaves, J.K. and C.J. Burns,
Electron density and electron content fluctuations in the auroral zone,
Radio Sci., **23**, 493-502, 1988.
- Holmgren, G., G. Marklund, L. Eliasson, H. Opgenoorth, E. Söraas, F. Primdahl, G. Haerendel and P.M. Kintner,
Ionospheric response to chemical releases in the high latitude E and F regions,
Adv. Space Res., **8**, 79-83, 1988.

- Hoppe, U.-P. and T.L. Hansen,
Studies of vertical motions in the upper mesosphere using the EISCAT UHF radar,
Ann. Geophys., 6, 181-186, 1988.
- Hoppe, U.-P., C.M. Hall and J. Röttger,
First observations of summer polar mesospheric backscatter echoes with a 224 MHz radar,
Geophys. Res. Lett., 15, 28-31, 1988.
- Huuskonen, A., P. Pollari, T. Nygrén and M.S. Lehtinen,
Range ambiguity effects in Barker-coded multipulse experiments with incoherent scatter radars,
J. Atm. Terr. Phys., 50, 265-276, 1988.
- Huuskonen, A., T. Nygrén, L. Jalonen, N. Björnå, T.L. Hansen, A. Brekke and T. Turunen,
Ion composition in sporadic E layers measured by the EISCAT UHF radar,
J. Geophys. Res., 93, 14603-14610, 1988.
- Jones, G.O.L., P.J.S. Williams, K.J. Winser, M. Lockwood and K. Suvanto,
Large plasma velocities along the magnetic field line in the auroral zone,
Nature, 336, 231-232, 1988.
- Kangas, J., A. Aikio and T. Pikkarainen,
Radar electric field measurements during an IPDP plasma wave event,
Planet. Space Sci., 36, 1103-1109, 1988.
- Kersley, L., S.E. Pryse and N.S. Wheadon,
Small-scale irregularities associated with a high-latitude electron density gradient: scintillation and EISCAT observations,
J. Atm. Terr. Phys., 50, 557-563, 1988.
- Kersley, L., S.E. Pryse and N.S. Wheadon,
Small-scale ionospheric irregularities near regions of soft-particle precipitation: scintillation and EISCAT observations,
J. Atm. Terr. Phys., 50, 1047-1055, 1988.
- Kirkwood, S., H.J. Opgenoorth and J.S. Murphree,
Ionospheric conductivities, electric fields and currents associated with auroral substorms measured by the EISCAT radar,
Planet. Space Sci., 36, 1359-1380, 1988.
- Kustov, A.V., M.V. Uspensky and P.J.S. Williams,
Effects of turbulent irregularities in the auroral electrojet,
(original title in Russian)
Geomag. Aeron., 28, 923-927, 1988.
- Lehtinen, M.,
On statistical inversion theory,
in: *Theory and Applications of Inverse Problems* (H. Haario, ed.), 46-57,
(Longman Scientific & Technical, Longman Group UK Ltd., 1988).
- Lockwood, M. and S.W.H. Cowley,
Observations at the magnetopause and in the auroral ionosphere of momentum transfer from the solar wind,
Adv. Space Res., 8, 281-299, 1988.
- Lockwood, M. and K.J. Winser,
On the determination of ion temperature in the auroral F-region ionosphere,
Planet. Space Sci., 36, 1295-1304, 1988.
- Lockwood, M., M.F. Smith, C.J. Farrugia and G.L. Siscoe,
Ionospheric ion upwelling in the wake of flux transfer events at the dayside magnetopause,
J. Geophys. Res., 93, 5641-5654, 1988.

- Lockwood, M., S.W.H. Cowley, H. Todd, D.M. Willis and C.R. Clauer, Ion flows and heating at a contracting polar-cap boundary, *Planet. Space Sci.*, 36, 1229-1253, 1988.
- Lockwood, M., K. Suvanto, J.-P. St.-Maurice, K. Kikuchi, B.J.I. Bromage, D.M. Willis, S.R. Crothers, H. Todd and S.W.H. Cowley, Scattered power from non-thermal, F-region plasma observed by EISCAT - evidence for coherent echoes?, *J. Atm. Terr. Phys.*, 50, 467-485, 1988.
- Lühr, H. and S. Buchert, Observational evidence for a link between currents in the geotail and the auroral ionosphere, *Ann. Geophys.*, 6, 169-176, 1988.
- Moorcroft, D.R. and K. Schlegel, Evidence for non-Maxwellian ion velocity distributions in the F-region, *J. Atm. Terr. Phys.*, 50, 455-465, 1988.
- Moorcroft, D.R. and K. Schlegel, E-region coherent backscatter at short wavelength and large aspect angle, *J. Geophys. Res.*, 93, 2005-2010, 1988.
- Nielsen, E., J. Bamber, Z.-S. Chen, A. Brekke, A. Egeland, J.S. Murphree, D. Venkatesan and W.I. Axford, Substorm expansion into the polar cap, *Ann. Geophys.*, 6, 559-571, 1988.
- Nielsen, E., C. Senior and H. Lühr, Hall conductivity deduced from ground-based measurements, *J. Geophys. Res.*, 93, 4125-4130, 1988.
- Nielsen, E., M.V. Uspensky, A. Kustov, A. Huuskonen and J. Kangas, On the dependence of Farley-Buneman turbulence level on ionospheric electric field, *J. Atm. Terr. Phys.*, 50, 601-605, 1988.
- Nordling, J.A., Å. Hedberg, G. Wannberg, T.B. Leyser, H. Derblom, H.J. Opgenoorth, H. Kopka, H. Kohl, P. Stubbe, M.T. Rietveld and C. La Hoz, Simultaneous bi-static European Incoherent Scatter UHF, 145-MHz radar and stimulated electromagnetic emission observations during HF ionospheric modification, *Radio Sci.*, 23, 809-819, 1988.
- Opgenoorth, H.J. and S. Kirkwood, Ground-based observations co-ordinated with Viking spacecraft measurements, *Proc. Roy. Soc.*, 1988 (in press).
- Oyama, K.I. and K. Schlegel, Observation of electron temperature anisotropy in the ionosphere: A review, *Ann. Geophys.*, 6, 389-400, 1988.
- Providakes, J., D.T. Farley, B.G. Fejer, J. Sahr, W.E. Swartz, I. Häggström, Å. Hedberg and J.A. Nordling, Observations of auroral E-region plasma waves and electron heating with EISCAT and a VHF radar interferometer, *J. Atm. Terr. Phys.*, 50, 339-356, 1988.
- Quegan, S., R.S. Gill and M. Lockwood, Comparisons between EISCAT observations and model calculations of the high-latitude ionosphere, *J. Atm. Terr. Phys.*, 50, 1057-1076, 1988.
- Rice, D., R.D. Hunsucker, L.J. Lanzerotti, G. Crowley, P.J.S. Williams, J.D. Craven and L. Frank, An observation of atmospheric gravity wave cause and effect during the October 1985 Worldwide Atmospheric Gravity Waves Study Campaign, *Radio Sci.*, 23, 919-930, 1988.

- Richmond, A.D., Y. Kamide, B.-H. Ahn, S.-I. Akasofu, D. Alcaydé, M. Blanc, O. de la Beaujardière, D.S. Evans, J.C. Foster, E. Friis-Christensen, T.J. Fuller-Rowell, J.M. Holt, D. Knipp, H.W. Kroehl, R.P. Lepping, R.J. Pellinen, C. Senior and A.N. Zaitsev, Mapping electrodynamic features of the high-latitude ionosphere from localized observations: combined incoherent-scatter radar and magnetometer measurements for January 18-19, 1984, *J. Geophys. Res.*, 93, 5760-5776, 1988.
- Rietveld, M.T., H. Kopka and P. Stubbe, Pc 1 ionospheric electric field oscillations, *Ann. Geophys.*, 6, 381-388, 1988.
- Rishbeth, H., A.P. van Eyken, B.S. Lanchester, T. Turunen, J. Röttger, C.M. Hall and U.-P. Hoppe, EISCAT VHF radar observations of periodic mesopause echoes, *Planet. Space Sci.*, 36, 423-428, 1988.
- Robinson, T.R., The excitation of plasma waves and instabilities in the ionosphere by means of high power radio waves, *Plasma Phys. Controll. Fusion*, 30, 45-56, 1988.
- Röttger, J., C. La Hoz, M.C. Kelley, U.-P. Hoppe and C.M. Hall, The structure and dynamics of polar mesosphere summer echoes observed with the EISCAT 224 MHz radar, *Geophys. Res. Lett.*, 15, 1353-1356, 1988.
- Schlegel, K., Auroral zone E-region conductivities during solar minimum derived from EISCAT data, *Ann. Geophys.*, 6, 129-138, 1988.
- Shirochkov, A.V., L.N. Makarova, S.A. Maurits and K. Schlegel, Structure of the ionosphere in the auroral zone during the magnetospheric substorm on 13 July 1984, (original title in Russian) *Geomagn. Aeron.*, 28, 416-421, 1988.
- Steen, Å. and P.N. Collis, High time-resolution imaging of auroral arc deformation at substorm onset, *Planet. Space Sci.*, 36, 715-732, 1988.
- Steen, Å., P.N. Collis and I. Häggström, On the development of folds in auroral arcs, *J. Atm. Terr. Phys.*, 50, 301-313, 1988.
- Steen, Å., D. Rees, P.N. Collis and J.S. Murphree, What role does the F-region neutral wind play in auroral intensifications? *Planet. Space Sci.*, 36, 851-868, 1988.
- Suvanto, K., Incoherent scattering of radar waves from non-thermal F-region plasma: Analytical methods of spectrum synthesis, *Radio Sci.*, 23, 989-996, 1988.
- Todd, H., S.W.H. Cowley, A. Etemadi, B.J.I. Bromage, M. Lockwood, D.M. Willis and H. Lühr, Flow in the high-latitude ionosphere: measurements at 15 s resolution made using the EISCAT 'POLAR' experiment, *J. Atm. Terr. Phys.*, 50, 423-446, 1988.
- Todd, H., S.W.H. Cowley, M. Lockwood, D.M. Willis and H. Lühr, Response time of the high-latitude dayside ionosphere to sudden changes in the north-south component of the IMF, *Planet. Space Sci.*, 36, 1415-1428, 1988.

- Turunen, T., T. Nygrén, A. Huuskonen and L. Jalonen,
Incoherent scatter studies of sporadic-E using 300 m resolution,
J. Atm. Terr. Phys., 50, 277-287, 1988.
- Turunen, E., P.N. Collis and T. Turunen,
Incoherent scatter spectral measurements of the summertime high-latitude D-region with the EISCAT UHF-radar,
J. Atm. Terr. Phys., 50, 289-299, 1988.
- Uspensky, M.V. and P.J.S. Williams,
The amplitude of auroral backscatter: I. Model estimates of the dependence on electron density,
J. Atm. Terr. Phys., 50, 73-79, 1988.
- Uspensky, M.V., A. Kustov, E. Nielsen, A. Huuskonen and J. Kangas,
Electron density estimations in the auroral E region using STARE data, (original title in Russian)
Geomagn. Aeron., 28, 688-691, 1988.
- Vallinkoski, M.,
Statistics of incoherent scatter spectrum multiparameter fits,
J. Atm. Terr. Phys., 50, 839-851, 1988.
- Williams, P.J.S., B. Jones, M.V. Uspensky and G. Starkov,
Multi-radar studies of auroral backscatter,
J. Atm. Terr. Phys., 50, 315-321, 1988.
- Williams, P.J.S., G. Crowley, K. Schlegel, T.S. Viridi, I. McCrea, G. Watkins, N. Wade, J.K. Hargreaves, T. Lachlan-Cope, H. Muller, J.E. Baldwin, P. Warner, A.P. van Eyken, M.A. Hapgood and A.S. Rodger,
The generation and propagation of atmospheric gravity waves observed during the Worldwide Atmospheric Gravity-wave Study (WAGS),
J. Atm. Terr. Phys., 50, 323-338, 1988.
- Winser, K.J., G.O.L. Jones and P.J.S. Williams,
Variations in field-aligned plasma velocity with altitude and latitude in the auroral zone: EISCAT observations and the physical interpretation,
Physica Scripta, 37, 640-644, 1988.
- Winser, K.J., A.D. Farmer, D. Rees and A. Aruliah,
Ion-neutral dynamics in the high latitude ionosphere: first results from the INDI experiment,
J. Atm. Terr. Phys., 50, 369-377, 1988.
- Winser, K.J., G.O.L. Jones and P.J.S. Williams,
Large field-aligned velocities observed by EISCAT,
J. Atm. Terr. Phys., 50, 379-382, 1988.
- Wright, J.W., R.I. Kressman, T.S. Viridi and P.N. Collis,
Comparisons of EISCAT and dynasonde ionospheric measurements: simple to moderately structured plasma densities,
J. Atm. Terr. Phys., 50, 405-421, 1988.
- Yau, A.W. and M. Lockwood,
Vertical ion flows in the polar ionosphere,
AGU Monograph, 44, 229-240, 1988.

Publications (Proceedings, Reports, Theses) 1988

- Brekke, A.,
The polar ionosphere,
WITS Handbook, 1, (C.H. Liu and B. Edwards, eds.), 94-126 (publ. by SCOSTEP Secretariat, Dept. Elec. Engin., University of Illinois, Urbana, IL, 1988).
- Buchert, S.,
Untersuchung über die Dynamik der Ionosphäre im Bereich des Nordlichts mit Hilfe des EISCAT-Ionosphärenradars,
Ph.D. thesis, Technische Universität München, 1988.
- Figuroa Martinez, D.R.,
Ionen-Neutrgas-Kopplung in der polaren Atmosphäre: Benutzung von EISCAT für die Berechnung von thermosphärischen Parametern,
Ph.D. thesis, Georg-August-Universität zu Göttingen, 1988.
- Grassmann, V.,
Inkohärente Rückstreuung von Radiowellen durch ein Plasma unter Berücksichtigung von Teilchen-Stößen,
Rpt. MPAE-W-100-88 07, Max Planck-Institut für Aeronomie, Katlenburg-Lindau, F.R.Germany, 1988 (Ph.D. thesis).
- Hanssen, A.,
The incoherent scatter plasma line used for the derivation of plasma parameters, with particular emphasis on the ion composition. Theory and EISCAT experiment,
Cand. scient. thesis, University of Tromsø, 1988.
- Huuskonen, A.,
High resolution studies of the lower E-region using the incoherent scatter method,
Ph.D. thesis, University of Oulu, 1988.
- Kirkwood, S.,
SPECTRUM - A computer algorithm to derive the flux-energy spectrum of precipitating particles from EISCAT electron density profiles,
IRF-Techn. Rpt. 034, Institute of Space Physics, Kiruna, Sweden, 1988.
- Markkanen, J.,
Revontulten synty,
esiteelmä Jyväskylän yliopiston Fysiikan laitoksella,
28 October 1988.
- Meyer, W.,
Untersuchungen groß- und kleinskaliger dynamischer Prozesse in der Mesosphäre und oberen Stratosphäre anhand von Wind- und Dichtemessungen über Nordskandinavien im Rahmen des MAP/WINE Projekts,
Ph.D. thesis, Rheinische Friedrich-Wilhelms-Universität, Bonn, 1988.
- Röttger, J.,
The instrumental principles of MST radars and incoherent scatter radars and the configuration of radar system hardware,
Lecture Journal, International School on Atmospheric Radar (S. Fukao, ed.), III, 1-81 (publ. by Radio Atmospheric Science Center, Kyoto, Japan, November 1988).
- Schlegel, K. and K.-I. Oyama,
Electron temperatures in the high latitude topside ionosphere from satellite and incoherent scatter data,
Res. Note No. 395, The Institute of Space and Astronautical Science, Tokyo, 1988.
- Steen, Å.,
Investigations of auroral dynamics: techniques and results,
IRF Scientific Rpt. 194, Swedish Institute of Space Physics, Kiruna, Sweden, 1988 (Ph.D. thesis).

Todd, H.,
Studies of flow in the high-latitude
ionosphere using the EISCAT radar,
Ph.D. thesis, University of London,
1988.

Treumann, R., and C. La Hoz,
Radio emission processes related to
solar flares,
in: Activity in Cool Star Envelopes,
O. Havnes (Ed.), 269-281, Kluwer,
1988.

Trondsen, T.S.,
Plasma line measurements with the
EISCAT spectrum analyzer,
Cand. scient. thesis, University of
Tromsø, 1988.

Virdi, T.S.,
Periodic phenomena in the high-latitude
thermosphere,
Ph.D. thesis, University College of
Wales, Aberystwyth, 1988.

Supplements 1984-1987

Journals, Books

Collis, P.N. and S. Kirkwood,
Localised features in the auroral D-
region observed by EISCAT,
Adv. Space Res., 7, 349-352, 1987.

Fuller-Rowell, T.J.,
Numerical investigations of thermo-
spheric/ionospheric coupling in the
polar regions,
Physica Scripta, T18, 229-239, 1987.

Kersley, L., S.E. Pryse and
N.S. Wheadon,
Amplitude and phase scintillation at
high latitudes over northern Europe,
in: The Effect of Ionosphere on
Communication, Navigation and Sur-
veillance Systems (J.M. Goodman, ed.),
591, (NRL, Washington, D.C., 1987).

Rishbeth, H. and D.M. Willis,
UK allocations of EISCAT observing
time,
Q. J. Roy. Astron. Soc., 28, 477-480,
1987.

Williams, P.J.S.,
EISCAT: Ar Ffiniau'r Gofod (EISCAT:
on the boundaries of space),
Y Gwyddonydd (The Scientist), 25, 19-
22, 1987.

Proceedings

Hargreaves, J.K. and C.J. Burns,
Electron density and electron content
fluctuations in the auroral zone,
Proc. of Symposium on The Effect of
the Ionosphere on Communication,
Navigation and Surveillance Systems,
675, Springfield, VA, 1987.

Theses

Farmer, A.D.,
Measurements of ionospheric structure:
winds, currents and electric fields,
Ph.D. thesis, University of London,
1984.

Winser, K.J.,
A combined radar and optical study of
the polar ionosphere,
Ph.D. thesis, Ulsier Polytechnic, 1984.

Fontaine, D.,
Les aurores diffuses boreales et
australes: une contribution theorique et
experimentale a l'etude du transport
des electrons dans la magnetosphere
terrestre,
Ph.D. thesis, l'Université Pierre &
Marie Curie, Paris, 1985.

Oakley, G.L.,
Differential carrier-phase observations
at high latitudes,
M.Sc. thesis, University College of
Wales, Aberystwyth, 1986.

Jones, G.O.L.,
EISCAT studies of the high-latitude E-
and F-regions,
Ph.D. thesis, University College of
Wales, Aberystwyth, 1987.

Pryse, S.E.,
Radio-wave scintillations and
ionospheric irregularities at high
latitudes,
Ph.D. thesis, University College of
Wales, Aberystwyth, 1987.

Russell, C.D.,
Observations of radio-wave scintil-
lations and ionospheric irregularities at
high latitudes,
M.Sc. thesis, University College of
Wales, Aberystwyth, 1987.

EISCAT REPORTS AND MEETINGS

Reports 1988:

EISCAT Annual Report 1987

Meeting reports:

C. La Hoz (Editor)
Proceedings of the EISCAT Annual Review Meeting 1988,
Riksgränsen, Sweden, 22-25 February, 1988.
EISCAT Meetings No. 88/13, 1988.

Meetings 1988:

COUNCIL	31st meeting 9-10 May 1988	Katlenburg-Lindau, Germany
	32nd meeting 10-11 November 1988	Kiruna, Sweden
SAC	34th meeting 25 March 1988	Bologna, Italy
	35th meeting 11-12 October 1988	Sodankylä, Finland
AFC	30th meeting 7 April 1988	Kiruna, Sweden
	31th meeting 29 September 1988	Oslo, Norway

BALANCE SHEET AT 31 DECEMBER 1988

	MSEK					
	At 31 Dec. 1987	Additions			Depre- ciations	At 31 Dec. 1988
		Pool	Cap. Op.	Other		
Assets						
FIXED ASSETS						
Buildings	8.2			0.2	8.0	
Transmitters	26.6	4.1		1.6	29.1	
UHF-antenna	14.7			1.3	13.4	
VHF-antenna	18.6			1.5	17.1	
Receivers	0.8			0.8		
Computers etc	5.8		0.2	1.3	4.7	
Other	2.2		0.9	0.7	2.4	
Total	76.9	4.1	1.1		7.4	74.7
CURRENT ASSETS						
Debtors	0.3				1.0	
Prepayments and accrued income	0.3				0.3	
Cash and Ordinary Bank Accounts	8.6				5.9	
Special Accounts	0.1				0.2	
Total	9.3					7.4
GRAND TOTAL	86.2					82.1

	MSEK	
	At 31 Dec. 1987	At 31 Dec. 1988
Liabilities		
CAPITAL		
Contributions		
Pool	88.6	92.7
Capital Operating in Kind	14.6	15.6
Other	25.1	25.1
	0.4	0.4
	128.7	133.8
Depreciations	51.8	59.1
Total Capital	76.9	74.7
RESERVES		
Pool	4.3	0.6
Capital Operating Other	0.8	0.9
	0.8	2.6
Total Reserves	5.9	4.1
Special Accounts	0.1	0.2
LIABILITIES		
Provisions	0.3	0.2
Other Liabilities	3.0	2.9
Total Liabilities	3.3	3.1
GRAND TOTAL	86.2	82.1

Totals may not match because of rounding. (MSEK = Million Swedish Crowns.)

EISCAT SCIENTIFIC ASSOCIATION 1988

	France	Finland	Federal Republic of Germany	Norway	Sweden	United Kingdom
COUNCIL	P. Bauer A. Berroir G. Caudal	O. Ranta A. Siivoia	W.L. Axford G. Haerendel G. Preiss	O. Havnes L. Westgaard	B. Hultqvist* M.O. Ottosson	W.J.G. Beynon T.B. Jones B.R. Martin
SAC	D. Fontaine W. Kofman	J. Kangas	W. Baumjohann K. Schlegel*	N. Björnå	H. Opgenoorth	S.W.H. Cowley P.J.S. Williams
AFC	J.P. Granier	O. Ranta	M. Meinecke	L. Westgaard*	J. Gustavsson	D. Morrell

SAC = Scientific Advisory Committee

AFC = Administrative and Finance Committee

Non-Associate SAC member: G. Kockarts

* = Chairman

HEADQUARTERS SENIOR STAFF

Director: J. Röttger (on secondment from MPG)

Assistant Directors: C. La Hoz, G. Wannberg

Business Manager: P. Hagström



THE EISCAT ASSOCIATES

Centre National de la Recherche Scientifique
France
(CNRS)

Suomen Akatemia
Finland
(SA)

Max-Planck-Gesellschaft
West Germany
(MPG)

Norges Almenvitenskapelige Forskningsråd
Norway
(NAVF)

Naturvetenskapliga Forskningsrådet
Sweden
(NFR)

Science and Engineering Research Council
The United Kingdom
(SERC)

